

Analysis of Mesoscopic Electromagnetic
Phenomena in Type III Superconductors
by the Fluxoid Dynamics Method

磁気量子動力学法による第二種超電導体中の
メゾスコピック電磁現象の解析

KAZUYUKI DEMACHI

田 町 泰 之

①

Analysis of Mesoscopic Electromagnetic
Phenomena in Type II Superconductors
by the Fluxoid Dynamics Method

磁束量子動力学法による第二種超電導体中の
メゾスコピック電磁現象の解析

KAZUYUKI DEMACHI

出町 和之

B.E., University of Tokyo
(1992)

M.E., University of Tokyo
(1994)

February 1996

Department of Quantum Engineering
and Systems Science,
Faculty of Engineering,
University of Tokyo

Acknowledgment

I would like to express my gratitude to Professor K. Miya for his excellent direction, heartfelt encouragement, and profitable discussion. I would also like to thank Assistant Professor M. Uesaka for his precise guidance and kind advises. I owe Assistant Professor Y. Yoshida great thank for his accurate instructions and kind cares in details.

I am very grateful to Dr. K. Morishita for his useful discussion and kindest help.

I am very thankful to Mr. R. C. Popa, Mr. A. Gillanyi, Mr. T. Uchimoto, Mr. Z. Chen and his wife Mrs. L. Wei, Mr. Y. Luo, Mr. M. Rabara and Mrs. W. Cheng for their fruitful discussion and deep friendship. I am also grateful to Mr. Y. Fukuzaki, Mr. R. Shinagawa, Mr. A. Takeshita, Mr. K. Kinoshita, Mr. T. Nakayamam, Mr. K. Takase, Mr. S. Shindo, Mr. K. Saito and Mr. T. Yamada for their kindest support. I would like to express my thanks to Ms. K. Kameta, Ms. A. Shimizu, Ms. K. Okamoto and Ms. S. Yoshitake for their kindest help.

Contents

1	Introduction	1
1.1	Background	2
1.2	Objectives and Outlines	6
1.2.1	Objectives	6
1.2.2	Outlines	6
2	Review of Electrodynamics of Superconductor	8
2.1	London theory for superconductors	9
2.1.1	London equations	9
2.1.2	Magnetic flux density around a fluxoid	11
2.1.3	Current density around a fluxoid	13
2.2	Ginzburg-Landau theory	14
2.2.1	Ginzburg-Landau free energy	14
2.2.2	Determination of coefficient α and β	15
2.2.3	Ginzburg-Landau equations	16
2.2.4	Ginzburg-Landau parameter	17
2.2.5	Quantization of magnetic flux	18
2.2.6	Upper critical field in bulk, H_{c2}	19
2.2.7	Abrikosov's lattice in type II superconductor	21
2.2.8	Upper critical field near the surface, H_{c3}	22
2.2.9	Time-dependent Ginzburg-Landau equations (TDGL eqs.)	24
2.2.10	Insulating boundary condition	26

2.3	Mixed state of superconductor	27
2.3.1	Critical state models	27
2.3.2	E-J constitutive relation	28
2.3.3	Flux Flow resistivity	29
3	Development of Fluxoid Dynamics Method and Simulation Codes	31
3.1	Numerical Simulation method for GL equations	32
3.1.1	Ginzburg-Landau equations of an isolated fluxoid	32
3.1.2	Discretized 1-dimensional GL equations	33
3.1.3	Distribution of order parameter and vector potential around an isolated fluxoid	35
3.1.4	Solution of TDGL equations	36
3.1.5	Discretization of 2-dimensional TDGL equations	36
3.1.6	Boundary condition of discretized 2D-TDGL equations	38
3.1.7	Time integral method of 2D-TDGL simulation	39
3.1.8	Computational model of YBCO thin film	42
3.1.9	Numerical results of YBCO thin film	43
3.2	2-dimensional fluxoid dynamics method	47
3.2.1	Kinetic equation of fluxoid	47
3.2.2	Viscous coefficient of fluxoid	48
3.2.3	Pinning force	49
3.2.4	Magnetic repulsive force between two fluxoids	52
3.2.5	Magnetic force due to Meissner current	53
3.2.6	Lorentz force due to transport current	53
3.2.7	Calculation of the electric field	54
3.2.8	Discretization of the kinetic equation	56
3.2.9	Periodic boundary condition	57
3.2.10	Insulating boundary condition	57
3.2.11	Initial distribution of fluxoids	58

3.3	3-dimensional fluxoid dynamics method	59
3.3.1	Governing equations of 3D-FD method	60
3.3.2	Pinning force and torque	61
3.3.3	Magnetic flux density due to each fluxoid	62
3.3.4	Magnetic flux density due to Meissner current	65
3.3.5	Magnetical repulsive force and torque	66
3.3.6	Lorentz force and torque due to transport current	67
3.3.7	Tension force	68
3.3.8	Viscous coefficient of fluxoid	70
3.3.9	Binding condition and edge condition	73
3.3.10	Solution of the governing equations	75
4	Prediction of critical current density of type II superconductor	78
4.1	2-dimensional analysis of the zero-field cooled NbTi	79
4.1.1	Computational model near the surface of NbTi bulk	79
4.1.2	Behaviors of fluxoids in NbTi bulk	81
4.1.3	Comparison with the Bean model	87
4.1.4	Relationship between J_c and B	87
4.2	2-dimensional analysis of the field cooled NbTi	91
4.2.1	Computational model	91
4.2.2	Flows of the fluxoids	92
4.2.3	Time-variation of Electric field : E_x	94
4.2.4	Relation between J_t and E_x	94
4.2.5	Constitutive relation between B_{cx} and J_c	97
5	Numerical analysis of the anisotropy of superconductor	99
5.1	3D analysis of anisotropy of the shielding current in NbTi	100
5.1.1	Computational model of 3-dimensional FD method	100
5.1.2	Initial distribution of fluxoids in equilibrium state	101

5.1.3	Flows of the fluxoids	104
5.1.4	Time-variation of electric field	109
5.1.5	Constitutive relation between J_t and E_x	111
5.1.6	Relation between B_{ex} and flow resistivity	112
5.1.7	Time-variation of electric field-2	113
5.1.8	Relation between B_{ex} and J_c	114
6	Conclusion	116
A	Appendix	126
A.1	126

Chapter 1

Introduction

1.1 Background

The superconductor exhibits two kinds of electromagnetic property.

The first one is the perfect conductivity. It was discovered by H. Kamerling Onnes in 1911. He made the experiment with use of platinum at low temperature in the first time and found that it shows an abrupt reduction in terms of electric resistance at a temperature while the drop depends on the purity of the specimen. Since mercury was known as the purest among all metals available at that time, he made the same experiment with use of the pure mercury to find that it showed also an abrupt drop of electric resistance at 4 K and it is impossible to be measured in the temperature range below 4 K. Then he thought that mercury changes at some critical temperature its state as to the electric resistance into a new one quite unlike those previously known. This was called the superconducting state.

The second one is the perfect diamagnetism. It was discovered by H. Meissner and R. Ochsenfeld in 1933. They found that the magnetic flux in the superconductor of normal conducting state was excluded when it became the superconducting state. This did not agree the expectation that the magnetic flux in superconductor should be kept constant when it became from the normal conducting state to the superconducting one. This phenomena is called the Meissner effect and it can not be explained only by the perfect conductivity.

After that, the theoretical progresses have been achieved by the London theory[1], the BCS theory, and the Ginzburg-Landau theory[2] and so on. The two electromagnetic properties of superconductor were shown by F. and H. London in 1935 that they could be expressed well using the London equations,

$$E = \frac{\partial}{\partial t}(\Lambda J_s), \quad (1.1)$$

$$H = \nabla \times (\Lambda J_s). \quad (1.2)$$

This equations indicated the penetration depth of the magnetic field from the surface of the superconductor, λ which explained the Meissner effect. The BCS theory was de-

rived by J. Barden, L. N. Cooper and J. R. Schrieffer in 1957 and suggested that the Bose-condensed two electrons, a Cooper pair, was not affected by the electric resistance and behaved as the superconducting electrons. The Ginzburg-Landau theory was suggested by V. L. Ginzburg and L. D. Landau in 1950. It succeeded to describe the free energy density in the superconductor as the function of the order parameter of the phase transition from the normal conducting state to the superconducting one, while the order parameter corresponded to the wave function in quantum mechanics. It suggested the coherence length of the phase, ξ , and the Ginzburg-Landau parameter, κ , dividing the the superconductor into 2 kinds, the type I superconductor ($\kappa < 1/\sqrt{2}$), and the type II one ($\kappa > 1/\sqrt{2}$). The High-Tc superconductor is included into the type II.

Since the High-Tc superconductor was discovered and the critical temperature exceeded the temperature of liquid nitrogen(77K), the "superconductor fever" arose being decaying at this moment in the pursuit of new application of the material. Recently the applications of superconductor are still now explored studied in various engineering and technological fields, while a success has been achieved in particular field of practical use. The most popular one is the superconducting levitation system such as the magnetic vehicles of linear motor cars. As the energy storage technology, SMES(Superconducting Magnetic Energy Storage) and SFW(Superconducting FlyWheel)[3][4] are under development not only in Japan but also in other countries. HTSC tape material[5] has developed rapidly and its easiness of transformation have attracted the attention of many researchers.

As regards the nuclear fusion reactor technology, the contribution of superconductor is indispensable. In fact, in the design of ITER (International Thermonuclear Experimental Reactor), the magnet system consist of many superconducting coils: the CS(Center Soleoid) coil to drive the large current in the plasma and the TF(Toroidal Field) and PF(Poloidal Field) coils to confine the plasma in the magnetic field. Furthermore, possibility of the High-Tc Superconducting Plasma Stabilizer was initiated for the studies[6].

It can be said that the scientific feasibility of the nuclear fusion reactor has been already

proved almost in the large tokamak machine such as JET, JT-60 and TFTR. However, as well known, further investigations and development activity are necessary for proceeding to demonstration of the technological feasibility of it. The output power density of ITER is about $1.5\text{MW}/\text{m}^3$ which is $2.0\sim 7.5\%$ of the nuclear fission reactors ($20\sim 60\text{MW}/\text{m}^3$). With regards to the output power density of fusion reactor, it is important to consider its parameter dependence like this,

$$P \propto \beta^2 B^4 a_p^2,$$

where β is the plasma β value, B is the magnitude of the magnetic flux density at the center of plasma and a_p is the minor radius of plasma. If it is possible to increase the magnetic flux density 3 times larger, the 81 times larger power density will be produced. Hence the development of the high efficient superconducting magnets is one of the most important issues for the realization of nuclear fusion reactors.

In such general practical applications, the superconductors are used in high magnetic field, which is usually higher than the critical magnetic field of the type I superconductor, H_c , and the lower critical field of the type II superconductor, H_{c1} . It means that only the type II superconductor in the mixed state ($H_{c1} < H < H_{c2}$) can be used for most practical applications.

In the type II superconductor in the mixed state, the magnetic flux is quantized in the form of fluxoids. The distribution of fluxoids is determined by the interaction with the impurities, other fluxoids and so on. The macroscopic electromagnetic phenomena of type II superconductors can be predicted by analyzing behaviors of fluxoids in the mesoscopic electromagnetic level.

Some physical models proposed up to now such as the critical state model [7]-[9] and the flux flow and creep one [10],[11] could be taken as the macroscopic constitutive model of the mixed state of type II superconductors. These models can be expressed as constitutive relations between the macroscopic electric field and the macroscopic current density. Such macroscopic mathematical models have been successfully applied so far to the numerical analysis of the shielding current field in type II superconductors [12]-[14]

and the simulation of the levitation force due to the superconducting magnets [15]-[18].

However, these models can not accurately describe the nonlinear electromagnetic phenomena in superconductors such as the electromagnetic anisotropy[19], [20] and the melting of the flux lattice[21]-[23] and so on. Therefore, development of new physical model based on the precise analysis of the behavior of fluxoids is expected.

In this study, a new theoretical analysis method of the behaviors of fluxoids in type II superconductor is proposed, which is based on the Molecular Dynamics method (MD method) [24]-[26] combined with the London and the Ginzburg-Landau theories. The prediction of some macroscopic electromagnetic phenomena and the evaluation of the anisotropy of type II superconductor were made. This analysis method was named the Fluxoid Dynamics method (FD method).

1.2 Objectives and Outlines

1.2.1 Objectives

This thesis presents the development of the new simulation method, Fluxoid Dynamics method (FD method). By this method, the nonlinear electromagnetic phenomena in type II superconductor which can not be explained by the conventional macroscopic method was investigated.

Then the thesis says the following four purposes:

- Development of the simulation method of the distribution of the superconducting electrons density and the magnetic flux density in type II superconductor by solving the Ginzburg-Landau equations.
- Development of 2-dimensional and 3-dimensional Fluxoid Dynamics (FD method) method and its simulation code. This method is based on the concept of the Molecular Dynamics method combined with the results of above simulation. The behavior of the fluxoids in the superconductor is predicted by solving the various interactions such as the fluxoids and the pinning centers.
- Prediction of the macroscopic electromagnetic phenomena of type II superconductor by the FD method, such as the relationship between the applied magnetic flux density and the critical current density.
- Evaluation of the anisotropy of type II superconductor by the FD method, such as the critical current density in NbTi due to the arrangement of the α -Ti pins.

1.2.2 Outlines

The thesis consists of seven chapters including this one.

In Chapter 2, through the London theory, the Ginzburg-Landau theory and some electrodynamics of superconductor reviewed are the fundamental theories necessary for the development of the FD method leading to a provision of the basic frame of the thesis.

In Chapter 3, the FD method was developed and its simulation code were implemented. Section 3.1 explains the 1-dimensional and 2-dimensional numerical simulation methods of Ginzburg-Landau equations. By this method, the structure of an isolated fluxoid in NbTi was analyzed and the formation of fluxoids lattice in YBCO thin film was simulated. In Section 3.2 the theory and the simulation method of 2-dimensional FD method was developed. In this theory five kinds of forces are taken into account: the pinning force F_p , the magnetic repulsive force between fluxoids F_f , the magnetic force due to the Meissner current F_M , the Lorentz force due to the transport current density F_J and the viscous force caused by the ohmic loss in the normal conducting core F_η . Section 3.3 describes the theory and the simulation method of 3-dimensional FD method. Here a fluxoid is regarded as a chain of short unit of fluxoid, and the tension F_T is added into consideration.

In Chapter 4 the critical current density, J_c , of NbTi was predicted by 2-dimensional FD method and the validity of these method was verified. The relation between the applied magnetic flux density and the critical current density agreed with the empirical model, Kim model.

In Chapter 5 the anisotropy of NbTi due to the arrangement of the α -Ti pinning centers were investigated by using 3-dimensional Fluxoid Dynamics Method. The dependence of J_c on the angle of the applied magnetic field was analyzed.

In Chapter 6, the total works in this thesis and the new knowledge from this study are concluded.

Chapter 2

Review of Electrodynamics of Superconductor

2.1 London theory for superconductors

Two fundamental properties of superconductor, the perfect conductivity and the perfect diamagnetism are described by the London theory. Moreover this theory can be not only a good approximation to the behaviors of the superconductors with high upper critical magnetic field, H_{c2} , hence some important characteristic features of them can be derived from this theory.

2.1.1 London equations

In the superconductor, the permanent current flows constantly. This phenomenon should be exactly described by the classical equation of motion of the superconducting electrons. In the superconductor, the electrons receive only the acceleration due to the electric field, thus we have

$$m^* \frac{dv_s}{dt} = -e^* E, \quad (2.1)$$

where m^* and $-e^*$ are respectively the mass and the electric charge of a Cooper pair. v_s is the velocity of a Cooper pair and E is the electric field. And the superconducting current density is written as

$$j_s = -n_s e^* v_s, \quad (2.2)$$

where n_s is the density of the Cooper pair. This substitution of eq. (2.2) into eq. (2.1) yields

$$E = \frac{m^*}{n_s e^{*2}} \frac{dj_s}{dt}. \quad (2.3)$$

The magnetic field, H and the magnetic flux density B are governed by the following Maxwell's equations:

$$\nabla \times E = \frac{\partial B}{\partial t}, \quad (2.4)$$

$$\nabla \times H = j_s. \quad (2.5)$$

where the displacement current density is neglected.

The constitutive equation between B and H are written as,

$$B = \mu_0 H. \quad (2.6)$$

By means of eqs.(2.3), (2.4) and (2.6), one can obtain

$$\frac{\partial}{\partial t} \left(B + \frac{m^*}{\mu_0 n_s e^{*2}} \nabla \times \nabla \times B \right) = 0, \quad (2.7)$$

London brothers showed that the Meissner effect can be explained when the following equation is satisfied,

$$B + \frac{m^*}{\mu_0 n_s e^{*2}} \nabla \times \nabla \times B = 0. \quad (2.8)$$

Equations (2.3) and (2.8) are called London equations. Employing the identity $\nabla \times \nabla \times B = \nabla(\nabla \cdot B) - \nabla^2 B$ and imposing $\nabla \cdot B = 0$, eq.(2.8) can be rewritten as

$$\nabla^2 B - \frac{1}{\lambda^2} B = 0, \quad (2.9)$$

where λ has the dimension of length and notes

$$\lambda = \left(\frac{m^*}{\mu_0 n_s e^{*2}} \right)^{1/2}, \quad (2.10)$$

Here, we consider a sufficiently large piece of superconductor material which occupies the region $x \geq 0$ as shown in Fig.2.1. Then $x < 0$ is the air region and $x = 0$ is the surface of the superconductor. When the external magnetic field $H_{ex} = H_{ex} e_z$ is applied parallel to the z -axis, it is thought that the direction of magnetic flux density B in the superconductor is also parallel to the z -axis and has a distribution in its magnitude only in x -direction.

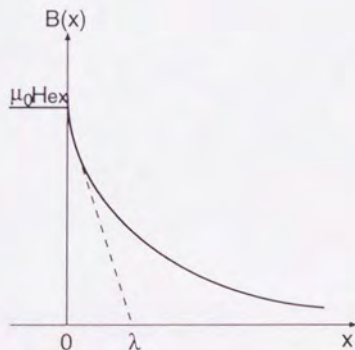


Figure 2.1: Distribution of magnetic flux density near the surface of the superconductor in the Meissner state

Therefore, eq.(2.9) is rewritten as

$$\frac{d^2 B}{dx^2} - \frac{B}{\lambda^2} = 0. \quad (2.11)$$

From the following boundary conditions,

$$\begin{cases} B(0) = \mu_0 H_{ez} \\ B \xrightarrow{x \rightarrow \infty} 0 \end{cases}, \quad (2.12)$$

the function of the magnetic flux density in the superconductor, $B(x)$ is obtained as,

$$B(x) = \mu_0 H_{ez} \exp\left(-\frac{x}{\lambda}\right). \quad (2.13)$$

This equation means that the magnetic field can penetrate the superconductor with the depth $\sim \lambda$. This depth λ is called the magnetic penetration depth.

2.1.2 Magnetic flux density around a fluxoid

In the case that the magnetic penetration depth λ is large enough than the coherence length ξ , the following London's equation is satisfied around a fluxoid,

$$\lambda^2 \nabla \times \nabla \times \mathbf{B}_f + \mathbf{B}_f = \Phi_0 \delta_2(\mathbf{r}) \mathbf{z}, \quad (2.14)$$

where $\delta_2(\mathbf{r})$ is the Delta function satisfying the following equation,

$$\int_S \delta_2(\mathbf{r}) dS = 1. \quad (2.15)$$

Equation (2.14) is rewritten by substituting $\nabla \cdot \mathbf{B}_f = 0$ as

$$\nabla^2 \mathbf{B}_f - \frac{\mathbf{B}_f}{\lambda^2} = -\frac{\Phi_0}{\lambda} \delta_2(\mathbf{r}) \mathbf{e}_z \quad (2.16)$$

Then, by substituting $\mathbf{B} = (0, 0, B)$ to eq. (2.16) because of the assumption of the uniformity in z-direction, eq. (2.14) is written in the cylindrical coordinate system as

$$\lambda^2 \frac{d^2 B_f}{dr^2} + \lambda^2 \frac{1}{r} \frac{dB_f}{dr} - B_f + \Phi_0 \delta_2(\mathbf{r}) = 0. \quad (2.17)$$

This is one kind of the modified Bessel equation ($n=0$), so the solution can be written as,

$$B_f(r) = C K_0\left(\frac{r}{\lambda}\right), \quad (2.18)$$

where C is a constant and K_0 is the modified Bessel function of the second kind ($n=0$).

Because the fluxoid has the flux quantum Φ_0 , the following equation is satisfied,

$$\Phi_0 = \int B_f(r) dS = \int_0^\infty 2\pi B_f(r) r dr = 2\pi C \int_0^\infty K_0\left(\frac{r}{\lambda}\right) r dr. \quad (2.19)$$

By applying $\lambda r' = r$ and $\lambda dr' = dr$, eq. (2.19) can be rewritten as,

$$\Phi_0 = 2\pi\lambda^2 C \int_0^\infty K_0(r') r' dr'. \quad (2.20)$$

Then substituting the differential equation concerning the modified Bessel function of the second kind,

$$\frac{d}{dx} \{x^\nu K_\nu(x)\} = -x^\nu K_{\nu-1}(x), \quad (2.21)$$

eq. (2.20) is rewritten as,

$$\Phi_0 = 2\pi\lambda^2 C [-r' K_1(r')]_0^\infty \quad (2.22)$$

Here, the function K_1 is presented as

$$K_1(r') = \left\{ \gamma + \ln\left(\frac{r'}{2}\right) \right\} + \frac{1}{2} \left(\frac{r'}{2}\right)^{-1} - \sum_{m=1}^{\infty} \frac{1}{m(m+1)} \left\{ 1 + \frac{1}{2} + \dots + \frac{1}{m} + \frac{1}{2(m+1)} \right\} \left(\frac{r'}{2}\right)^{2m+1} \quad (2.23)$$

where I_1 is the modified Bessel function of the first kind ($n=1$) and γ is the Euler's constant, $\gamma = 0.5772166 \dots$. From eq. (2.23) the following equation is obtained because the second term is dominant when r' goes to zero ($r' \rightarrow 0$),

$$\lim_{r' \rightarrow 0} (-r' K_1(r')) \simeq \lim_{r' \rightarrow 0} \left\{ -r' \frac{1}{2} \left(\frac{r'}{2}\right)^{-1} \right\} = -1. \quad (2.24)$$

On the other hand, K_1 can be approximated as follows when r' is large enough,

$$K_1(r') \simeq \sqrt{\frac{\pi}{2r'}} \exp(-r'). \quad (2.25)$$

Then the following equation is obtained,

$$\lim_{r' \rightarrow \infty} (-r' K_1(r')) = 0. \quad (2.26)$$

Substituting eq.(2.24) and (2.26) to eq.(2.22), the constant C is obtained as

$$C = \frac{\Phi_0}{2\pi\lambda^2} \frac{1}{0 - (-1)} = \frac{\Phi_0}{2\pi\lambda^2}. \quad (2.27)$$

Then, the magnetic flux density around a fluxoid $B(r)$ is expressed as

$$B_f(r) = \frac{\Phi_0}{2\pi\lambda^2} K_0\left(\frac{r}{\lambda}\right). \quad (2.28)$$

However, this equation is satisfied in the case that the radius r is greater than the coherence length, $r > \xi$. Fig.2.2 shows the distribution of the magnetic flux density around a fluxoid when it is approximated that the magnetic flux density at the center of the fluxoid, $B(0)$ is mostly equal to the magnetic flux density at radius $r = \xi$.

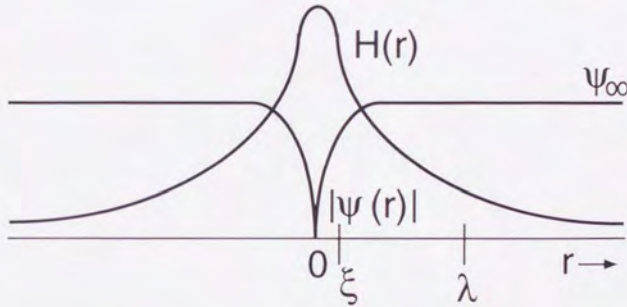


Figure 2.2: Distribution of magnetic flux density around a fluxoid

2.1.3 Current density around a fluxoid

When a fluxoid is parallel to the z -axis, the distribution of shielding current density around a fluxoid, $J_s(r)$ is expressed by using the magnetic flux density around a fluxoid, B_f , as

$$\mathbf{J}_s = J_s \mathbf{e}_\theta = \frac{1}{\mu_0} \nabla \times (B_f \mathbf{e}_z) = -\frac{1}{\mu_0} \frac{\partial B_f}{\partial r} \mathbf{e}_\theta. \quad (2.29)$$

By substituting eq.(2.28) to eq.(2.29), $J_s(r)$ can be calculated as,

$$J_s(r) = -\frac{1}{\mu_0} \frac{\Phi_0}{2\pi\lambda^2} \frac{\partial K_0\left(\frac{r}{\lambda}\right)}{\partial r} = \frac{\Phi_0}{2\mu_0\pi\lambda^3} K_1\left(\frac{r}{\lambda}\right). \quad (2.30)$$

As described above, the magnetic flux density and the shielding current density around a fluxoid can be represented using the modified Bessel functions of the second kind, K_0 and K_1 .

2.2 Ginzburg-Landau theory

2.2.1 Ginzburg-Landau free energy

In the Ginzburg-Landau (GL) theory, the superconducting electrons density, n_s , is given as the square of the complex function $\psi(\mathbf{r})$ as

$$n_s = |\psi(\mathbf{r})|^2. \quad (2.31)$$

This function $\psi(\mathbf{r})$ is called the order parameter and is similar to the wave function in the quantum theory.

Generally, the free energy density of superconducting state, ϵ_s , depends on the superconducting electrons density, n_s , and then ϵ_s is given as the function of n_s . In GL theory, it is considered that ϵ_s can be expanded with $|\psi|^2$ as,

$$\epsilon_s = \text{const.} + \alpha|\psi|^2 + \frac{\beta}{2}|\psi|^4 + \dots, \quad (2.32)$$

where α and β are unknown coefficients.

On the other hand, when the magnetic field exists, the order parameter ψ can vary in space. In such a case, the expectation of the kinetic energy density is derived from the quantum theory as,

$$U_k = \frac{1}{2m^*} \left| \left(\frac{\hbar}{i} \nabla + e^* \mathbf{A} \right) \psi \right|^2, \quad (2.33)$$

where m^* and $-e^*$ are the mass and the electrical charge of a Cooper pair, and \mathbf{A} is the magnetic vector potential. Furthermore, the magnetic energy is given as,

$$U_m = \frac{B^2}{2\mu_0} \quad (2.34)$$

where B is the magnetic flux density and μ_0 is the magnetic permeability in vacuum. From eqs. (2.32), (2.33) and (2.34), the free energy density of the superconducting state can be written as

$$\epsilon_s = \epsilon_{n0} + \alpha|\psi|^2 + \frac{\beta}{2}|\psi|^4 + \frac{1}{2m^*} \left| \left(\frac{\hbar}{i} \nabla + e^* \mathbf{A} \right) \psi \right|^2 + \frac{B^2}{2\mu_0}, \quad (2.35)$$

where ϵ_{n0} is the free energy density of the normal conducting state in the case $B = 0$.

2.2.2 Determination of coefficient α and β

We consider such a case that there is no gradient of superconducting electrons density ($\nabla|\psi|^2 = 0$), and there is no magnetic field ($\mathbf{B} = 0$), so that the vector potential \mathbf{A} can be zero without the loss of generality. In such a case, the free energy density of superconducting state can be rewritten as

$$\varepsilon_s - \varepsilon_{n0} = \alpha|\psi|^2 + \frac{\beta}{2}|\psi|^4 = \frac{\beta}{2} \left(|\psi|^2 + \frac{\alpha}{\beta} \right)^2 - \frac{\alpha^2}{2\beta}. \quad (2.36)$$

When the temperature is lower than the critical temperature ($T < T_c$), the energy $\varepsilon_s - \varepsilon_n$ has the minimum value less than 0 realizing the superconducting state (see Fig.2.3). And the superconducting electron density which gives the minimum $\varepsilon_s - \varepsilon_{n0}$ must be $|\psi|^2 > 0$. From such conditions, the following equations are obtained,

$$|\psi|^2 = |\psi_\infty|^2 = -\frac{\alpha}{\beta} > 0, \quad (2.37)$$

$$\varepsilon_s - \varepsilon_{n0} = -\frac{\alpha^2}{2\beta} < 0, \quad (2.38)$$

where ψ_∞ is the order parameter at the fully superconducting region where the magnetic field is shielded completely and there is no gradient of the order parameters. From eqs. (2.37) and (2.38), the followings are derived,

$$\alpha < 0, \quad \beta > 0. \quad (2.39)$$

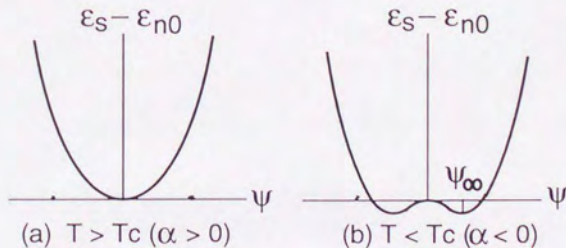


Fig. 2.3: Function $\varepsilon_s - \varepsilon_{n0}$ in the cases (a) $T > T_c$ and (b) $T < T_c$

On the other hand, the free energy density without the magnetic flux density is equal to the Gibbs's free energy density, eq. (2.38) can be rewritten as,

$$\varepsilon_s - \varepsilon_{n0} = g_s|_{B=0} - g_n|_{B=0} = -\frac{\mu_0 H_c^2}{2}, \quad (2.40)$$

where g_s and g_n are the Gibbs's free energy density in the superconducting and the normal conducting state, respectively. H_c is the thermodynamical critical magnetic field.

Furhtermore, from London theory, the magnetic penetration depth, λ is given as eq. (2.10) by using n_s , the following equation is derived,

$$|\psi_\infty|^2 = n_s = \frac{m^*}{\mu_0 e^* \lambda^2}. \quad (2.41)$$

By solving the simultaneous equations, eqs. (2.37), (2.38), (2.39), (2.40) and (2.41), the coefficients α and β are obtained as,

$$\alpha = -\frac{e^{*2} \mu_0^2 H_c^2 \lambda^2}{m^*}, \quad (2.42)$$

$$\beta = \frac{e^{*4} \mu_0^3 H_c^2 \lambda^4}{m^{*2}}. \quad (2.43)$$

2.2.3 Ginzburg-Landau equations

The free energy of the superconducting state, E_s is expressed as the volume integral of eq.(2.32),

$$\begin{aligned} E_s &= \int_v \varepsilon_s \, dv \\ &= \int_v \left[\varepsilon_{n0} + \alpha |\psi|^2 + \frac{\beta}{2} |\psi|^4 + \frac{1}{2m^*} \left| \left(\frac{\hbar}{i} \nabla + e^* \mathbf{A} \right) \psi \right|^2 + \frac{(\nabla \times \mathbf{A})^2}{2\mu_0} \right] dv. \end{aligned} \quad (2.44)$$

The functions $\psi(\mathbf{r})$ and $\mathbf{A}(\mathbf{r})$ are given so that the free energy E_s becomes minimum.

Here, the variation of E_s is written as follows (see Appendix A),

$$\begin{aligned} \delta E_s &= \int_v \left[\left\{ \alpha \psi + \beta |\psi|^2 \psi + \frac{1}{2m^*} \left(\frac{\hbar}{i} \nabla + e^* \mathbf{A} \right)^2 \psi \right\} \delta \psi^* + \{C.C.\} \delta \psi \right. \\ &\quad + \left. \left\{ \frac{1}{2m^*} \left(\frac{\hbar e^*}{i} (\psi^* \nabla \psi - \psi \nabla \psi^*) + 2e^{*2} \mathbf{A} |\psi|^2 \right) + \frac{1}{\mu_0} (\nabla \times \nabla \times \mathbf{A}) \right\} \delta \mathbf{A} \right] dv \\ &\quad + \int_S \left[\frac{1}{2m^*} \left\{ -\frac{\hbar}{i} \delta \psi^* \left(\frac{\hbar}{i} \nabla \psi + e^* \mathbf{A} \psi \right) + (C.C.) \right\} + \frac{1}{\mu_0} \delta \mathbf{A} \times (\nabla \times \mathbf{A}) \right] dS, \end{aligned} \quad (2.45)$$

where ψ^* is the complex conjugated order parameter. Here, by selecting the $\delta\psi$, $\delta\psi^*$ and $\delta\mathbf{A}$ which becomes 0 at the surface of the superconductor, the following equations are derived from the condition that $\delta E_s = 0$,

$$\alpha\psi + \beta|\psi|^2\psi + \frac{1}{2m^*} \left(\frac{\hbar}{i} \nabla + e^* \mathbf{A} \right)^2 \psi = 0, \quad (2.46)$$

$$\mathbf{j} = -\frac{\hbar e^*}{2m^* i} (\psi^* \nabla \psi - \psi \nabla \psi^*) - \frac{e^{*2} \mathbf{A}}{m^*} |\psi|^2, \quad (2.47)$$

where

$$\mathbf{j} = \frac{1}{\mu_0} \nabla \times \nabla \times \mathbf{A}. \quad (2.48)$$

Equation (2.47) corresponds to the equation of current density in the quantum mechanics and (2.48) corresponds to the Ampere's law.

Equations (2.46) and (2.47) are called the Ginzburg-Landau equations.

2.2.4 Ginzburg-Landau parameter

In the case of zero magnetic field, the magnetic vector potential \mathbf{A} can be selected as $\mathbf{A} = 0$, and eq.(2.46) can be expressed as

$$\alpha\psi + \beta|\psi|^2\psi - \frac{\hbar^2}{2m^*} \nabla^2 \psi = 0, \quad (2.49)$$

where ψ can be a real function. By assuming that ψ changes only in x-direction and by substituting the normalized order parameter,

$$\Psi = \frac{\psi}{|\psi_\infty|}, \quad (2.50)$$

eq. (2.49) is written as

$$\frac{\hbar}{2m^* |\alpha|} \frac{d^2 \Psi}{dx^2} + \Psi - |\Psi|^2 \Psi = 0. \quad (2.51)$$

Considering that order parameter change f is little enough ($\Psi = 1 - f$), eq.(2.51) is written,

$$\frac{\hbar}{2m^* |\alpha|} \frac{d^2 f}{dx^2} - 2f = 0. \quad (2.52)$$

The solution of eq. (2.52) is given as

$$f \sim \exp\left(-\frac{\sqrt{2}|x|}{\xi}\right), \quad (2.53)$$

where $\xi = \hbar/(2m^*|\alpha|)^{1/2}$. Then the order parameter changes in the space within the length ξ and this length is called the coherence length. By substituting eq. (2.42), ξ is written as following,

$$\xi = \frac{\hbar}{(2m^*|\alpha|)^{1/2}} = \frac{\hbar}{\sqrt{2}e^*\mu_0 H_c \lambda} \quad (2.54)$$

2.2.5 Quantization of magnetic flux

Assuming that the order parameter is expressed by the phase θ as

$$\psi = |\psi| \exp(-i\theta), \quad (2.55)$$

eq. (2.47) is transformed as

$$\mathbf{j} = \frac{e^*\hbar}{m^*} |\psi|^2 \nabla\theta - \frac{e^{*2}}{m^*} |\psi|^2 \mathbf{A}. \quad (2.56)$$

Now, we consider the closed loop C in the superconductor and assume that it is so large enough that the magnetic flux density is zero ($B = 0$) and the current density is zero ($j = 0$) along the loop C . Then \mathbf{A} on C is written from eq. (2.56) as followings,

$$\mathbf{A} = \frac{\hbar}{e^*} \nabla\theta. \quad (2.57)$$

The linear integration of \mathbf{A} on C gives the flux enclosed by C ,

$$\oint_C \mathbf{A} \cdot d\boldsymbol{\ell} = \int \nabla \times \mathbf{A} \cdot d\mathbf{S} = \Phi = \int \mathbf{B} \cdot d\mathbf{S} = \Phi. \quad (2.58)$$

By substituting eq.(2.57) to (2.58), Φ is written as

$$\Phi = \frac{\hbar}{e^*} \int_C \nabla\theta \cdot d\boldsymbol{\ell} = \frac{\hbar}{e^*} \Delta\theta, \quad (2.59)$$

where $\Delta\theta$ is the gain of phase after making one round of C . Therefore, $\Delta\theta$ must be integral multiples of 2π , and the following equation is derived.

$$\Phi = \frac{\hbar}{e^*} \cdot 2\pi n = n\Phi_0, \quad (n \in Z) \quad (2.60)$$

where Φ_0 is the minimum unit of the magnetic flux given by

$$\Phi_0 = \frac{h}{e^*}. \quad (2.61)$$

Φ_0 is called the quantized flux. Then the Ginzburg-Landau theory shows that the magnetic flux can exist as the quantized flux in the type-II superconductor.

2.2.6 Upper critical field in bulk, H_{c2}

It is assumed that the external magnetic field is near the upper critical magnetic field, $H \simeq H_{c2}$. In such a case, the order parameter is $|\psi| \ll |\psi_\infty|$. Then the second term of eq. (2.46) is neglected and the following linearized GL equation is obtained,

$$\left(\frac{\nabla}{i} + \frac{2\pi A}{\Phi_0} \right)^2 \psi = -\frac{2m^* \alpha}{\hbar^2} = \frac{1}{\xi^2} \psi. \quad (2.62)$$

Here, we assumed that the magnetic field H is parallel to z -axis, and select the gauge condition as,

$$A = (A_x, A_y, A_z) = (0, \mu_0 H x, 0). \quad (2.63)$$

Substituting eq. (2.63) to eq. (2.62), the following equation is derived,

$$\left[-\nabla^2 - \frac{4\pi i}{\Phi_0} \mu_0 H x \frac{\partial}{\partial x} + \left(\frac{2\pi \mu_0 H}{\Phi_0} \right)^2 x^2 \right] \psi = \frac{1}{\xi^2} \psi \quad (2.64)$$

Here, we assume that ψ is written as

$$\psi(x, y, z) = e^{ik_y y} e^{ik_z z} f(x). \quad (2.65)$$

Substituting eq. (2.65) to eq. (2.64), the equation concerning $f(x)$ is derived,

$$-\frac{d^2 f(x)}{dx^2} + \left(\frac{2\pi \mu_0 H}{\Phi_0} \right)^2 (x - x_0)^2 f(x) = \left(\frac{1}{\xi^2} - k_z^2 \right) f(x), \quad (2.66)$$

where

$$x_0 = -\frac{k_y \Phi_0}{2\pi \mu_0 H}. \quad (2.67)$$

Equation (2.66) is equal to the Schrödinger equation of a harmonic oscillator having force constant $(2\pi \hbar \mu_0 H / \Phi_0)^2 / m^*$. Therefore the eigen value of this harmonic oscillator is given

as,

$$\epsilon_n = \left(n + \frac{1}{2}\right) \hbar \omega_c = \left(n + \frac{1}{2}\right) \hbar \left(\frac{2\pi \hbar \mu_0 H}{m^* \Phi_0}\right) = \frac{\hbar^2}{2m^*} \left(\frac{1}{\xi^2} - k_z^2\right), \quad (n \in \mathcal{Z}) \quad (2.68)$$

and the magnetic field H is written as

$$H = \frac{\Phi_0}{2\pi \mu_0 (2n + 1)} \left(\frac{1}{\xi^2} - k_z^2\right). \quad (2.69)$$

When the magnetic field is decreasing, the maximum magnetic field in which the superconducting core can be driven, H_{c2} , is defined as the maximum value of H in eq. (2.69).

This is the upper critical magnetic field H_{c2} and is given in the case that $k_z = 0$ and $n = 0$ as

$$H_{c2} = \frac{\Phi_0}{2\pi \mu_0 \xi^2}. \quad (2.70)$$

Furthermore, the eigen function $f(x)$ is obtained as,

$$f(x) = \exp \left[-\frac{(x - x_0)^2}{2\xi^2} \right]. \quad (2.71)$$

From eq. (2.54), the thermodynamical critical magnetic field H_c is expressed as

$$H_c = \frac{\hbar}{\sqrt{2} e^* \mu_0 \xi \lambda} \quad (2.72)$$

By defining the Ginzburg-Landau parameter as

$$\kappa = \frac{\lambda}{\xi}, \quad (2.73)$$

the relation between H_c and H_{c2} is obtained as,

$$H_{c2} = \sqrt{2} \kappa H_c. \quad (2.74)$$

Therefore, in the case $\kappa < 1/\sqrt{2}$, the superconductor is the type-I superconductor because $H_{c2} < H_c$. On the other hand, in the case $\kappa > 1/\sqrt{2}$, it is the type-II superconductor because $H_c < H_{c2}$.

$$\begin{cases} \kappa < 1/\sqrt{2} & H_c > H_{c2} : \text{type I} \\ \kappa > 1/\sqrt{2} & H_c < H_{c2} : \text{type II} \end{cases} \quad (2.75)$$

2.2.7 Abrikosov's lattice in type II superconductor

When the applied magnetic field is parallel to z -axis, $\mathbf{H}_{ez} \parallel \hat{z}$, the order parameter ψ can be written in the same manner as eq.(2.65),

$$\psi(x, y) = e^{-ik_y y} \psi'(x). \quad (2.76)$$

And by assuming that $H_{ez} \simeq H_{c2}$, the constant x_0 in eq.(2.67) can be rewritten as,

$$x_0 = \frac{k_y \Phi_0}{2\pi\mu_0 H_{ez}} \simeq \frac{k_y \Phi_0}{2\pi\mu_0 H_{c2}} = \frac{k_y \Phi_0}{2\pi\mu_0} \left(\frac{\Phi_0}{2\pi\mu_0 \xi^2} \right)^{-1} = k_y \xi^2. \quad (2.77)$$

Substituting eqs.(2.76) and (2.77) to eq.(2.66), the following equation is obtained concerning ψ' ,

$$-\xi^2 \frac{d^2 \psi'}{dx^2} + \left[\left(\frac{x}{\xi} - k_y \xi \right)^2 - 1 \right] \psi' = 0. \quad (2.78)$$

The solution of this equation is given as

$$\psi'(x) \sim \exp \left[-\frac{1}{2} \left(\frac{x}{\xi} - k_y \xi \right)^2 \right]. \quad (2.79)$$

Because k_y is the arbitrary constant, $\psi(x, y)$ can be written from eqs.(2.76) and (2.79) as,

$$\psi(x, y) = \sum_n C_n e^{-in k_y y} \exp \left[-\frac{1}{2} \left(\frac{x}{\xi} - n k_y \xi \right)^2 \right]. \quad (2.80)$$

By choosing the constant $C_{2m} = C_0$ and $C_{2m+1} = iC_0$, the superconducting electrons density $|\psi|^2$ is calculated as [27],

$$|\psi|^2 = |C_0|^2 3^{-1/4} \left[1 + 2 \exp \left(-\frac{\pi}{\sqrt{3}} \right) \left[\cos \left\{ \frac{2\pi}{a_f} \left(\frac{2}{\sqrt{3}} x \right) \right\} + \cos \left\{ \frac{2\pi}{a_f} \left(\frac{x}{\sqrt{3}} - y \right) \right\} - \cos \left\{ \frac{2\pi}{a_f} \left(\frac{x}{\sqrt{3}} + y \right) \right\} \right] \right], \quad (2.81)$$

where $a_f = 2\pi/k$. Because $2 \exp \left(-\frac{\pi}{\sqrt{3}} \right) \simeq 0.326 \simeq 1/3$, this $|\psi|^2$ becomes 0 at the locations,

$$(x, y) = \left(\sqrt{3} \left(p \pm \frac{1}{4} \right) a_f, \left(q \mp \frac{1}{4} \right) a_f \right). \quad (p, n \in N) \quad (2.82)$$

Then it is found that the triangle lattice is constructed as shown in Fig.2.4. This is called Abrikosov's triangle lattice[28].

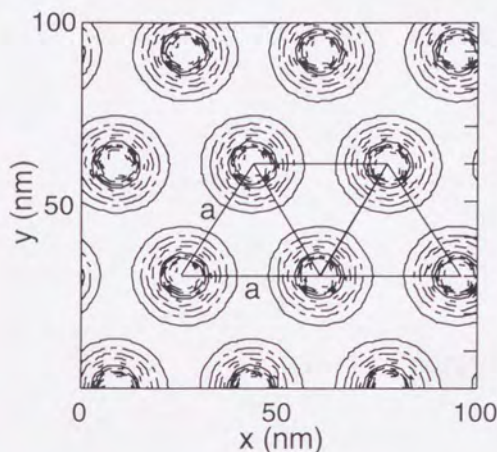


图 2.4: Abrikosov's triangle lattice

2.2.8 Upper critical field near the surface, H_{c3}

The upper critical magnetic field, H_{c2} in section 2.1.6 is realized in the superconductor bulk. Near the surface of the superconductor, however, different property can be expected.

The boundary condition at the surface of the superconductor is represented as follows,

$$\mathbf{p} \cdot \mathbf{n} = \left(\frac{\nabla}{i} + \frac{2\pi\mathbf{A}}{\Phi_0} \right) \psi \Big|_{\mathbf{n}} = 0, \quad (2.83)$$

where \mathbf{p} is the momentum of the Cooper pair. For the magnetic field which is perpendicular to the surface, $\mathbf{H}_{ex} \parallel \hat{z}$, eq.(2.83) is satisfied by choosing $k_z = 0$ in eq.(2.65), because $\mathbf{A} \parallel \hat{y}$ and $\hat{y} \perp \mathbf{n}$.

Then, we consider that $x \geq 0$ gives the semi-infinitely large superconductor and the magnetic field is applied parallel to the surface, $\mathbf{H}_{ex} \parallel \hat{z}$. The vector potential can be

chosen as expressed in eq.(2.63) too, and eq.(2.83) is rewritten as,

$$\left. \frac{\partial \psi}{\partial x} \right|_{x=0} = 0. \quad (2.84)$$

From this boundary condition and eq.(2.71), the order parameter can be assumed to be represented as follows,

$$\psi = e^{ik_y y} f(x) = e^{-ax^2} e^{ik_y y}, \quad (2.85)$$

where a is a constant. This function ψ gives the symmetrical order parameter and the reflected image is extended to the outside of the superconductor as shown in Fig.2.5.

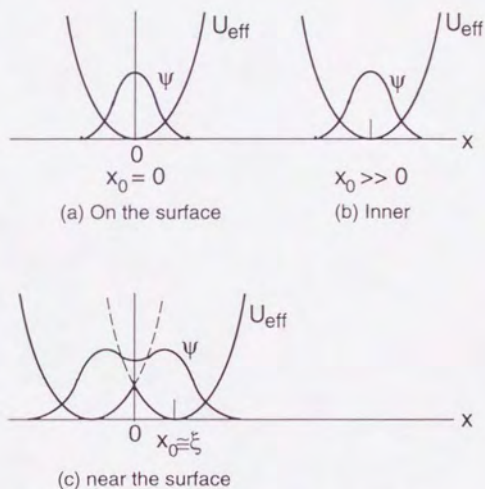


图 2.5: Distribution of order parameter of type-II superconductor

The approximated Gibbs's free energy per unit length is given as

$$G - G_n = \frac{\hbar^2}{2m^*} \int_0^\infty \left[-\frac{1}{\xi} |\psi|^2 + \left| \left(\frac{\nabla}{i} - \frac{2\pi}{\Phi_0} \mathbf{A} \right) \psi \right|^2 \right] dx, \quad (2.86)$$

where G_n is the Gibbs's free energy per unit length in the normal conducting state.

Substituting eq.(2.85) to eq.(2.86), the following equation is obtained,

$$G - G_n = \frac{\hbar^2}{4m^*} \left[\left(\frac{\pi}{2a} \right)^{1/2} \left(k_y^2 - \frac{1}{\xi^2} \right) - 2 \frac{\pi \mu_0 H_{cz}}{\Phi_0 a} k_y + \left(\frac{\pi}{2a^3} \right)^{1/2} \left(a^2 + \left(\frac{\pi \mu_0 H_{cz}}{\Phi_0} \right)^2 \right) \right]. \quad (2.87)$$

From this equation, k_y which minimizes G is given as,

$$k_y = \left(\frac{2}{\pi a} \right)^{1/2} \frac{\pi \mu_0 H_{cz}}{\Phi_0}. \quad (2.88)$$

Substituting eq.(2.88), eq.(2.87) is transformed as,

$$G' - G_n = \frac{\hbar^2}{4m^*} \left(\frac{\pi}{2} \right)^{1/2} \left[a^{1/2} - \frac{1}{\xi^2} a^{-1/2} + \left(\frac{\pi \mu_0 H_{cz}}{\Phi_0} \right)^2 \left(1 - \frac{2}{\pi} \right) a^{-3/2} \right]. \quad (2.89)$$

Furthermore, from the following condition,

$$\frac{\partial G'}{\partial a} = 0, \quad G'(a) - G_n = 0, \quad (2.90)$$

the constant a and the magnetic field H_{c3} are calculated as,

$$a = \frac{1}{2\xi^2}, \quad (2.91)$$

$$H_{c3} = \frac{\Phi_0}{2\pi\mu_0\xi^2} \sqrt{\frac{\pi}{\pi-2}} = H_{c2} \sqrt{\frac{\pi}{\pi-2}} \simeq 1.66H_{c2}. \quad (2.92)$$

The more accurate value of H_{c3} was calculated by Saint-James and de Gennes[29] as

$$H_{c3} = 1.695H_{c2}. \quad (2.93)$$

As mentioned above, in the magnetic field which is parallel to the surface of the superconductor, the generation of fluxoids begins in the 70% higher magnetic field than H_{c2} .

2.2.9 Time-dependent Ginzburg-Landau equations (TDGL eqs.)

The time-dependent Ginzburg-Landau equations were suggested derived by Gor'kov and Eliashberg[30]-[33]. The TDGL equations are expressed as,

$$\frac{1}{D} \left(\frac{\partial}{\partial t} + i \frac{e^* \phi}{\hbar} \right) \Delta = - \left(\frac{\nabla}{i} + \frac{e^* \mathbf{A}}{\hbar} \right)^2 \Delta - \frac{1}{\xi^2} (|\Delta|^2 - 1) \Delta, \quad (2.94)$$

$$\sigma \left(\frac{\partial \mathbf{A}}{\partial t} + \nabla \phi \right) = Re \left(\Delta^* \left(\frac{\nabla}{i} + \frac{e^* \mathbf{A}}{\hbar} \right) \Delta \right) \frac{\hbar}{\mu_0 e^* \lambda^2} - \frac{\nabla \times \nabla \times \mathbf{A}}{\mu_0}, \quad (2.95)$$

where D is the diffusion coefficient of the Cooper pairs in normal conducting state, σ is the conductivity in normal conducting state, and ϕ is the electric scalar potential. Δ is the order parameter, which is normalized by the equilibrium value in zero field,

$$\Delta_0 = \pi k_B [2(T_c^2 - T^2)]^{\frac{1}{2}}, \quad (2.96)$$

where T_c is the critical temperature and k_B is the Boltzmann constant. ξ is the coherence length and it is represented by

$$\xi = \frac{\hbar}{\phi_0} \sqrt{\frac{6D}{\tau_s}}, \quad (2.97)$$

where τ is the scattering time of spin flop,

$$\tau_s = \frac{\pi \hbar}{8k_B(T_c - T)}. \quad (2.98)$$

λ is the magnetic penetration depth, represented by

$$\lambda = \frac{\hbar}{\sqrt{8\pi\sigma\tau_s\Delta_0}}. \quad (2.99)$$

Equations (2.94) and (2.95) are called the time-dependent Ginzburg-Landau equations.

Next, in order to eliminate the scalar potential, ϕ , the modified vector potential method[34] was applied to (2.94) and (2.95). By this method, the modified vector potential and scalar potential, $\tilde{\mathbf{A}}$ and $\tilde{\phi}$ can be introduced as:

$$\tilde{\mathbf{A}} = \mathbf{A} - \nabla\chi, \quad (2.100)$$

$$\tilde{\phi} = \phi + \frac{\partial\chi}{\partial t} = 0. \quad (2.101)$$

According to these gauge transformation, the order parameter $\tilde{\Delta}$ can be rewritten as follows,

$$\tilde{\Delta} = \Delta \exp\left(i\frac{2\pi}{\Phi_0}\chi\right) = \Delta \exp\left(i\frac{e^*}{\hbar}\chi\right), \quad (2.102)$$

where Φ_0 is the magnetic flux quantum. By substituting (2.101) and (2.102) to (2.94) and (2.95), the following equations can be obtained,

$$\frac{1}{D} \frac{\partial \tilde{\Delta}}{\partial t} = -\left(\frac{\nabla}{i} + \frac{e^*}{\hbar} \tilde{\mathbf{A}}\right)^2 \tilde{\Delta} - \frac{1}{\xi^2} (|\tilde{\Delta}|^2 - 1) \tilde{\Delta}, \quad (2.103)$$

$$\sigma \frac{\partial \tilde{\mathbf{A}}}{\partial t} = \Re \left[\tilde{\Delta}^* \left(\frac{\nabla}{i} + \frac{e^*}{\hbar} \tilde{\mathbf{A}} \right) \tilde{\Delta} \right] \frac{\hbar}{\mu_0 e^* \lambda^2} - \frac{\nabla \times \nabla \times \tilde{\mathbf{A}}}{\mu_0}. \quad (2.104)$$

Here, the following dimensionless variables and operator are defined [35]-[42],

$$\tau = t/\tau_s, \quad (2.105)$$

$$\mathbf{b} = \frac{1}{\mu_0 H_{c2}} \mathbf{B}, \quad (2.106)$$

$$\mathbf{a} = \frac{1}{\mu_0 \xi H_{c2}} \tilde{\mathbf{A}} = \frac{e^* \xi}{\mu_0 \hbar} \tilde{\mathbf{A}}, \quad (2.107)$$

$$\nabla' = \xi \nabla. \quad (2.108)$$

By substituting (2.105)–(2.108) to (2.103) and (2.104), the following dimensionless TDGL equations can be derived:

$$\frac{\partial \tilde{\Delta}}{\partial \tau} = -\frac{1}{12} \left[\left[\frac{\nabla'}{i} + \mathbf{a} \right]^2 \tilde{\Delta} + (|\tilde{\Delta}|^2 - 1) \tilde{\Delta} \right], \quad (2.109)$$

$$\frac{\partial \mathbf{a}}{\partial \tau} = \Re \left[\tilde{\Delta}^* \left(\frac{\nabla'}{i} + \mathbf{a} \right) \tilde{\Delta} \right] - \kappa^2 \nabla' \times \nabla' \times \mathbf{a}, \quad (2.110)$$

where κ denotes the Ginzburg-Landau parameter, $\kappa = \lambda/\xi$.

2.2.10 Insulating boundary condition

As a boundary condition for the surface of the superconductor, the insulating boundary condition is adopted. It is represented as

$$\mathbf{p} \cdot \mathbf{n} = \left(\frac{\nabla'}{i} + \frac{e^*}{\hbar} \tilde{\mathbf{a}} \right) \tilde{\Delta} \cdot \mathbf{n} = 0, \quad (2.111)$$

where \mathbf{p} and \mathbf{n} are the momentum of a Cooper pair and the unit vector normal to the boundary. This equation means that the Cooper pair does not go through the surface of the superconductor.

2.3 Mixed state of superconductor

The Lorentz force is expressed as $F_L = J \times B$. When the current density J exceeds a critical value and the Lorentz force acting on a fluxoid in the type-II superconductor becomes larger than the pinning force, the fluxoid can be released from the pinning center and move around. This critical value of the current density is called the critical current density, J_c . Then the fluxoid is trapped by another pinning center and the new constant magnetic field distribution is formed. Therefore, the magnetic field distribution can be assumed to be determined from the condition that the Lorentz force is equal to the pinning force. The critical state model modifies the electromagnetic phenomenon of the type-II superconductor based on this assumption.

2.3.1 Critical state models

If the magnetic flux density B and the current density J are perpendicular to each other in the superconductor, $F_L = JB$. Because the pinning force F_p is equal to the Lorentz force due to the critical current density, $F_L = J_c B$ according to the critical state model, the critical current density is represented as,

$$J_c = \frac{F_p(B)}{B}. \quad (2.112)$$

Concerning F_p in eq. (2.112), some models have been proposed. Here, we introduce three models, the Bean model, the Kim model and the Yasukochi model.

1. Bean model[7]

The critical current density J is assumed to have a constant value,

$$J_c = J_{c0}, \quad (2.113)$$

where J_{c0} is a constant. In this model it is assumed that $F_p(B)$ is proportional to B .

2. Kim model [8]

Kim et al. proposed an empirical relation, which fits to many experimental results,

$$J_c = \frac{J'_{c0}}{B + B_0}, \quad (2.114)$$

where B_0 and J'_{c0} are constants. The equation corresponds to Bean model when $B \ll B_0$. And it means that $F_p = \text{const.}$ when $B \gg B_0$.

3. Yasukochi model [9]

In this model, the dependence of J_c on B is expressed as

$$J_c = \frac{J''_{c0}}{\sqrt{B}}, \quad (2.115)$$

where J''_{c0} is the critical current density when $B = 1$ T.

In Fig.2.6, the J_c - B relation for these three models are depicted.

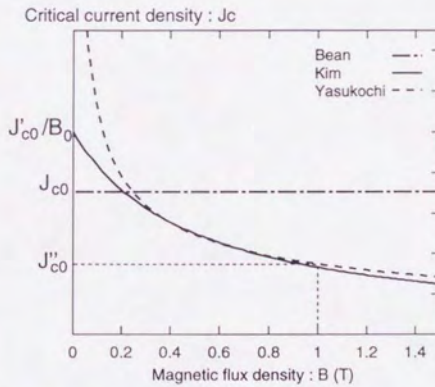


Figure 2.6: Conceptual drawing of J_c - B relation by Critical State models

2.3.2 E-J constitutive relation

When the fluxoids moves in the magnetic flux density B , with velocity v , the following speed electromotive force E is yielded,

$$E = B \times v. \quad (2.116)$$

When the fluxoids moves in the type II superconductor, the kinetic equation is given as

$$\eta_f \mathbf{v} = \mathbf{J} \times \mathbf{B} - \mathbf{F}_p, \quad (2.117)$$

where η_f is the viscous coefficient for a fluxoid, \mathbf{J} is the shielding current density and \mathbf{F}_p is the pinning force. The critical current density J_c is defined as the maximum current density which does not cause the fluxoids' movement. By substituting $\mathbf{v} = \mathbf{0}$ into eq. (2.117), J_c is given as

$$J_c = \frac{F_p}{B}. \quad (2.118)$$

By substituting eq.(2.118) to eq.(2.116), the electric field is obtained as

$$\mathbf{E} = \frac{B^2}{\eta_f} (\mathbf{J} - \mathbf{J}_c) = \rho_f (\mathbf{J} - \mathbf{J}_c), \quad (2.119)$$

where ρ_f is the flux flow resistivity. From eq. (2.119), the relation between E and J is shown in Fig. 2.7.

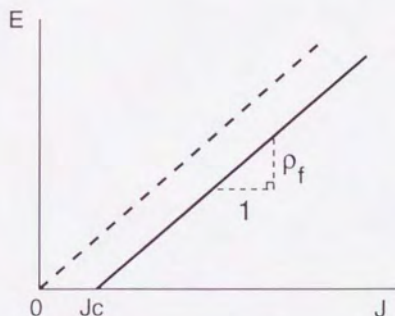


Figure 2.7: Relation between E and J

2.3.3 Flux Flow resistivity

When a fluxoid moves, the fluxoid motion in the type-II superconductor causes ohmic energy loss, because of the normal conducting electrons flow inside and outside the flux-

oid. Accordingly, a corresponding electric resistivity can be measured. Next, the flow resistivity will be determined.

The power loss inside the normal conducting core of the fluxoid, per unit length, is written as

$$W_1 = \pi \xi^2 \frac{\mu_0^2 H_{c2}^2 v^2}{\rho_n} \left(1 + \frac{B}{2\mu_0 H_{c2}} \right)^2, \quad (2.120)$$

where v is the velocity of the fluxoid and ρ_n is the normal conducting resistivity.

Outside of the normal conducting core, the power loss per unit length is

$$\begin{aligned} W_2 &= 2\pi \int_{\xi}^{R_0} \frac{r dr}{\rho_n} \left[\left(\frac{\Phi_0 v}{2\pi} \right) \frac{1}{r^4} + \left(\frac{Bv}{2} \right)^2 \right] \\ &= \frac{\pi R_0^2 \mu_0 H_{c2} B}{2\rho_n} \left(1 - \frac{B^2}{4\mu_0^2 H_{c2}^2} \right) v^2. \end{aligned} \quad (2.121)$$

The equivalent power loss can be expressed as a function of an equivalent resistance ρ_f as follows;

$$W_3 = \frac{\pi R_0^2 B^2 v^2}{\rho_f}. \quad (2.122)$$

By assuming that the equivalent power loss is equal to the whole power loss $W_1 + W_2$, the equivalent resistivity ρ_f can be written,

$$\rho_f = \frac{B}{\mu_0 H_{c2}} \left(1 + \frac{B}{2\mu_0 H_{c2}} \right)^{-1} \rho_n. \quad (2.123)$$

When the distance between each fluxoid is large enough, then $B \ll \mu_0 H_{c2}$, and this equation becomes

$$\rho_f = \frac{B}{\mu_0 H_{c2}} \rho_n. \quad (2.124)$$

corresponding to the well known experimental results. This formulation is called the Bardeen-Stephen model[43].

Chapter 3

Development of Fluoxid Dynamics Method and Simulation Codes

3.1 Numerical Simulation method for GL equations

3.1.1 Ginzburg-Landau equations of an isolated fluxoid

If the induced magnetic field in a type-II superconductor is just slightly higher than the lower critical magnetic field, H_{c1} , only a few numbers of fluxoids exist in the superconductor. It follows that the distance between fluxoids is enough large as compared to the coherence length ξ , to consider that each fluxoid is isolated, and to neglect its interactions with any other fluxoids (see Fig.3.1). Then the axial symmetry is satisfied for a fluxoid, regarding the distribution of the order parameter and of the magnetic flux density.

Next, the Ginzburg-Landau simulation concerning an isolated fluxoid will be presented.

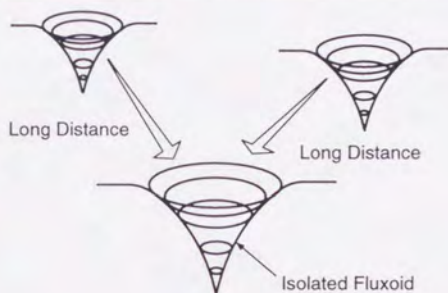


Figure 3.1: Each isolated fluxoid

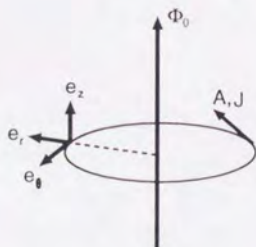


Figure 3.2: Axial symmetry and uniformity in z-direction of a fluxoid

By assuming axial symmetry around z axis and the uniformity in z direction (see Fig.3.2), the following equations are obtained.

$$\begin{cases} \psi = |\psi_\infty| f(r) e^{i\theta}, \\ \mathbf{A} = A(r) \mathbf{e}_\theta, \\ \mathbf{J} = J(r) \mathbf{e}_\theta. \end{cases} \quad (3.1)$$

where $f(r)$ is the order parameter normalized by $|\psi_\infty|$ and $f(r)$ becomes 1 in the superconducting region.

If we substitute eq.(3.1) in eqs.(2.46) and (2.47), the GL equations for an isolated fluxoid are obtained as

$$f - f^3 - \xi^2 \left[\left(\frac{1}{r} - \frac{2\pi A}{\Phi_0} \right)^2 f - \frac{1}{r} \frac{d}{dr} \left(r \frac{df}{dr} \right) \right] = 0, \quad (3.2)$$

$$J = \frac{e^* \hbar}{m^*} |\psi_\infty|^2 \left(\frac{1}{r} - \frac{2\pi A}{\Phi_0} \right) f^2, \quad (3.3)$$

$$\mu_0 J = -\frac{1}{r} \frac{dA}{dr} + \frac{A^2}{r^2} - \frac{dA^2}{dr^2} \quad (3.4)$$

where Φ_0 is the flux quantum, $\Phi_0 = h/e^*$.

At the center of the fluxoid, the order parameter equals zero because the superconducting electrons density is zero. Also, both the vector potential $A(r)$ and the current density $J(r)$ become zero, due to the axis symmetry. On the other hand, at $r \gg \lambda$, $f(r)$ equals one because the normalized superconducting electron density is one. Because the flux enclosed by the circle of radius r is the flux quantum, for $r \gg \lambda$ we can write also

$$\Phi_0 = \int B \cdot dS = \oint \mathbf{A} \cdot d\mathbf{l} = 2\pi r A(r). \quad (3.5)$$

Then, the boundary conditions for $f(r)$, $A(r)$ and $J(r)$ are represented by,

$$(r=0) \begin{cases} f = 0 \\ A = 0 \\ J = 0 \end{cases}, \quad (r \gg 3\lambda) \begin{cases} f = 1 \\ A = \frac{\Phi_0}{2\pi r} \\ J = 0 \end{cases} \quad (3.6)$$

3.1.2 Discretized 1-dimensional GL equations

The 1-dimensional GL eqs. (3.2), (3.3) and (3.4) can be discretized in the region where radius is $0 \leq r \leq R$ by using the finite difference method,

$$f_i - f_i^3 - \xi^2 \left[\left(\frac{1}{r_i} - \frac{2\pi A_i}{\Phi_0} \right)^2 f_i - \frac{1}{r_i} \frac{f_{i+1} - f_{i-1}}{2\Delta r} - \frac{f_{i+1} + f_{i-1} - 2f_i}{(\Delta r)^2} \right] = 0 \quad (3.7)$$

$$J_i = \frac{e^* \hbar}{m^*} |\psi_\infty|^2 f_i^2 \left(\frac{1}{r_i} - \frac{2\pi A_i}{\Phi_0} \right) \quad (3.8)$$

$$\mu_0 J_i = -\frac{1}{r_i} \frac{A_{i+1} - A_{i-1}}{2\Delta r_i} + \frac{A_i}{r_i^2} - \frac{A_{i+1} + A_{i-1} - 2A_i}{(\Delta r)^2} \quad (3.9)$$

where N is the number of radial divisions and $i = 1, \dots, N+1$. Δr is the distance between two nodes: $\Delta r = r_{i+1} - r_i$; And $r_1 = 0$; $r_{N+1} = R$.

By using eq.(3.6), the corresponding boundary conditions for the discretization eqs.(3.7)–(3.9) are given by

$$\begin{cases} f_1 = 0 \\ A_1 = 0 \\ J_1 = 0 \end{cases}, \quad \begin{cases} f_{N+1} = 1 \\ A_{N+1} = \frac{\phi_0}{2\pi N \Delta r} \\ J_{N+1} = 0 \end{cases} \quad (3.10)$$

Because eq.(3.7) contains the nonlinear term, $-f_i^3$, the first two terms were solved into factors as

$$f_i - f_i^3 = f_i^*(1 + f_i^*)(1 - f_i^*), \quad (3.11)$$

where f^* is the value at the previous time step.

The calculation was carried out by implementing eqs.(3.7) ~ (3.10). The flow chart of the program is shown in Fig.3.3.

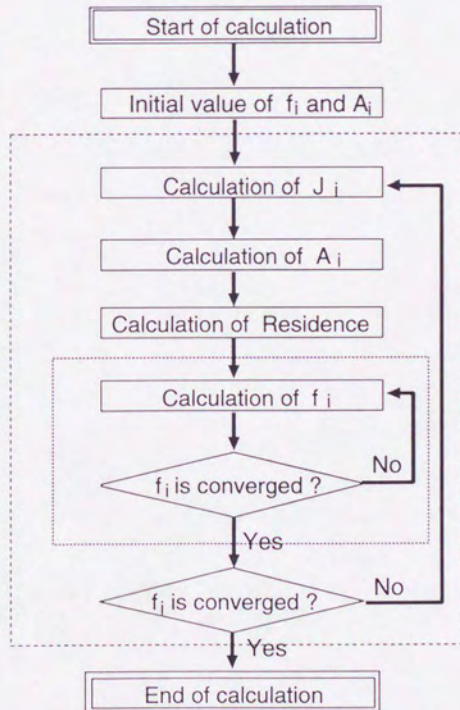


Figure 3.3: Flow chart of 1-dimensional GL simulation

3.1.3 Distribution of order parameter and vector potential around an isolated fluxoid

Fig. 3.4 shows the computed result for the normalized order parameter $f(r)$ and for the vector potential $A(r)$ in the case of NbTi ($\xi = 5.2\text{nm}$, $\lambda = 210\text{nm}$). As expected, $f(r)$ was proportional to the radius r for $r \simeq 0$, and it was saturated at $f(r) = 1$ for $r \gg 3\lambda$. The result agrees well with the approximate solution:

$$n_s = |\psi_\infty|^2 f^2(r) = \tanh^2 \frac{r}{\xi}, \quad (3.12)$$

where n_s is the superconducting electron density.

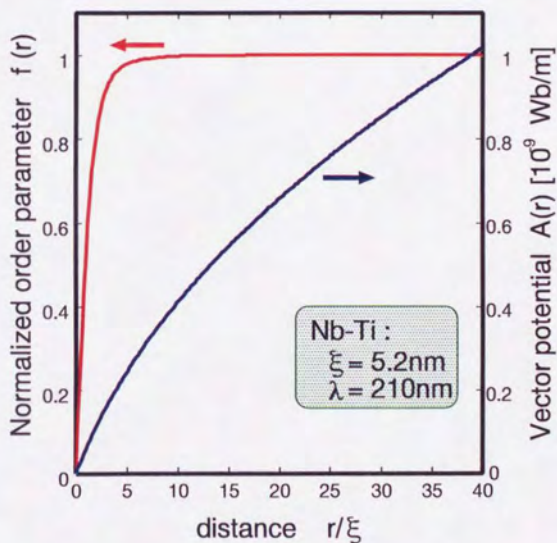


Figure 3.4: Numerical result for order parameter and vector potential of an isolated fluxoid (NbTi : $\xi = 5.2\text{nm}$, $\lambda = 210\text{nm}$)

3.1.4 Solution of TDGL equations

In this section, the numerical results of the magnetization process of type II superconductors based on the TDGL simulation for 2-dimensional model will be shown.

The derivation of the Time-Dependent Ginzburg-Landau equations were expressed as eqs. (3.13) and (3.14) in section 2.2.9., as follows,

$$\frac{\partial \Delta}{\partial \tau} = -\frac{1}{12} \left[\left(\frac{\nabla}{i} + \mathbf{a} \right)^2 \Delta + (|\Delta|^2 - 1)\Delta \right], \quad (3.13)$$

$$\frac{\partial \mathbf{a}}{\partial \tau} = \Re \left[\Delta^* \left(\frac{\nabla}{i} + \mathbf{a} \right) \Delta \right] - \kappa^2 \nabla \times \nabla \times \mathbf{a}, \quad (3.14)$$

For the discretization of these TDGL equations, the finite difference method (FDM) was applied. And for the time-integration, the forward difference method and the backward difference method were applied for eq. (3.13) and eq. (3.14), respectively.

Furthermore, for the iterative calculation of eq.(3.14), the 2-direction SLOR method was applied[44],[45] Then in x-direction SLOR method, the simultaneous equations are given as

$$a_1 x_{i,j-1}^{(k+1)} + a_2 x_{i,j}^{(k+1)} + a_3 x_{i,j+1}^{(k+1)} a_4 x_{i-1,j}^{(k)} + a_5 x_{i+1,j}^{(k)} = b, \quad (3.15)$$

where superscripts $(k+1)$ and (k) mean the present and the previous time steps, respectively. On the other hand, in y-direction SLOR method, the simultaneous equations are given by

$$a_1 x_{i-1,j}^{(k+1)} + a_2 x_{i,j}^{(k+1)} + a_3 x_{i+1,j}^{(k+1)} a_4 x_{i,j-1}^{(k)} + a_5 x_{i,j+1}^{(k)} = b. \quad (3.16)$$

In this simulation, the x-direction SLOR and the y-direction SLOR were repeated until convergence was obtained.

3.1.5 Discretization of 2-dimensional TDGL equations

Here, the 2-dimensional problem in xy plane is assumed. The right hand side of eq. (3.14) can be transformed as follows;

$$-\frac{1}{12} \left[\left(\frac{\nabla}{i} + \mathbf{a} \right)^2 \Delta + (|\Delta|^2 - 1)\Delta \right]$$

$$\begin{aligned}
&= -\frac{1}{12} \left[\left(\frac{\nabla}{i} + \mathbf{a} \right) \left(\frac{\nabla}{i} \Delta + \mathbf{a} \Delta \right) + (|\Delta|^2 - 1) \Delta \right] \\
&= -\frac{1}{12} \left[\left(-\nabla^2 \Delta + \frac{\nabla}{i} (\mathbf{a} \Delta) + \mathbf{a} \frac{\nabla}{i} \Delta + a^2 \Delta \right) + (|\Delta|^2 - 1) \Delta \right], \quad (3.17)
\end{aligned}$$

By substituting $\nabla \cdot \mathbf{a} = 0$, eq. (3.13) can be discretized as,

$$\begin{aligned}
\frac{\partial \Delta}{\partial \tau} &= \frac{1}{12} \left[\nabla^2 \Delta - 2\mathbf{a} \cdot \frac{\nabla}{i} \Delta + a^2 \Delta - (|\Delta|^2 - 1) \Delta \right] \\
&= \frac{1}{12} \left[\frac{\partial^2 \Delta}{\partial x^2} + \frac{\partial^2 \Delta}{\partial y^2} + 2i(a_x, a_y) \cdot \left(\frac{\partial \Delta}{\partial x}, \frac{\partial \Delta}{\partial y} \right) - (|\Delta|^2 - 1 - a^2) \Delta \right], \quad (3.18)
\end{aligned}$$

where $d\tau$ is the time step division.

Equation (3.18) can be discretized as follows,

$$\begin{aligned}
&\frac{\Delta'(j, k) - \Delta(j, k)}{d\tau} \\
&= \frac{1}{12} \left[\frac{\Delta(j-1, k) - 2\Delta(j, k) + \Delta(j+1, k)}{(dx)^2} + \frac{\Delta(j, k-1) - 2\Delta(j, k) + \Delta(j, k+1)}{(dy)^2} \right. \\
&\quad \left. + 2i \left(a_x(j, k) \frac{\Delta(j+1, k) - \Delta(j-1, k)}{2dx} + a_y(j, k) \frac{\Delta(j, k+1) - \Delta(j, k-1)}{2dy} \right) \right. \\
&\quad \left. - \{ |\Delta(j, k)|^2 - 1 - a^2(j, k) \} \Delta(j, k) \right], \quad (3.19)
\end{aligned}$$

where the prime(') denotes the unknown value.

Next, the second term of the righthand side of eq. (3.14) is rewritten as

$$-\kappa^2 \nabla \times \nabla \times \mathbf{a} = -\kappa^2 (\nabla (\nabla \cdot \mathbf{a}) - \nabla^2 \mathbf{a}) = \kappa^2 \nabla^2 \mathbf{a}. \quad (3.20)$$

where the gauge $\nabla \cdot \mathbf{a} = 0$ is used. By using eq.(3.20), eq.(3.14) can be rewritten as

$$\begin{aligned}
\frac{\partial \mathbf{a}}{\partial \tau} &= \Re \left[-i \Delta^* \nabla \Delta + |\Delta|^2 \mathbf{a} \right] + \kappa^2 \nabla^2 \mathbf{a} \\
&= \Re \left[-i \Delta^* \left(\frac{\partial \Delta}{\partial x}, \frac{\partial \Delta}{\partial y} \right) + |\Delta|^2 \mathbf{a} + \kappa^2 \left(\frac{\partial^2 a_x}{\partial x^2} + \frac{\partial^2 a_x}{\partial y^2}, \frac{\partial^2 a_y}{\partial x^2} + \frac{\partial^2 a_y}{\partial y^2} \right) \right]. \quad (3.21)
\end{aligned}$$

Then, eq.(3.21) is discretized as follows,

$$\begin{aligned}
\frac{a'_x(j, k) - a_x(j, k)}{d\tau} &= \Re \left(-i \Delta^*(j, k) \frac{\Delta(j+1, k) - \Delta(j-1, k)}{2dx} + |\Delta(j, k)|^2 a_x(j, k) \right. \\
&\quad \left. + \kappa^2 \left(\frac{a_x(j-1, k) - 2a_x(j, k) + a_x(j+1, k)}{(dx)^2} \right. \right. \\
&\quad \left. \left. + \frac{a_x(j, k-1) - 2a_x(j, k) + a_x(j, k+1)}{(dy)^2} \right) \right), \quad (3.22)
\end{aligned}$$

$$\begin{aligned} \frac{a'_y(j, k) - a_y(j, k)}{d\tau} = & \Re \left(-i\Delta^*(j, k) \frac{\Delta(j+1, k) - \Delta(j-1, k)}{2dy} \right) + |\Delta(j, k)|^2 a_y(j, k) \\ & + \kappa^2 \left(\frac{a_y(j-1, k) - 2a_y(j, k) + a_y(j+1, k)}{(dx)^2} \right. \\ & \left. + \frac{a_y(j, k-1) - 2a_y(j, k) + a_y(j, k+1)}{(dy)^2} \right), \end{aligned} \quad (3.23)$$

3.1.6 Boundary condition of discretized 2D-TDGL equations

As a boundary condition at superconductor surface, we adopted the insulating boundary condition:

$$\mathbf{p} \cdot \mathbf{n} = \left(\frac{\nabla}{i} + \frac{e^*}{\hbar} \mathbf{a} \right) \Delta \cdot \mathbf{n} = 0, \quad (3.24)$$

where \mathbf{p} and \mathbf{n} are the momentum of a Cooper pair and the unit vector normal to the boundary. If the surface of the superconductor is parallel to x axis, and the boundaries are at $y = 0$ and $y = L_y$, the normal vector \mathbf{n} is written as

$$\mathbf{n} = (0, \pm 1). \quad (3.25)$$

From eq.(3.25) and eq.(3.24), the following boundary condition is obtained concerning the order parameter Δ ,

$$i \frac{\partial \Delta}{\partial y} - a_y \Delta = 0. \quad (3.26)$$

Equation (3.26) can be discretized at $y = 0$ and $y = L_y$ as,

$$\begin{aligned} (y = 0) \quad & i \frac{\Delta(j, 3) - \Delta(j, 1)}{2dy} - a_y(j, 2) \Delta(j, 2) = 0, \\ (y = L_y) \quad & i \frac{\Delta(j, N_y + 3) - \Delta(j, N_y + 1)}{2dy} - a_y(j, N_y + 2) \Delta(j, N_y + 2) = 0. \end{aligned} \quad (3.27)$$

Furthermore, the boundary condition of the vector potential \mathbf{a} at boundary $y = 0$ and $y = L_y$ is expressed as

$$\frac{\partial a_y}{\partial x} - \frac{\partial a_x}{\partial y} = b_{ex,z}, \quad (3.28)$$

where $b_{ex,z}$ is the external magnetic flux density. Furthermore, the following conditions are applied for eq.(3.28) as

$$\frac{\partial a_y}{\partial x} = 0, \quad \frac{\partial a_x}{\partial y} = -b_{ex,z}. \quad (3.29)$$

Equation (3.29) is discretized as

$$\begin{aligned}
 (y=0) \quad & \frac{a_x(j, 3) - a_x(j, 1)}{2dy} = -b_{ex}, \\
 (y=L_y) \quad & \frac{a_x(j, N_y + 3) - a_x(j, N_y + 1)}{2dy} = -b_{ex}, \\
 (y=0) \quad & \frac{a_y(j+1, 2) - a_y(j-1, 2)}{2dx} = 0, \\
 (y=L_y) \quad & \frac{a_y(j+1, N_y + 2) - a_y(j-1, N_y + 2)}{2dx} = 0,
 \end{aligned} \tag{3.30}$$

Furthermore, the periodical boundary condition was applied for x-direction. It is expressed as follows,

$$\begin{cases} \Delta(1, k) = \Delta(N_y + 1, k), \\ a_y(1, k) = a_y(N_y + 1, k), \\ a_x(1, k) = a_x(N_y + 1, k), \end{cases} \tag{3.31}$$

$$\begin{cases} \Delta(N_y + 3, k) = \Delta(3, k), \\ a_x(N_y + 3, k) = a_x(3, k), \\ a_y(N_y + 3, k) = a_y(3, k). \end{cases} \tag{3.32}$$

3.1.7 Time integral method of 2D-TDGL simulation

From (3.21), the stability condition of the Crank-Nicolson's scheme is derived:

$$1 \geq 2\kappa^2(1-\theta)d\tau \left(\frac{1}{\Delta x^2} + \frac{1}{\Delta y^2} \right). \tag{3.33}$$

The Ginzburg-Landau parameter of high T_c superconductor is large enough ($\kappa = 50 \sim 500$) to cause the instability for the forward difference scheme ($\theta = 0$) according to (3.33). Therefore, for time-integration, the forward difference scheme was applied to (3.19), and the backward difference scheme ($\theta = 1$) was applied to (3.23).

In order to solve eq.(3.23), 2-direction SLOR method was used [44],[45]. Fig.3.5 shows the mesh division of the analytical region and the concept of the 2-direction SLOR method. The unknowns are at \times -marked nodes, and the knowns are at \circ -marked nodes.

(x-direction SLOR)

$$\frac{a'_z(j, k) - a_z(j, k)}{d\tau} = \Re \left(-i\Delta^*(j, k) \frac{\Delta(j+1, k) - \Delta(j-1, k)}{2dx} \right) + |\Delta(j, k)|^2 a'_z(j, k)$$

$$\begin{aligned}
& +\kappa^2 \left(\frac{a_x(j-1, k) - 2a'_x(j, k) + a_x(j+1, k)}{(dx)^2} \right. \\
& \left. + \frac{a'_x(j, k-1) - 2a'_x(j, k) + a'_x(j, k+1)}{(dy)^2} \right), \quad (3.34)
\end{aligned}$$

$$\begin{aligned}
\frac{a'_y(j, k) - a_y(j, k)}{d\tau} &= \Re \left(-i\Delta^*(j, k) \frac{\Delta(j+1, k) - \Delta(j-1, k)}{2dy} \right) + |\Delta(j, k)|^2 a'_y(j, k) \\
& + \kappa^2 \left(\frac{a_y(j-1, k) - 2a'_y(j, k) + a_y(j+1, k)}{(dx)^2} \right. \\
& \left. + \frac{a'_y(j, k-1) - 2a'_y(j, k) + a'_y(j, k+1)}{(dy)^2} \right), \quad (3.35)
\end{aligned}$$

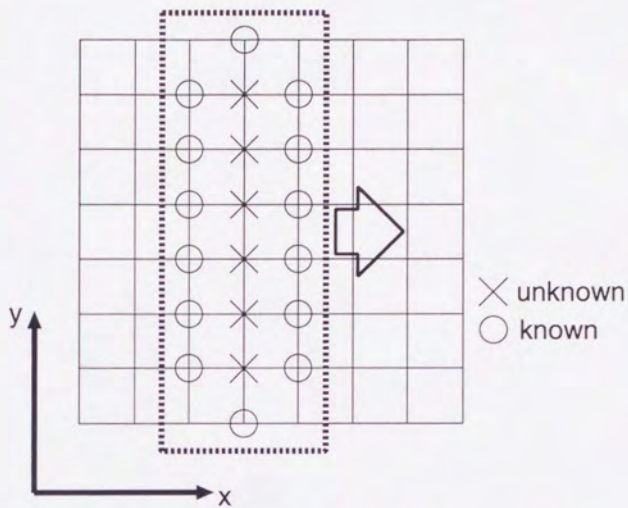
(y-direction SLOR)

$$\begin{aligned}
\frac{a'_x(j, k) - a_x(j, k)}{d\tau} &= \Re \left(-i\Delta^*(j, k) \frac{\Delta(j+1, k) - \Delta(j-1, k)}{2dx} \right) + |\Delta(j, k)|^2 a'_x(j, k) \\
& + \kappa^2 \left(\frac{a'_x(j-1, k) - 2a'_x(j, k) + a'_x(j+1, k)}{(dx)^2} \right. \\
& \left. + \frac{a_x(j, k-1) - 2a'_x(j, k) + a_x(j, k+1)}{(dy)^2} \right), \quad (3.36)
\end{aligned}$$

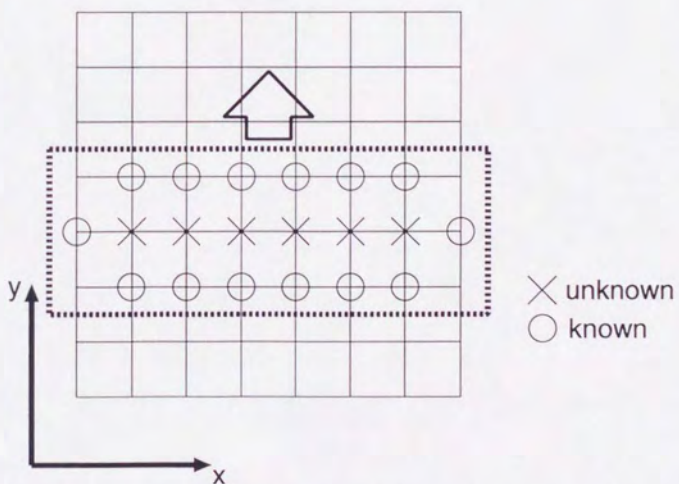
$$\begin{aligned}
\frac{a'_y(j, k) - a_y(j, k)}{d\tau} &= \Re \left(-i\Delta^*(j, k) \frac{\Delta(j+1, k) - \Delta(j-1, k)}{2dy} \right) + |\Delta(j, k)|^2 a'_y(j, k) \\
& + \kappa^2 \left(\frac{a'_y(j-1, k) - 2a'_y(j, k) + a'_y(j+1, k)}{(dx)^2} \right. \\
& \left. + \frac{a_y(j, k-1) - 2a'_y(j, k) + a_y(j, k+1)}{(dy)^2} \right). \quad (3.37)
\end{aligned}$$

where again the prime (') denotes the unknown values.

Equations (3.19) and (3.20) are used for the calculation of $\Delta'(j, k)$, eqs. (3.34) and (3.35) for the calculation of $a'_x(j, k)$, and eqs.(3.36) and (3.37) for $a'_y(j, k)$.



(a) x direction SOR



(b) y direction SOR

Figure 3.5: 2-direction SOR method

3.1.8 Computational model of YBCO thin film

Fig.3.6 shows the computational model of the type-II superconductor thin film for the 2-dimensional TDGL simulation. As superconductor material, $\text{YBa}_2\text{Cu}_3\text{O}_{6+x}$ was employed.

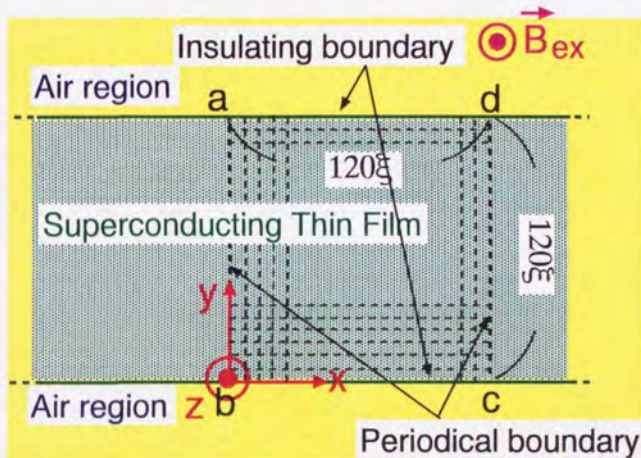


Figure 3.6: Schematic drawing for the computational model of 2-dimensional TDGL simulation

The material and simulation parameters are as follows,

- Coherence length : 3.0nm
- Magnetic penetration depth : 150nm
- Size of the analytical region : $L_x = L_y = 60\xi$
- Mesh division numbers : $n_x \times n_y = 60 \times 60$

The x- and y-axes are normalized with the coherence length ξ . The insulating boundary condition was used for the boundary \overline{ad} and \overline{bc} , and the periodic boundary condition, for the boundary \overline{ab} , \overline{dc} .

It is assumed that a constant and uniform magnetic field, B_{ex} , was applied to the superconductor, and that the superconductor was then cooled in this magnetic field until the superconducting state is established (Field-Cooling), as shown in Fig.3.7. The

formation of the vortex lattice in such an occasion was simulated by this computational method.

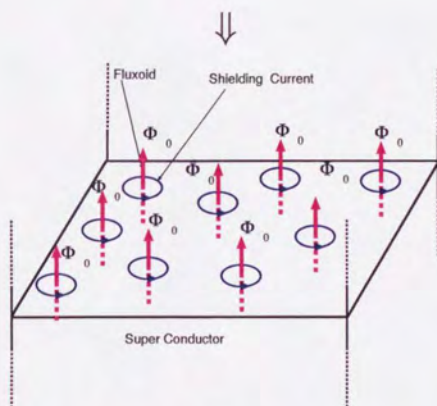
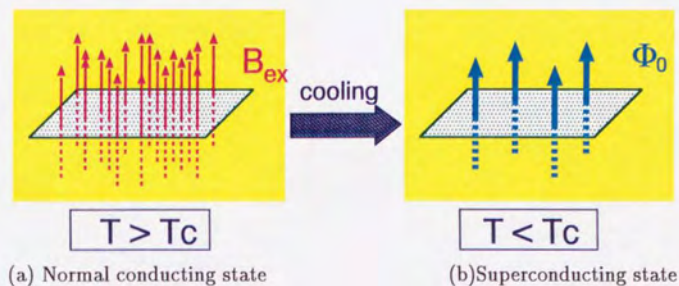


Figure 3.7: Field cooling of the $\text{YBa}_2\text{Cu}_3\text{O}_{x+6}$ thin film

3.1.9 Numerical results of YBCO thin film

Fig.3.8 shows the time-variation of the superconducting electrons distribution density, $|\Delta|^2$, normalized by $|\Delta_\infty|^2$, for the case when the applied magnetic flux density is $B_{ex} = 0.03\mu_0 H_{c2}$. In the superconducting region, $|\Delta|^2$ becomes 1.0. Around the fluxoid, $|\Delta|^2 \in$

(0, 1) because of the normal conducting core. The simulation shows that 12 cavities of $|\Delta|^2$ are constructed. These 12 fluxoids formed the well-known triangular vortex lattice, indicating that the superconductor is in the mixed state.

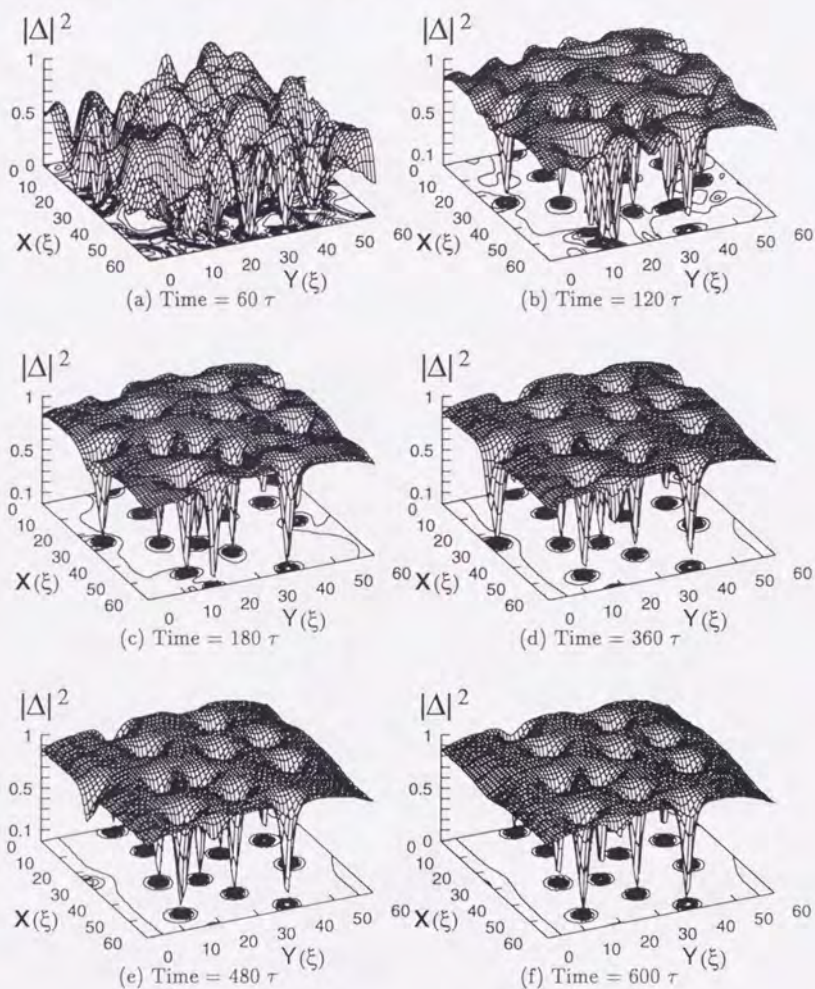


Figure 3.8: Formation of the vortex lattice in YBCO thin film (Superconducting electrons density)

Fig.3.9 shows the time-variation of the distribution of magnetic flux density, B . It is found that the locations of the peaks for the magnetic flux density correspond to the locations of the cavities of the superconducting electrons density.

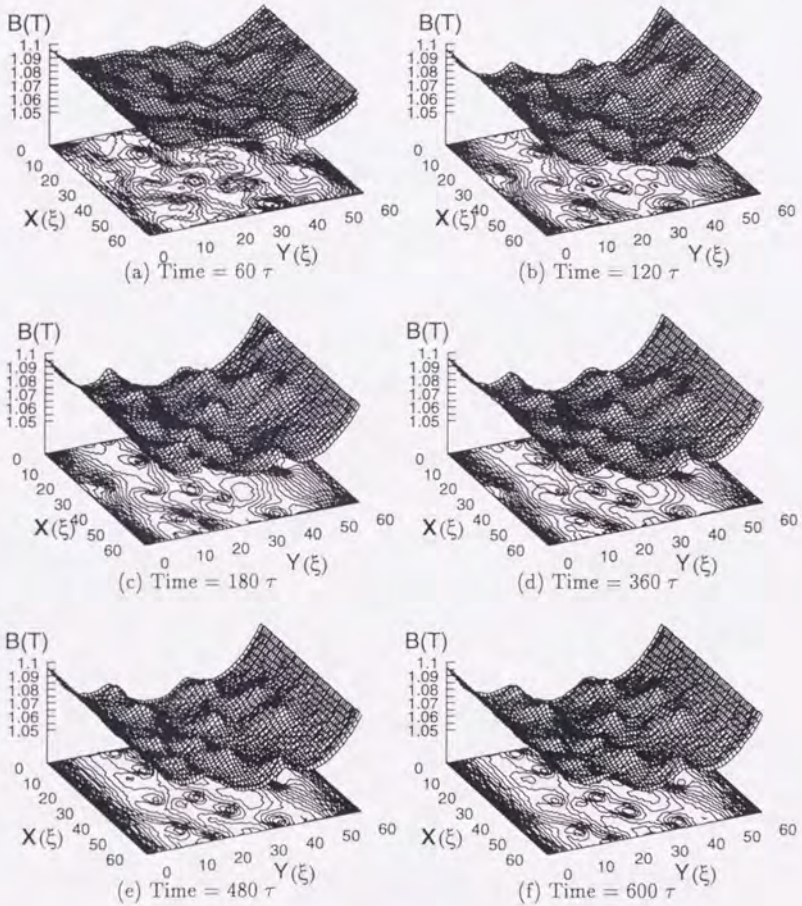


Figure 3.9: Formation of the vortex lattice in YBCO thin film (Magnetic flux density)

By comparing with the spread of the superconducting electrons density around a fluxoid, it can be noticed that the spread pattern of the magnetic flux density peak is much broader than that of superconducting electrons density. This is because the magnetic penetration depth, λ , is 50 times larger than the coherence length, ξ .

Near the surface of the superconductor, it is found that the magnetic flux density decreases from the surface exponentially. This magnetic flux density corresponds to the Meissner field.

3.2 2-dimensional fluxoid dynamics method

3.2.1 Kinetic equation of fluxoid

In the 2-dimensional FD method of type-II superconductor, the fluxoids are considered to be affected by 5 kinds of forces (see Fig.3.10) and they move until the equilibrium of the forces is attained. In the 2-dimensional Fluxoid Dynamics method, the tensional force due to the curvature of the fluxoid is neglected by making the assumption of uniformity in z-direction. Then, kinetic equation of fluxoid movement is written as [46],[47]:

$$\eta_f \frac{\partial \mathbf{r}_i}{\partial t} = \sum_j \mathbf{F}_p(\mathbf{r}_{ij}) + \sum_k \mathbf{F}_f(\mathbf{r}_{ik}) + \mathbf{F}_M(\mathbf{r}_i) + \mathbf{F}_J(\mathbf{r}_i). \quad (3.38)$$

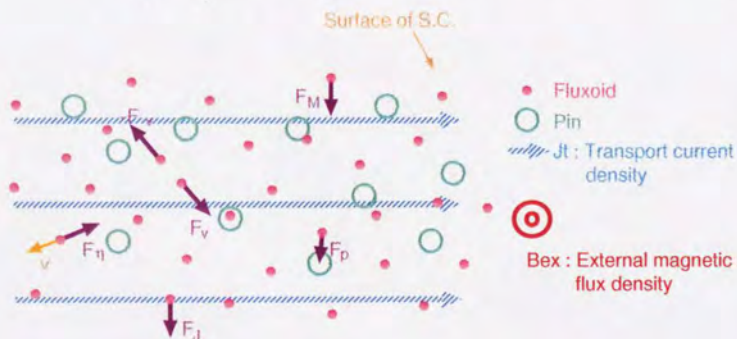


Figure 3.10: 5 kinds of forces in 2-dimensional FD method

Here the inertial term was neglected because the mass of electrons around a fluxoid is negligibly small [46]. The vectors and the coefficient in eq. (3.38) correspond to the followings,

- \mathbf{r}_i : position vector of i -th fluxoid
- \mathbf{r}_{ij} : relative position vector between i -th fluxoid and j -th pinning center
- \mathbf{r}_{ik} : relative position vector between i -th and k -th fluxoids
- η_f : viscous coefficient
- \mathbf{F}_p : pinning force
- \mathbf{F}_f : repulsive force between two fluxoids
- \mathbf{F}_M : Lorentz force due to Meissner current
- \mathbf{F}_J : Lorentz force due to transport current

The left side of eq. (3.38) corresponds to the viscous force $-\mathbf{F}_\eta$. This equation was discretized to calculate the location of i -th fluxoid, \mathbf{r}_i . The value of time increment is chosen enough small that each fluxoid does not skip over any pinning center. Next, the evaluation of the forces \mathbf{F}_p , \mathbf{F}_f , \mathbf{F}_J and \mathbf{F}_M , and of the viscous coefficient η will be described.

3.2.2 Viscous coefficient of fluxoid

When the fluxoids move in the type-II superconductor, the viscous force appears due to the Joule's loss of the normal conducting electrons around the fluxoids is yielded as shown in Fig. 3.11. Here, we assume that the viscous force per unit length of a fluxoid can be expressed as,

$$\mathbf{F}_\eta = -\eta_f \mathbf{v} \quad (3.39)$$

where η_f and \mathbf{v}_i are the viscous coefficient and the velocity of the fluxoid. We try to evaluate the value of η_f . The energy dispersion per unit length of fluxoid, W_1 , is written as,

$$W_1 = -\mathbf{F}_\eta \cdot \mathbf{v} = \eta_f v^2 \quad (3.40)$$

Next, we evaluate the energy dispersion due to the Joule's loss of the normal conducting electrons around a fluxoid.

This energy dispersion per unit length of fluxoid is written as

$$W_2 = \int_S \frac{\mathbf{J}_n^2}{\sigma_e} dS = \int_S \frac{(en_n \mathbf{v})^2}{\sigma_e} dS = \frac{e^2 v^2}{\sigma_e} \int_S n_n^2 dS \quad (3.41)$$

where

- \mathbf{J}_n : current density due to normal conducting electrons
- σ_e : macroscopic conductivity in normal conducting state
- e : electric charge of an electron
- n_n : normal conducting electrons density

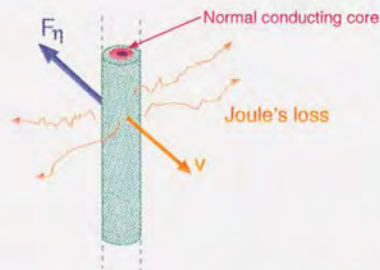


Figure 3.11: Viscous force and Joule's loss of a fluxoid

Under the assumption that these two energy dispersion are equal, the viscous coefficient η_f can be obtained from eq.(3.40) and eq.(3.41) as,

$$\eta_f = \frac{e^2}{\sigma_e} \int_S n_n^2 dS \quad (3.42)$$

The normal conducting electrons density n_n is given by following equation,

$$n_n = |\psi_\infty|^2 - n_s = |\psi_\infty|^2 - |\psi_\infty|^2 \hat{f}^2 = |\psi_\infty|^2 (1 - \hat{f}^2) \quad (3.43)$$

By substituting eq. (3.43) to eq. (3.42), η_f is obtained as

$$\eta_f = \frac{e^2 |\psi_\infty|^4}{\sigma_e} \int_S (1 - \hat{f}^2)^2 dS \quad (3.44)$$

3.2.3 Pinning force

Here we assume that the uniformity in z -direction is satisfied. We consider an isolated fluxoid which is parallel to z -axis, so that the axial symmetry is satisfied around a fluxoid. If this fluxoid is considered isolated, the Ginzburg-Landau's free energy density is given by

$$\begin{aligned} \varepsilon_{s1}(\tau) = \varepsilon_n - \mu_0 H_c^2 \left[\hat{f}^2(\tau) - \frac{1}{2} \hat{f}^4(\tau) - \xi^2 \left\{ \left(\frac{d\hat{f}(\tau)}{d\tau} \right)^2 \right. \right. \\ \left. \left. + \left(\frac{1}{\tau} - \frac{2\pi \hat{A}(\tau)}{\Phi_0} \right)^2 \hat{f}^2(\tau) \right\} \right] + \frac{B^2}{2\mu_0} \quad (3.45) \end{aligned}$$

where τ , ε_n , H_c and B are the distance from the center of the fluxoid, the free energy density in normal conducting state, the critical magnetic field and the magnetic flux density, respectively. $\hat{f}(\tau)$ and $\hat{A}(\tau)$ are numerical results of the normalized order parameter and of the vector potential around a fluxoid in NbTi ($\xi = 5.2nm$ and $\lambda = 210nm$) and are shown in Fig. 3.4.

On the other hand, at a location far from the fluxoid, the variables f and A satisfy the following equations:

$$f = 1, \quad (3.46)$$

$$\frac{df}{d\tau} = 0, \quad (3.47)$$

$$A = \frac{\Phi_0}{2\pi\tau}. \quad (3.48)$$

By substituting eqs. (3.46) ~ (3.48) into eq. (3.45), the free energy density at a location far from the fluxoid ϵ_{s2} can be obtained as:

$$\epsilon_{s2} = \epsilon_n - \frac{\mu_0 H_c^2}{2} + \frac{B^2}{2\mu_0}. \quad (3.49)$$

Fig. 3.12 shows the conceptual model of the distribution of free energy density, ϵ , in three cases:

- (a) the fluxoid is outside of the pinning center,
- (b) the fluxoid touches the pinning center.
- (c) the fluxoid invades the pinning center.

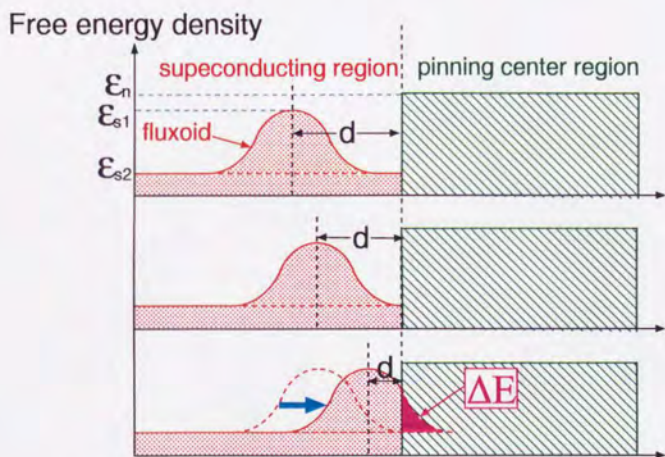


Figure 3.12: Variation of the distribution of free energy density

In this figure, d is the distance between the center of the fluxoid and the surface of the pinning center. In the pinning center region, $\epsilon = \epsilon_n$ is satisfied because the normal conducting state is kept in this region. Therefore, the free energy changes when the fluxoid invades the pinning center (see case (c)). Thus, the variation of the free energy ΔE can be written as:

$$\Delta E = \int_{S_p} \{\epsilon_{s2} - \epsilon_{s1}(\tau)\} dS$$

$$= -\mu_0 H_c^2 \int_{S_p} \left[\frac{(\hat{f}^2 - 1)^2}{2} + \xi^2 \left\{ \left(\frac{d\hat{f}}{dr} \right)^2 + \left(\frac{1}{r} - \frac{2\pi\hat{A}}{\Phi_0} \right)^2 \hat{f}^2 \right\} \right] dS. \quad (3.50)$$

Now we assume that the pinning center is large enough comparing to the fluxoid (see Fig. 3.13), and the boundary of the pinning center region is almost straight. In this case, the pinning force per unit length of fluxoid, F_p , can be obtained from the following equation:

$$\begin{aligned} F_p(d) &= \frac{\partial \Delta E}{\partial d} \mathbf{n} \\ &= \frac{\partial}{\partial d} \left\{ \int_{S_p} \{ \varepsilon_{s2} - \varepsilon_{s1}(r) \} dS \right\} \mathbf{n} \\ &= \left\{ \int_{\partial S_p} (\varepsilon_{s2} - \varepsilon_{s1}(\sqrt{d^2 + \ell^2})) d\ell \right\} \mathbf{n} \quad (\because r = \sqrt{d^2 + \ell^2}) \\ &= \left[-\mu_0 H_c^2 \int_{-\infty}^{\infty} \left\{ \frac{(\hat{f}^2 - 1)^2}{2} + \xi^2 \left(\left(\frac{d\hat{f}}{dr} \right)^2 + \left(\frac{1}{r} - \frac{2\pi\hat{A}}{\Phi_0} \right)^2 \hat{f}^2 \right) \right\} d\ell \right] \mathbf{n} \quad (3.51) \end{aligned}$$

where d is the distance between the fluxoid's center and the surface of the pinning center and \mathbf{n} is the normal vector at the surface of the pinning center (see Fig. 3.13).

Fig. 3.14 shows the numerical result for the pinning force per unit length, $F_p(d)$, calculated according to eq. (3.84). F_p keeps $F_p < 0$ everywhere and $|F_p|$ has a maximum at the surface of the pinning center.

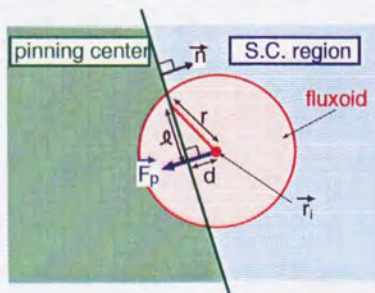


Figure 3.13: The fluxoid invading the pinning center

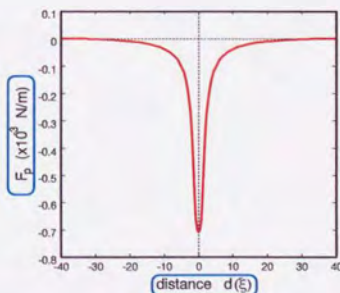


Figure 3.14: Numerical result of the pinning force F_p

3.2.4 Magnetic repulsive force between two fluxoids

Generally, the magnetic energy is expressed as

$$E = \frac{B^2}{2\mu_0} \quad (3.52)$$

where B is the magnetic flux density. Fig. 3.15 shows the distribution of the magnetic flux density due to two fluxoids. By using the symmetry, the magnetic energy is written as

$$\begin{aligned} E &= \int_S \{B_i(\mathbf{r}) + B_k(\mathbf{r})\} \cdot \{B_i(\mathbf{r}) + B_k(\mathbf{r})\} dS \\ &= \frac{\Phi_0}{2\mu_0} \cdot [B_i(\mathbf{r}_i) + B_i(\mathbf{r}_k) + B_k(\mathbf{r}_i) + B_k(\mathbf{r}_k)] \\ &= \frac{\Phi_0}{\mu_0} B_i(\mathbf{r}_i) + \frac{\Phi_0}{\mu_0} B_i(\mathbf{r}_k), \quad (\because B_i(\mathbf{r}_k) = B_k(\mathbf{r}_i)) \end{aligned} \quad (3.53)$$

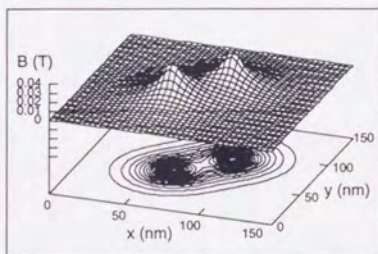


Figure 3.15: Magnetic flux density by two fluxoids

where \mathbf{r}_i and \mathbf{r}_k are the position vectors for the i -th and k -th fluxoid, respectively. The second term of the right side of eq. (3.53) corresponds to the magnetic interactive energy between i -th and k -th fluxoids, E_{ik} . By substituting eq. (2.28), E_{ik} is obtained as

$$E_{ik} = \frac{\Phi_0}{\mu_0} B_i(\mathbf{r}_k) = \frac{\Phi_0^2}{2\pi\mu_0\lambda^2} K_0\left(\frac{r_{ik}}{\lambda}\right), \quad (3.54)$$

where $r_{ik} = |\mathbf{r}_i - \mathbf{r}_k|$.

From eq. (3.54) the repulsive force between two fluxoids can be expressed as the differential of E_{ik} with respect to r_{ik} like,

$$\begin{aligned} F_f(\mathbf{r}_{ik}) &= -\nabla E_{ik} = -\frac{\partial E_{ik}}{\partial r} \frac{\mathbf{r}_{ik}}{r_{ik}} = \frac{\Phi_0^2}{2\pi\mu_0\lambda^3} K_1\left(\frac{r_{ik}}{\lambda}\right) \frac{\mathbf{r}_{ik}}{r_{ik}}, \\ &\left(\because \frac{d}{dr} K_0(r) = -K_1(r)\right) \end{aligned} \quad (3.55)$$

3.2.5 Magnetic force due to Meissner current

The Meissner field at the location of i -th fluxoid can be written as follows,

$$B_M(\mathbf{r}_i) = B_{ex} \exp\left(-\frac{d_i^M}{\lambda}\right) \mathbf{e}_z, \quad (3.56)$$

where B_{ex} and d_i^M are the external magnetic flux density and the distance between the air boundary of the superconductor and i -th fluxoid, respectively.

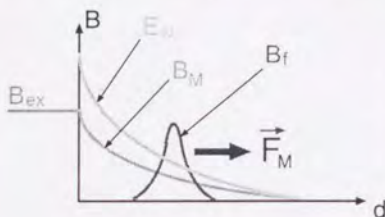


Figure 3.16: Meissner field and magnetic repulsive force

Then, the magnetic interactive energy between the Meissner field B_M , and the magnetic flux density due to i -th fluxoid B_i is expressed in the same manner as in eq. (3.54),

$$\begin{aligned} E_{M,i} &= \frac{1}{\mu_0} \Phi_0 \cdot B_M \\ &= \frac{\Phi_0 B_{ex}}{\mu_0} \exp\left(-\frac{d_i^M}{\lambda}\right) \end{aligned} \quad (3.57)$$

The Lorentz force due to the Meissner field on the i -th fluxoid is obtained by differentiating $E_{M,i}$ with respect to d_i^M ,

$$F_M(\mathbf{r}_i) = -\nabla E_{M,i} = -\nabla \left\{ \frac{\Phi_0 B_{ex}}{\mu_0} \exp\left(-\frac{d_i^M}{\lambda}\right) \right\} = -\frac{\Phi_0 B_{ex}}{\mu_0 \lambda} \exp\left(-\frac{d_i^M}{\lambda}\right) \mathbf{n}, \quad (3.58)$$

where \mathbf{n} is the normal vector at the air surface of the superconductor (see Fig. 3.16).

3.2.6 Lorentz force due to transport current

When the transport current flows in the type-II superconductor, the corresponding Lorentz force acts on the fluxoid in the superconductor. In 2-dimensional coordinate system, the transport current density J_t can be written as

$$\mathbf{J}_t = (J_{tx}, J_{ty}, J_{tz})^T = (J_{tx}, J_{ty}, 0)^T. \quad (3.59)$$

From the uniformity in z -direction, the magnetic flux density due to the transport current, $B_J = (0, 0, B_J)$ can be defined, and \mathbf{J}_t can be expressed by rotation of B_J as follows;

$$\mathbf{J}_t = \frac{1}{\mu_0} \nabla \times B_J = \left(\frac{1}{\mu_0} \frac{\partial B_{Jz}}{\partial y}, -\frac{1}{\mu_0} \frac{\partial B_{Jz}}{\partial x}, 0 \right)^T \quad (3.60)$$

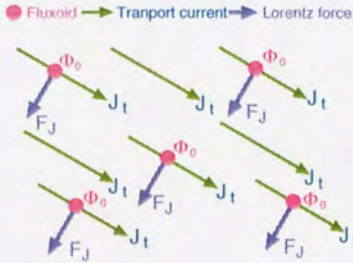


Figure 3.17: Lorentz force due to transport current

Then the Lorentz force due to the transport current acting on the fluxoid is obtained as,

$$\begin{aligned}
 F_J &= -\nabla \cdot E_J \\
 &= -\Phi_0 \left(\frac{1}{\mu_0} \frac{\partial B_J}{\partial x}, \frac{1}{\mu_0} \frac{\partial B_J}{\partial y}, \frac{1}{\mu_0} \frac{\partial B_J}{\partial z} \right)^T \\
 &= \Phi_0 (J_{ty}, -J_{tx}, 0)^T \\
 &= \begin{pmatrix} J_{tx} \\ J_{ty} \\ J_{tz} \end{pmatrix} \times \begin{pmatrix} 0 \\ 0 \\ \Phi_0 \end{pmatrix} \\
 &= \mathbf{J}_t \times \Phi_0
 \end{aligned} \tag{3.62}$$

The magnetic interactive energy between the magnetic flux density due to the fluxoid (\mathbf{B}), and the magnetic flux density due to the transport current (\mathbf{B}_J) is given by

$$E_J = \int_S \frac{\mathbf{B} \cdot \mathbf{B}_J}{\mu_0} dS = \frac{\Phi_0 \cdot \mathbf{B}_J}{\mu_0} = \frac{\Phi_0 B_J}{\mu_0} \tag{3.61}$$

3.2.7 Calculation of the electric field

When i -th fluxoid move with speed \mathbf{v} , the electromotive force acting upon the unit electric charge at location (x, y) is

$$E_{e,i} = \mathbf{B}_i \times \mathbf{v}_i \delta_2(x, y) \tag{3.63}$$

where $\delta_2(x, y)$ is the 2-dimensional Delta function. Then the average electrical field in x direction along \overline{AB} ($\overline{E}_{x,AB}$) and the voltage difference between AB (V_{AB}) in Fig. 3.18 are written as

$$\overline{E}_{x,AB}(y) = V_{AB}(y) = \int_{-\frac{L_x}{2}}^{\frac{L_x}{2}} F_x dx = \sum_{i=1}^N \int_{-\frac{L_x}{2}}^{\frac{L_x}{2}} (\mathbf{B}_i(x, y) \times \mathbf{v}_i)_x \delta(x, y) dx \tag{3.64}$$

The average electric field in $\square abcd$ (E_x) can be obtained as follows;

$$\begin{aligned}
 E_x &= \frac{1}{L_y} \int_0^{L_y} \overline{E}_{x,AB}(y) dy \\
 &= \frac{1}{L_x L_y} \int_0^{L_y} \int_{-\frac{L_x}{2}}^{\frac{L_x}{2}} V_{AB}(y) dy
 \end{aligned}$$

$$\begin{aligned}
 &= \frac{1}{L_x L_y} \sum_{i=1}^N \left\{ \left(\int_0^{L_y} \int_{-\frac{L_x}{2}}^{\frac{L_x}{2}} \mathbf{B}_i(x, y) \delta_2(x, y) dx dy \right) \times \mathbf{v}_i \right\} \\
 &= \frac{1}{L_x L_y} \sum_{i=1}^N (\Phi_{0,i} \times \mathbf{v}_i) \quad (3.65)
 \end{aligned}$$

E_y can be obtained in a similar way. Then the average electrical field \bar{E} is expressed as

$$\bar{E} = \frac{1}{L_x L_y} \sum_{i=1}^N (\Phi_{0,i} \times \mathbf{v}_i) \quad (3.66)$$

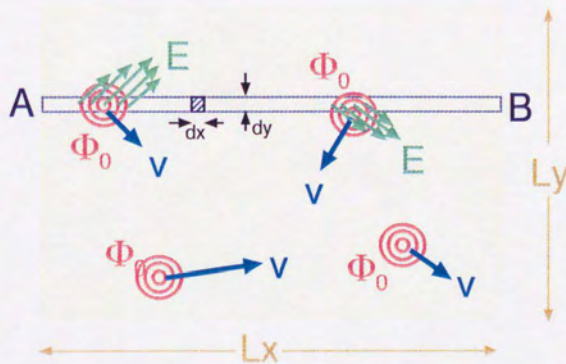


Figure 3.18: Evaluation of average electric field

3.2.8 Discretization of the kinetic equation

The kinetic equation, eq. (3.38) was discretized like,

$$\begin{aligned} \eta_f \frac{\partial r_{x,i}}{\partial t} &= \sum_j F_{pz}(r_{x,j}^p - r_{x,i}, r_{y,j}^p - r_{y,i}) + \sum_k F_{fz}(r_{x,k} - r_{x,i}, r_{y,k} - r_{y,i}) \\ &+ F_{Mz}(r_{x,i}, r_{y,i}) + F_{Jz}(r_{x,i}, r_{y,i}), \end{aligned} \quad (3.67)$$

$$\begin{aligned} \eta_f \frac{\partial r_{y,i}}{\partial t} &= \sum_j F_{py}(r_{x,j}^p - r_{x,i}, r_{y,j}^p - r_{y,i}) + \sum_k F_{fy}(r_{x,k} - r_{x,i}, r_{y,k} - r_{y,i}) \\ &+ F_{My}(r_{x,i}, r_{y,i}) + F_{Jy}(r_{x,i}, r_{y,i}). \end{aligned} \quad (3.68)$$

By applying the explicit method concerning the time integration, eq. (3.68) is rewritten as

$$\begin{aligned} \eta_f \frac{r'_{x,i} - r_{x,i}}{\Delta t} &\simeq \sum_j F_{pz}(r_{x,j}^p - r_{x,i}, r_{y,j}^p - r_{y,i}) + \sum_k F_{fz}(r_{x,k} - r_{x,i}, r_{y,k} - r_{y,i}) \\ &+ F_{Mz}(r_{x,i}, r_{y,i}) + F_{Jz}(r_{x,i}, r_{y,i}), \end{aligned} \quad (3.69)$$

$$\begin{aligned} \eta_f \frac{r'_{y,i} - r_{y,i}}{\Delta t} &\simeq \sum_j F_{py}(r_{x,j}^p - r_{x,i}, r_{y,j}^p - r_{y,i}) + \sum_k F_{fy}(r_{x,k} - r_{x,i}, r_{y,k} - r_{y,i}) \\ &+ F_{My}(r_{x,i}, r_{y,i}) + F_{Jy}(r_{x,i}, r_{y,i}), \end{aligned} \quad (3.70)$$

where Δt is the time division and $\mathbf{r}'_i = (r'_{x,i}, r'_{y,i})$ is the position vector of i -th fluxoid at the new time step. From eq. (3.70), the position vector at the new time step can be obtained by the following equation,

$$\begin{aligned} r'_{x,i} &= r_{x,i} + \frac{\Delta t}{\eta_f} \left\{ \sum_j F_{pz}(r_{x,j}^p - r_{x,i}, r_{y,j}^p - r_{y,i}) + \sum_k F_{fz}(r_{x,k} - r_{x,i}, r_{y,k} - r_{y,i}) \right. \\ &\left. + F_{Mz}(r_{x,i}, r_{y,i}) + F_{Jz}(r_{x,i}, r_{y,i}) \right\}, \end{aligned} \quad (3.71)$$

$$\begin{aligned} r'_{y,i} &= r_{y,i} + \frac{\Delta t}{\eta_f} \left\{ \sum_j F_{py}(r_{x,j}^p - r_{x,i}, r_{y,j}^p - r_{y,i}) + \sum_k F_{fy}(r_{x,k} - r_{x,i}, r_{y,k} - r_{y,i}) \right. \\ &\left. + F_{My}(r_{x,i}, r_{y,i}) + F_{Jy}(r_{x,i}, r_{y,i}) \right\}, \end{aligned} \quad (3.72)$$

where Δt was determined so small that no fluxoid would skip any pinning center around within 1 time step.

3.2.9 Periodic boundary condition

For saving the computing memory and shortening the simulation time, the periodic boundary condition was applied for the computational model. Fig. 3.19 shows the 2-dimensional

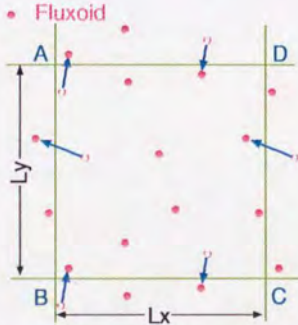


Figure 3.19: 2-dimensional periodic boundary condition

boundary condition. From the x direction periodic boundary condition, the fluxoid exits through the boundary CD(AB) at $(\pm L_x/2, y)$ was applied as the another fluxoid enters through the boundary AB(CD) at $(\mp L_x/2, y)$. It is the same manner in the case of the y direction periodic boundary condition.

3.2.10 Insulating boundary condition

In the case that the fluxoid exists near the surface of the superconductor, the reflected image of the fluxoid must be taken into consideration. This is an established method and it is applied for satisfying the condition that the shielding current around the fluxoid is parallel to the surface. When the fluxoid is near the surface of the superconductor at the location $(x, L_y - d_y)$, the reflected image of the fluxoid is located at $(x, L_y + d_y)$ as shown in Fig. 3.20), Then the shielding current density at $y = L_y$ due to the two fluxoids are written as,

$$\begin{aligned} \mathbf{J}_{sur} &= \nabla'_1 \times \frac{\Phi_0}{2\pi\lambda^2} K_0 \left(-\frac{r_1}{\lambda} \right) \mathbf{e}_z + \nabla'_2 \times \left(-\frac{\Phi_0}{2\pi\lambda^2} K_0 \left(-\frac{r_2}{\lambda} \right) \mathbf{e}_z \right) \\ &= \frac{\Phi_0}{2\pi\lambda^2} \left\{ \nabla'_1 \times K_0 \left(-\frac{\sqrt{(x' - x)^2 + dy^2}}{\lambda} \right) \mathbf{e}_z \right. \\ &\quad \left. - \nabla'_2 \times K_0 \left(-\frac{\sqrt{(x' - x)^2 + (-dy)^2}}{\lambda} \right) \mathbf{e}_z \right\} \end{aligned}$$

$$\begin{aligned}
&= \frac{\Phi_0}{2\pi\lambda^3} \left(K_1 \left(-\frac{\sqrt{(x'-x)^2 + dy^2}}{\lambda} \right) \mathbf{e}_{\theta 1} - K_1 \left(-\frac{\sqrt{(x'-x)^2 + (-dy)^2}}{\lambda} \right) \mathbf{e}_{\theta 2} \right) \\
&= \frac{\Phi_0}{2\pi\lambda^3} K_1 \left(-\frac{\sqrt{(x'-x)^2 + dy^2}}{\lambda} \right) \left\{ \left(\frac{\frac{dy}{\sqrt{(x'-x)^2 + dy^2}}}{\frac{x'-x}{\sqrt{(x'-x)^2 + dy^2}}} \right) - \left(\frac{-\frac{dy}{\sqrt{(x'-x)^2 + d_y^2}}}{\frac{x'-x}{\sqrt{(x'-x)^2 + d_y^2}}} \right) \right\} \\
&= \frac{2d_y\Phi_0}{2\pi\lambda^3\sqrt{(x'-x)^2 + d_y^2}} K_1 \left(-\frac{\sqrt{(x'-x)^2 + dy^2}}{\lambda} \right) \mathbf{e}_x \quad (3.73)
\end{aligned}$$

Then the current density becomes parallel to the surface, and the required condition is satisfied.

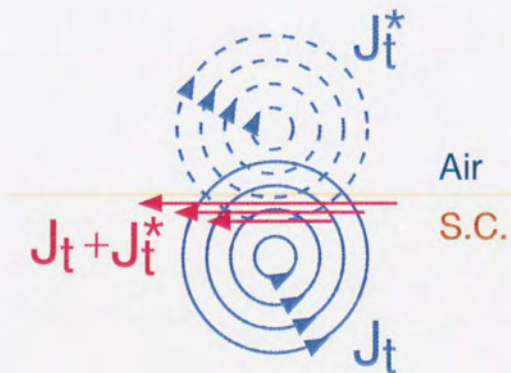


Figure 3.20: Reflected image of the fluxoid near the surface

3.2.11 Initial distribution of fluxoids

In the case that the magnetic flux density $B = B_0 \neq 0$ at time $t = 0$, the initial distribution of the fluxoids were calculated according to the Abrikosov's triangle lattice. The length of the side of the triangle is written as

$$a = \sqrt{\frac{2\Phi_0}{\sqrt{3}B_0}} \quad (3.74)$$

3.3 3-dimensional fluxoid dynamics method

In the previous chapter, the behaviors of the fluxoids in NbTi were simulated by the 2-dimensional Fluxoid Dynamics Method. From the numerical results the evaluation and the prediction of the electromagnetic phenomena have been done and the validity of this method was verified. In this chapter, the development of the 3-dimensional Fluxoid Dynamics Method will be described.

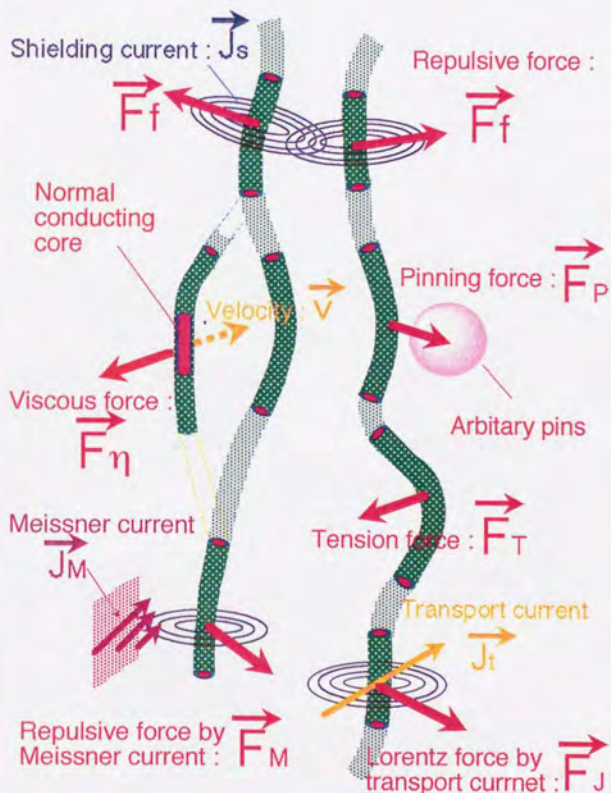


Figure 3.21: 6 kinds of forces acting on the fluxoid

3.3.1 Governing equations of 3D-FD method

In the 3-dimensional FD method, the fluxoids are considered to be affected by 6 kinds of forces as shown in Fig.3.21. Here, the tension due to the curvature of the fluxoid is taken into consideration. In the 2-dimensional FD method, this force was neglected by assuming the uniformity in z-direction.

- F_η : viscous force
- F_p : pinning force
- F_f : repulsive force between two fluxoids
- F_M : Lorentz force due to Meissner current
- F_J : Lorentz force due to transport current
- F_T : Tension

In the 3-dimensional Fluxoid Dynamics, a fluxoid was discretized with the N circular arc elements as shown in Fig.3.22. r_i and r_{i+1} are the location vectors of the nodes which are the both edges of the i -th element and ℓ_i is the length of the i -th element. o_i and R_i are the location vector of the center of curvature and the radius of curvature of the i -th element. n_i is the normal vector which points from the center of the i -th element to o_i . F_i and C_i are the force and torque which are acting on i -th element.

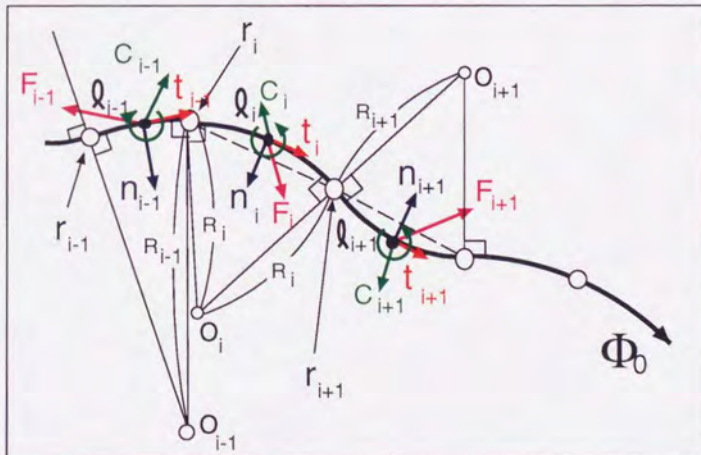


Figure 3.22: Discretization of a fluxoid with arc elements

The governing equations of the 3-dimensional FD method concerning the force and torque are written as follows,

$$\eta_F \mathbf{v}_i = -\mathbf{F}_i^\eta = \sum_j \mathbf{F}_{i,j}^p + \sum_{k,k \neq i} \mathbf{F}_{i,k}^f + \mathbf{F}_i^M + \mathbf{F}_i^J + \mathbf{F}_i^T, \quad (3.75)$$

$$-\mathbf{C}_i^\eta = \sum_j \mathbf{C}_{i,j}^p + \sum_{k,k \neq i} \mathbf{C}_{i,k}^f + \mathbf{C}_i^M + \mathbf{C}_i^J + \mathbf{F}_i^T, \quad (3.76)$$

where the subscripts are the same as the 2-dimensional FD method. The forces and torques are calculated as the line integral of the 2-dimensional forces and torques per unit length along the fluxoid, as follows,

$$\mathbf{F}_i = \int_{-\frac{\ell_i}{2}}^{\frac{\ell_i}{2}} d\mathbf{f}_i d\ell, \quad (3.77)$$

$$\mathbf{C}_i = \int_{-\frac{\ell_i}{2}}^{\frac{\ell_i}{2}} (\mathbf{r} - \mathbf{r}_{g,i}) \times d\mathbf{f}_i d\ell, \quad (3.78)$$

where $d\mathbf{f}_i$ is the force per unit length of i -th element according to the 2-dimensional FD method. And $\mathbf{r}_{g,i}$ is the location vector of center of gravity of the i -th element given as

$$\mathbf{r}_{g,i} \simeq \frac{\mathbf{r}_i + \mathbf{r}_{i+1}}{2} + \frac{\mathbf{w}_i}{3}, \quad (3.79)$$

where \mathbf{w}_i is the deflection vector of the i -th element.

3.3.2 Pinning force and torque

Fig.3.23 shows the pinning force acting on the infinitely small element with length $d\ell$. This force $d\mathbf{f}^p$ can be written as

$$d\mathbf{f}^p = \hat{f}^p(R) \frac{R}{R} d\ell, \quad (3.80)$$

where $\hat{f}^p(R)$ is the amplitude of the pinning force per unit length and \mathbf{r} is the location vector of the arbitrary point on the i -th element. \mathbf{r}_k^p is the location vec-

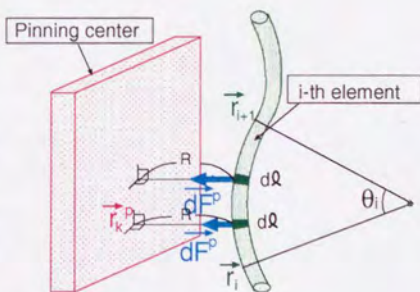


Figure 3.23: Pinning force on i -th element

tor of the perpendicular from \mathbf{r} onto the surface of the k -th pinning center. \mathbf{R} is the vector, $\mathbf{R} = \mathbf{r}_k^p - \mathbf{r}_i$. Then the pinning force and the pinning torque between the i -th element and the k -th pinning center are given as the line integral:

$$\mathbf{F}_i^p = \int_{-\frac{\ell_i}{2}}^{\frac{\ell_i}{2}} d\mathbf{F}^p = \int_{-\frac{\ell_i}{2}}^{\frac{\ell_i}{2}} \hat{f}_p(R) \frac{\mathbf{R}}{R} d\ell, \quad (3.81)$$

$$\mathbf{C}_i^p = \int_{-\frac{\ell_i}{2}}^{\frac{\ell_i}{2}} (\mathbf{r} - \mathbf{r}_{g,i}) \times d\mathbf{F}^p = \int_{-\frac{\ell_i}{2}}^{\frac{\ell_i}{2}} \hat{f}_p(R) (\mathbf{r} - \mathbf{r}_{f,i}) \times \frac{\mathbf{R}}{R} d\ell. \quad (3.82)$$

By applying the Gaussian integral, eqs. (3.81) and (3.82) are transformed as,

$$\mathbf{F}_i^p = \frac{\ell_i}{2} \sum_{k=1}^m \left\{ H_j \hat{f}_p(R(a_k)) \frac{\mathbf{R}(a_k)}{R(a_k)} \right\}, \quad (3.83)$$

$$\mathbf{C}_i^p = \frac{\ell_i}{2} \sum_{k=1}^m \left\{ H_k \hat{f}_p(R(a_k)) (\mathbf{r}(a_k) - \mathbf{r}_{g,i}) \times \frac{\mathbf{R}(a_k)}{R(a_k)} \right\}, \quad (3.84)$$

where H_k and a_k are the weighting coefficient and the representative points of the Gaussian integral.

3.3.3 Magnetic flux density due to each fluxoid

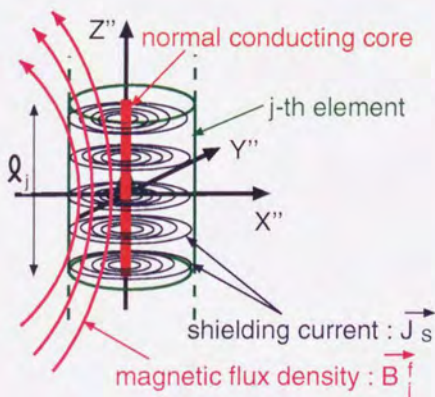


Figure 3.24: Shielding current loop around a fluxoid element

Next, the magnetic flux density which a fluxoid yields will be evaluated. The j -th fluxoid element has the shielding current loops which lie in piles with the length ℓ_j as shown in Fig.3.24. These shielding current loops has the current density,

$$\begin{aligned} \mathbf{j}_s &= j_s(r) \mathbf{e}_\theta \\ &= \frac{\Phi_0}{2\pi\lambda^3} K_1 \left(-\frac{r}{\lambda} \right) \mathbf{e}_\theta \end{aligned} \quad (3.85)$$

where K_1 is the modified Bessel function of the second kind ($n=1$).

Fig.3.25 shows the 2-dimensional shielding current loop which flows in the xy plane and the magnetic flux density $\mathbf{b} = (b_r, 0, b_z)$ due to the plane current loop. These components of the the magnetic flux density \mathbf{b} can be written by using j_s as follows.

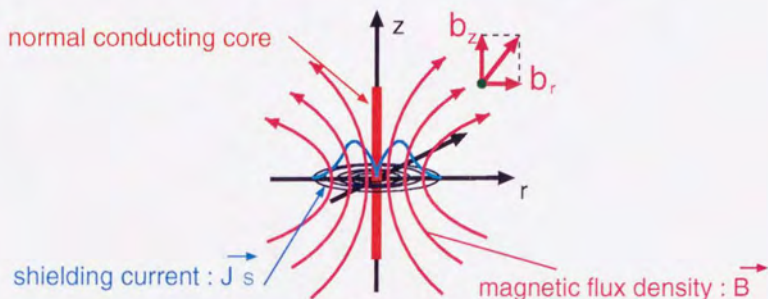


Figure 3.25: Shielding current loop in xy plane and the magnetic field

$$b_r(r, z) = \int_0^\infty \frac{\mu_0 j_s(a)}{2\pi} \frac{z}{r\sqrt{(a+r)^2 + z^2}} \left[\frac{a^2 + r^2 + z^2}{(a-r)^2 + z^2} E - K \right] da, \quad (3.86)$$

$$b_z(r, z) = \int_0^\infty \frac{\mu_0 j_s(a)}{2\pi} \frac{1}{\sqrt{(a+r)^2 + z^2}} \left[\frac{a^2 - r^2 - z^2}{(a-r)^2 + z^2} E + K \right] da, \quad (3.87)$$

where a is the radius around the fluxoid and $j_s(a)$ is the magnitude of the shielding current density at radius= a around a fluxoid. Fig. 3.26 shows the calculation result of $j_s(a)$.

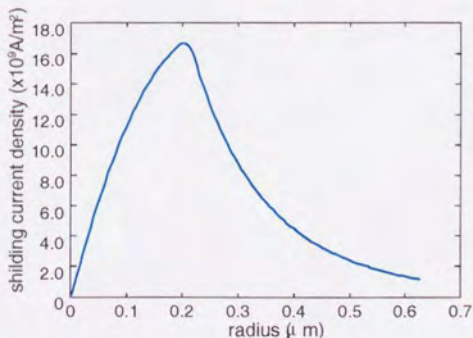


Figure 3.26: Calculation result of the shielding current density $J_s(r)$

And K and E are the complete elliptic integrals,

$$K = \int_0^{\frac{1}{2}\pi} \frac{d\theta}{\sqrt{1 - k^2 \sin^2 \theta}}, \quad (3.88)$$

$$E = \int_0^{\frac{1}{2}\pi} \sqrt{1 - k^2 \sin^2 \theta} d\theta, \quad (3.89)$$

$$k^2 = \frac{4ar}{(a+r)^2 + z^2}$$

Fig. 3.27 shows the calculation results of $b_r(r, z)$ and $b_z(r, z)$.

Here, we consider the j -th fluxoid element which is parallel to z -axis and whose center corresponds to the origin of the coordinate. The magnetic flux density $\mathbf{B}_j = (B_r, 0, B_z)$ yielded by the j -th fluxoid element at the location (r, θ, z) can be written as follows,

$$B_r(r, \theta, z) = \int_{-\frac{\ell_j}{2}}^{\frac{\ell_j}{2}} b_r(r, z - z') dz' = \frac{\ell_j}{2} \sum_{k=1}^m H_k b_r(r, z - \frac{\ell_j}{2} \alpha_k), \quad (3.90)$$

$$B_z(r, \theta, z) = \int_{-\frac{\ell_j}{2}}^{\frac{\ell_j}{2}} b_z(r, z - z') dz' = \frac{\ell_j}{2} \sum_{k=1}^m H_k b_z(r, z - \frac{\ell_j}{2} \alpha_k), \quad (3.91)$$

where H_k and α_k are the weighting coefficient and the representative points of the Gaussian integral.

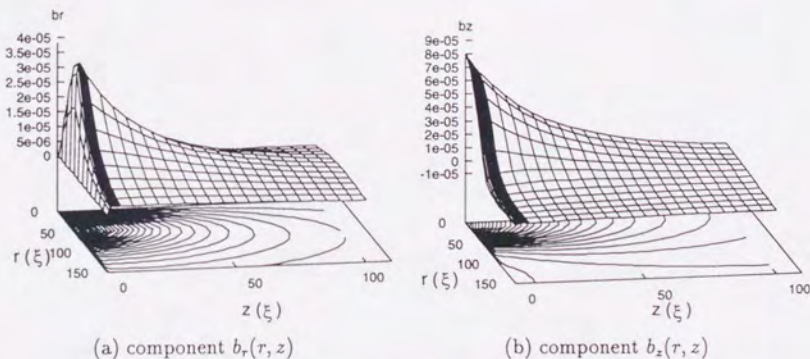


Figure 3.27: Calculation results of $b_r(r, z)$, $b_z(r, z)$

3.3.4 Magnetic flux density due to Meissner current

Next, the magnetic force and torque due to the Meissner current will be derived.

Fig.3.28 shows the magnetic flux density near the surface of the superconductor. The square corresponds to the surface of the superconductor, and the both sides of the square means the superconductor region and the air region, respectively.

B_{ex} is the external magnetic field, and this can be divided to the 2 components as,

$$B_{ex} = B_{ex,n} + B_{ex,t} = B_{ex,n} \mathbf{n} + B_{ex,t} \mathbf{t} \quad (3.92)$$

where \mathbf{n} and \mathbf{t} is the normal and tangential vector of the surface of the superconductor.

The tangential component of the external magnetic flux density inside of the superconductor, $B_{in,t}$, is shielded by the Meissner current and decreases exponentially, as

$$B_{in,t}(d_i) = B_{ex,t} \exp\left(-\frac{d_i}{\lambda}\right), \quad (3.93)$$

where d_i is the distance from the surface of the superconductor and λ is the London's magnetic penetration depth. Then the magnetic flux density which the Meissner current yields, B_M is obtained as follows,

$$\begin{aligned} B_M(d_i) &= B_{in,t} - B_{ex,t} \\ &= B_{ex,t} \left\{ \exp\left(-\frac{d_i}{\lambda}\right) - 1 \right\} \end{aligned} \quad (3.94)$$

As shown in Fig. 3.28, this magnetic flux density has only the component which is parallel to the surface of the superconductor.

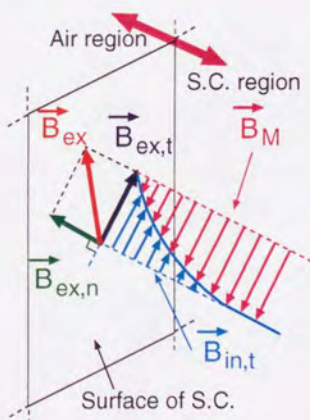


Figure 3.28: Meissner field near the surface of the superconductor

3.3.5 Magnetical repulsive force and torque

From the previous sections, it was found that the total magnetic flux density at the arbitrary location \mathbf{r} can be given as follows,

$$\mathbf{B}(\mathbf{r}) = \mathbf{B}_f(\mathbf{r}) + \mathbf{B}_M(\mathbf{r}). \quad (3.95)$$

Then the calculation method of the magnetical repulsive force and torque flux density \mathbf{F}_m and \mathbf{C}_m due to the total magnetic flux density \mathbf{B} will be derived.

Here, we consider the i -th element of fluxoid which is parallel to the z -axis and whose radius is a_{eff} . Furthermore we consider the rectangular prism which is circumscribed with the i -th element as shown in Fig.3.29.

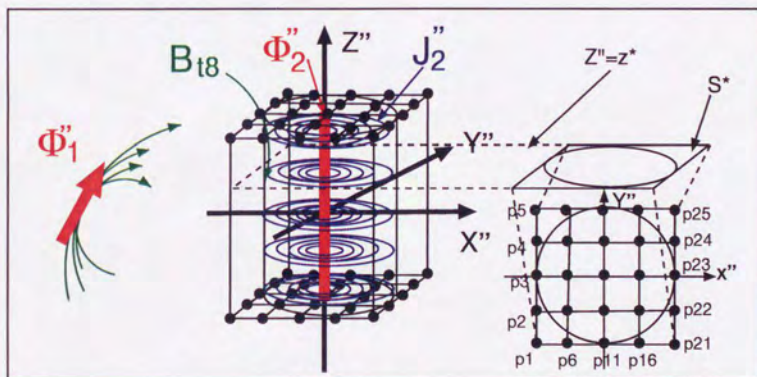


Figure 3.29: The i -th element and magnetic flux density at 25 nodes

The Lorentz force acting on the infinitely small length of the i -th element, $d\ell$, can be written as

$$d\mathbf{f}_{i,j}^f = \mathbf{J}_{s,i} \times \mathbf{B}_{f,j}, \quad (3.96)$$

where $\mathbf{B}_{f,j}$ is the magnetic flux density by the j -th element and $\mathbf{J}_{s,i}$ is the shielding current density around the i -th element.

Then the magnetic force and torque acting on the i -th element from the j -th element can be written as the integral of eq.(3.96) around the i -th element as follows

$$F_{i,j}^f = \int_{-\frac{\ell_i}{2}}^{\frac{\ell_i}{2}} \int_0^\infty \int_0^{2\pi} df_{i,j}^f d\theta dr d\ell, \quad (3.97)$$

$$C_{i,j}^f = \int_{-\frac{\ell_i}{2}}^{\frac{\ell_i}{2}} \int_0^\infty \int_0^{2\pi} (\mathbf{r} - \mathbf{r}_{ci}) \times df_{i,j}^f d\theta dr d\ell. \quad (3.98)$$

3.3.6 Lorentz force and torque due to transport current

The transport current flowing in the type-II superconductor interact with the magnetic field around the fluxoid and yields the Lorentz force. This Lorentz force per unit length acting on the i -th fluxoid element can be written as

$$dF_i^J = \int_0^{2\pi} \int_0^\infty \mathbf{J}_t \times \mathbf{B}^J(r') dr' d\theta = \mathbf{J}_t \times (\Phi_0 \mathbf{t}), \quad (3.99)$$

where \mathbf{t} is the tangential vector of $d\ell$ and Φ_0 is the quantumized flux as shown in Fig. 3.30.

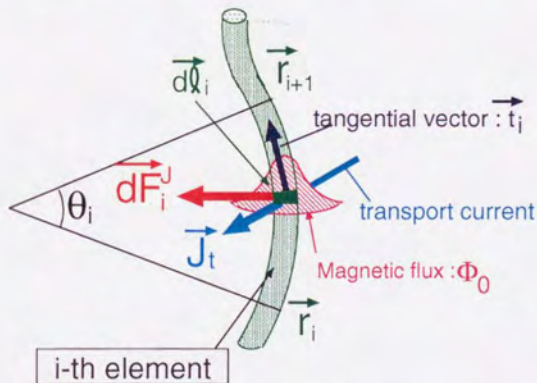


Figure 3.30: Lorentz force acting on the infinitely small length $d\ell$

Then the Lorentz force and torque acting on the i -th element can be obtained as the line integral of dF_i^J along the i -th element as follows,

$$\mathbf{F}_i^J = \int_{-\frac{\ell_i}{2}}^{\frac{\ell_i}{2}} dF_i^J d\ell_i = \int_{-\frac{\ell_i}{2}}^{\frac{\ell_i}{2}} \mathbf{J}_t \times (\Phi_0 \mathbf{t}_i) d\ell_i, \quad (3.100)$$

$$C_i^J = \int_{-\frac{\ell_i}{2}}^{\frac{\ell_i}{2}} (\mathbf{r} - \mathbf{r}_{gi}) \times d\mathbf{F}_i^J d\ell_i' = \int_{-\frac{\ell_i}{2}}^{\frac{\ell_i}{2}} (\mathbf{r} - \mathbf{r}_{gi}) \times (\mathbf{J}_i \times (\Phi_0 \mathbf{t}_i)) d\ell_i'. \quad (3.101)$$

By applying the Gaussian integral, eqs. (3.100) and (3.101) are transformed as,

$$\mathbf{F}_i^J = \frac{\Phi_0 \ell_i}{2} \sum_{k=1}^m H_k \mathbf{J}_i \times \mathbf{t}_i(a_k), \quad (3.102)$$

$$C_i^J = \frac{\Phi_0 \ell_i}{2} \sum_{k=1}^m H_k \{(\mathbf{r}(a_k) - \mathbf{r}_{gi}) \times \mathbf{t}_i(a_k)\} \quad (3.103)$$

where H_k and a_k are the weighting coefficient and the representative points of the Gaussian integral.

3.3.7 Tension force

When the fluxoid has the curvature, the tension force acts on the fluxoid. By assuming that the curvature is constant in a fluxoid element, the tension force per unit length of the i -th element can be written as

$$\mathbf{f}_i^T = \frac{\Phi_0^2}{2\mu_0 S} \frac{1}{R_{c,i}} \mathbf{n}_i \quad (3.104)$$

where $R_{c,i}$ is the radius of curvature and S is the cross section of the i -th element. \mathbf{n}_i is the unit vector pointing from the center of the i -th element to the center of curvature of the i -th element (see Fig.3.31).

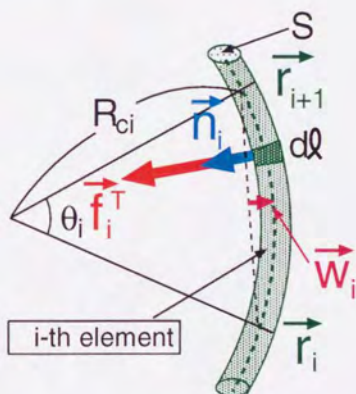


Figure 3.31: Tension acting on the infinitely small length dl

Then the tension force and torque acting on the i -th element are obtained as the line integral along the length of the i -th element as follows,

$$\mathbf{F}_i^T = \int_{-\frac{\ell_i}{2}}^{\frac{\ell_i}{2}} \mathbf{f}_i^T dl = \frac{\Phi_0^2}{2\mu_0 S} \frac{1}{R_{c,i}} \int_{-\frac{\ell_i}{2}}^{\frac{\ell_i}{2}} \mathbf{n}_i dl, \quad (3.105)$$

$$C_i^T = \int_{-\frac{\ell_i}{2}}^{\frac{\ell_i}{2}} (\mathbf{r} - \mathbf{r}_{c,i}) \times \mathbf{f}_i^T d\ell = \frac{\Phi_0^2}{2\mu_0 S} \frac{1}{R_{c,i}} \int_{-\frac{\ell_i}{2}}^{\frac{\ell_i}{2}} (\mathbf{r} - \mathbf{r}_{c,i}) \times \mathbf{n}_i d\ell. \quad (3.106)$$

Here, eq.(3.106) can be rewritten because of the symmetry about $\mathbf{r}_{c,i}$ written as

$$C_i^T = 0. \quad (3.107)$$

The normal vector \mathbf{n}_i can be divided to two components as follows,

$$\mathbf{n}_i = \mathbf{n}_{c,i} \cos \theta' - \mathbf{t}_{c,i} \sin \theta', \quad (3.108)$$

where $\mathbf{n}_{c,i}$ and $\mathbf{t}_{c,i}$ are the normal and tangential vectors at the center of the i -th element.

Then the line integral of eq.(3.108) becomes

$$\begin{aligned} \int_{-\frac{\ell_i}{2}}^{\frac{\ell_i}{2}} \mathbf{n}_i d\ell' &= \int_{-\frac{\theta_i}{2}}^{\frac{\theta_i}{2}} \mathbf{n}_i R_{c,i} d\theta' \\ &= R_{c,i} \left\{ \mathbf{n}_{c,i} \int_{-\frac{\theta_i}{2}}^{\frac{\theta_i}{2}} \cos \theta' d\theta' - \mathbf{t}_{c,i} \int_{-\frac{\theta_i}{2}}^{\frac{\theta_i}{2}} \sin \theta' d\theta' \right\} \\ &= \mathbf{n}_{c,i} \left\{ 2R_{c,i} \sin \left(\frac{\theta_i}{2} \right) \right\}, \end{aligned} \quad (3.109)$$

where θ_i is the angle of the i -th arc element, and is represented by using the bending vector of i -th element \mathbf{w}_i as follows,

$$\theta_i = 2 \sin^{-1} \left(\frac{|\mathbf{w}_i|}{\sqrt{|\mathbf{w}_i|^2 + \left(\frac{|\mathbf{r}_{i+1} - \mathbf{r}_i|}{2} \right)^2}} \right). \quad (3.110)$$

Furthermore, the normal vector $\mathbf{n}_{c,i}$, can be rewritten as

$$\mathbf{n}_{c,i} = -\frac{\mathbf{w}_i}{|\mathbf{w}_i|}. \quad (3.111)$$

Substituting eqs.(3.109) and (3.111) into eq.(3.105), the tension force \mathbf{F}_i^T can be obtained as,

$$\mathbf{F}_i^T = -\frac{\Phi_0^2}{\mu_0 S |\mathbf{w}_i|} \sin \left(\frac{\theta_i}{2} \right) \mathbf{w}_i. \quad (3.112)$$

3.3.8 Viscous coefficient of fluxoid

In the 2-dimensional Fluxoid Dynamics, the viscous coefficient per unit length of the fluxoid was obtained from the Ginzburg-Landau theory as

$$\hat{\eta} = 6.1993 \times 10^{-8} \text{ (N} \cdot \text{s/m)}. \quad (3.113)$$

In this section, the 3-dimensional viscous force and torque will be evaluated using $\hat{\eta}$.

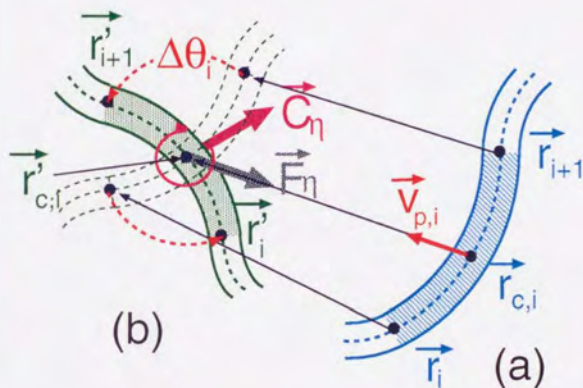


Figure 3.32: The translation and rotation of the i -th fluxoid element

Fig.3.32 shows the translation and rotation of the i -th fluxoid element. Here, the translation vector, $\mathbf{v}_{p,i}$, and the rotation vector, $\mathbf{v}_{c,i}$ of the arbitrary point on the i -th element can be written as

$$\begin{aligned} \mathbf{v}_{p,i} &\simeq \frac{\partial}{\partial t} \left\{ \mathbf{r}_{c,i} + \left(\frac{|\ell'|}{\ell_i/2} - 1 \right) \mathbf{w}_i \right\} = \frac{\partial}{\partial t} \left\{ \frac{\mathbf{r}_{i+1} + \mathbf{r}_i}{2} + \mathbf{w}_i + \left(\frac{|\ell'|}{\ell_i/2} - 1 \right) \mathbf{w}_i \right\} \\ &= \frac{\partial}{\partial t} \left(\frac{\mathbf{r}_{i+1} + \mathbf{r}_i}{2} + \frac{|\ell'|}{\ell_i/2} \mathbf{w}_i \right) \\ &= \frac{\mathbf{r}_i^{(k+1)} + \mathbf{r}_{i+1}^{(k+1)} - \mathbf{r}_i^{(k)} - \mathbf{r}_{i+1}^{(k)}}{2\Delta t} + \frac{2|\ell'|}{\ell_i} \frac{\mathbf{w}_i^{(k+1)} - \mathbf{w}_i^{(k)}}{\Delta t}, \end{aligned} \quad (3.114)$$

$$\mathbf{v}_{c,i} = \ell' \frac{\partial \hat{\theta}_i}{\partial t} \hat{\theta}_i = \ell' \frac{\Delta \hat{\theta}_i}{\Delta t} \hat{\theta}_i = \ell' \frac{\hat{\theta}_i^{(k+1)} - \hat{\theta}_i^{(k)}}{\Delta t} \hat{\theta}_i, \quad (3.115)$$

where $\mathbf{r}_{c,i}$ and \mathbf{w}_i are the location vector and the deflection vector at the center of the i -th element. ℓ' is the parameter which means the distance between the arbitrary point on the i -th element and the center of the i -th element ($-\ell_i/2 \leq \ell' \leq \ell_i/2$). θ_i is the angle of rotation of the i -th element and $\hat{\theta}_i$ is the unit vector of rotation. Δt is the time division. The subscripts (k) and $(k+1)$ mean the numbers of the time steps.

Using eq.(3.114), the viscous force acting on the i -th element can be obtained as,

$$\begin{aligned} \mathbf{F}_{\eta i} &= \int_{-\frac{\ell_i}{2}}^{\frac{\ell_i}{2}} -\hat{\eta} \mathbf{v}_{p,i} d\ell' \\ &= -\frac{\hat{\eta} \ell_i}{2\Delta t} (\mathbf{r}_i^{(k+1)} + \mathbf{r}_{i+1}^{(k+1)} - \mathbf{r}_i^{(k)} - \mathbf{r}_{i+1}^{(k)}) - \frac{\hat{\eta}}{\ell_i \Delta t} \left(\int_{-\frac{\ell_i}{2}}^{\frac{\ell_i}{2}} 2|\ell'| d\ell' \right) (\mathbf{w}_i^{(k+1)} - \mathbf{w}_i^{(k)}) \\ &= -\frac{\hat{\eta} \ell_i}{2\Delta t} \{ (\mathbf{r}_i^{(k+1)} + \mathbf{w}_i^{(k+1)} + \mathbf{r}_{i+1}^{(k+1)}) - (\mathbf{r}_i^{(k)} + \mathbf{w}_i^{(k)} + \mathbf{r}_{i+1}^{(k)}) \} \end{aligned} \quad (3.116)$$

Next, the arbitrary point on the i -th element can be expressed using the unit vector $\hat{\mathbf{r}}$ as follows,

$$\mathbf{r} = \mathbf{r}_{c,i} + \ell' \hat{\mathbf{r}}. \quad (3.117)$$

Substituting eq.(3.117), the viscous torque is represented as,

$$\begin{aligned} C_{\eta i} &= \int_{-\frac{\ell_i}{2}}^{\frac{\ell_i}{2}} (\mathbf{r} - \mathbf{r}_{c,i}) \times (-\hat{\eta} \mathbf{v}_{c,i}) d\ell' = \int_{-\frac{\ell_i}{2}}^{\frac{\ell_i}{2}} (\mathbf{r} - \mathbf{r}_{c,i}) \times \left(-\hat{\eta} \ell' \frac{\Delta \theta_i}{\Delta t} \right) \hat{\theta}_i d\ell' \\ &= -\hat{\eta} \frac{\Delta \theta_i}{\Delta t} \left(\int_{-\frac{\ell_i}{2}}^{\frac{\ell_i}{2}} \ell'^2 d\ell' \right) \hat{\mathbf{r}} \times \hat{\theta}_i \\ &= -\frac{\hat{\eta} \ell_i^3 \Delta \theta_i}{12\Delta t} \hat{\mathbf{r}} \times \hat{\theta}_i. \end{aligned} \quad (3.118)$$

The vector $\hat{\mathbf{r}} \times \hat{\theta}_i$ corresponds to the following vector product,

$$\begin{aligned} \hat{\mathbf{r}} \times \hat{\theta}_i &= \frac{(\mathbf{r}_{i+1}^{(k)} - \mathbf{r}_i^{(k)}) \times (\mathbf{r}_{i+1}^{(k+1)} - \mathbf{r}_i^{(k+1)})}{|\mathbf{r}_{i+1}^{(k+1)} - \mathbf{r}_i^{(k+1)}| |\mathbf{r}_{i+1}^{(k)} - \mathbf{r}_i^{(k)}| \sin \Delta \theta} \simeq \frac{(\mathbf{r}_{i+1}^{(k)} - \mathbf{r}_i^{(k)}) \times (\mathbf{r}_{i+1}^{(k+1)} - \mathbf{r}_i^{(k+1)})}{|\mathbf{r}_{i+1}^{(k)} - \mathbf{r}_i^{(k)}|^2 \Delta \theta} \\ &= \frac{(\mathbf{r}_{i+1}^{(k)} - \mathbf{r}_i^{(k)}) \times (\mathbf{r}_{i+1}^{(k+1)} - \mathbf{r}_i^{(k+1)})}{|\mathbf{g}_i|^2 \Delta \theta} \\ &= \frac{1}{|\mathbf{g}_i|^2 \Delta \theta} \left\{ \begin{aligned} &(\mathbf{r}_{i+1}^{(k)} - \mathbf{r}_i^{(k)})_y (\mathbf{r}_{i+1}^{(k+1)} - \mathbf{r}_i^{(k+1)})_z - (\mathbf{r}_{i+1}^{(k)} - \mathbf{r}_i^{(k)})_z (\mathbf{r}_{i+1}^{(k+1)} - \mathbf{r}_i^{(k+1)})_y \\ &(\mathbf{r}_{i+1}^{(k)} - \mathbf{r}_i^{(k)})_z (\mathbf{r}_{i+1}^{(k+1)} - \mathbf{r}_i^{(k+1)})_x - (\mathbf{r}_{i+1}^{(k)} - \mathbf{r}_i^{(k)})_x (\mathbf{r}_{i+1}^{(k+1)} - \mathbf{r}_i^{(k+1)})_z \\ &(\mathbf{r}_{i+1}^{(k)} - \mathbf{r}_i^{(k)})_x (\mathbf{r}_{i+1}^{(k+1)} - \mathbf{r}_i^{(k+1)})_y - (\mathbf{r}_{i+1}^{(k)} - \mathbf{r}_i^{(k)})_y (\mathbf{r}_{i+1}^{(k+1)} - \mathbf{r}_i^{(k+1)})_x \end{aligned} \right\} \end{aligned}$$

$$= \frac{1}{|\mathbf{g}_i|^2 \Delta t} \begin{bmatrix} 0 & g_{i,x} & -g_{i,y} & 0 & 0 & 0 & 0 & -g_{i,x} & g_{i,y} \\ -g_{i,x} & 0 & g_{i,x} & 0 & 0 & 0 & g_{i,x} & 0 & -g_{i,x} \\ g_{i,y} & -g_{i,x} & 0 & 0 & 0 & 0 & -g_{i,y} & g_{i,x} & 0 \end{bmatrix} \begin{Bmatrix} \tau_{i,x}^{(k+1)} \\ \tau_{i,y}^{(k+1)} \\ \tau_{i,z}^{(k+1)} \\ w_{i,x}^{(k+1)} \\ w_{i,y}^{(k+1)} \\ w_{i,z}^{(k+1)} \\ \tau_{i+1,x}^{(k+1)} \\ \tau_{i+1,y}^{(k+1)} \\ \tau_{i+1,z}^{(k+1)} \end{Bmatrix}, \quad (3.119)$$

where \mathbf{g}_i is the vector $\mathbf{g}_i = \mathbf{r}_{i+1}^{(k)} - \mathbf{r}_i^{(k)}$. From eqs.(3.118) and (3.119), the viscous torque $C_{\eta,i}$ is obtained as,

$$C_{\eta,i} = -\frac{\hat{\eta} \ell_i^3}{12 \Delta t |\mathbf{g}_i|^2} \begin{bmatrix} 0 & g_{i,x} & -g_{i,y} & 0 & 0 & 0 & 0 & -g_{i,x} & g_{i,y} \\ -g_{i,x} & 0 & g_{i,x} & 0 & 0 & 0 & g_{i,x} & 0 & -g_{i,x} \\ g_{i,y} & -g_{i,x} & 0 & 0 & 0 & 0 & -g_{i,y} & g_{i,x} & 0 \end{bmatrix} \begin{Bmatrix} \tau_{i,x}^{(k+1)} \\ \tau_{i,y}^{(k+1)} \\ \tau_{i,z}^{(k+1)} \\ w_{i,x}^{(k+1)} \\ w_{i,y}^{(k+1)} \\ w_{i,z}^{(k+1)} \\ \tau_{i+1,x}^{(k+1)} \\ \tau_{i+1,y}^{(k+1)} \\ \tau_{i+1,z}^{(k+1)} \end{Bmatrix} \quad (3.120)$$

Furthermore, eqs.(3.116) and (3.120) can be transformed to the following matrix equations,

$$-\mathbf{F}_{\eta,i} = [M_{F,i}] \{X_i^{(k+1)}\} - [M_{F,i}] \{X_i^{(k)}\} \quad (3.121)$$

$$-\mathbf{C}_{\eta,i} = [M_{C,i}] \{X_i^{(k+1)}\}, \quad (3.122)$$

where

$$\begin{aligned} \{X_i^{(k)}\} &= \{\mathbf{r}_i^{(k)}, \mathbf{w}_i^{(k)}, \mathbf{r}_{i+1}^{(k)}\}^T \\ &= \{\tau_{i,x}^{(k)}, \tau_{i,y}^{(k)}, \tau_{i,z}^{(k)}, w_{i,x}^{(k)}, w_{i,y}^{(k)}, w_{i,z}^{(k)}, \tau_{i+1,x}^{(k)}, \tau_{i+1,y}^{(k)}, \tau_{i+1,z}^{(k)}\}^T \end{aligned} \quad (3.123)$$

$$[M_{\eta,F}] = \frac{\hat{\eta} \ell_i}{2 \Delta t} [I_9] \quad (3.124)$$

$$[M_{\eta,C}] = \frac{\hat{\eta} \ell_i^3}{12 \Delta t |\mathbf{g}_i|^2} \begin{bmatrix} 0 & g_{i,x} & -g_{i,y} & 0 & 0 & 0 & 0 & -g_{i,x} & g_{i,y} \\ -g_{i,x} & 0 & g_{i,x} & 0 & 0 & 0 & g_{i,x} & 0 & -g_{i,x} \\ g_{i,y} & -g_{i,x} & 0 & 0 & 0 & 0 & -g_{i,y} & g_{i,x} & 0 \end{bmatrix} \quad (3.125)$$

$[I_9]$ is the eigen matrix (9×9).

3.3.9 Binding condition and edge condition

(1) Binding condition

For the binding condition between adjacent two elements, it was assumed that the two tangential vectors of the i -th and $(i+1)$ -th elements at the i -th node, $-t_i^2$, t_i^1 are equal as shown in Fig.3.33. The tangential vectors t_i^2 and t_i^1 are represented as follows,

$$t_i^2 = \frac{r_i^{(k+1)} - r_{i-1}^{(k+1)} - |g_{i-1}| \tan\left(\frac{\theta_{i-1}}{2}\right) \frac{w_{i-1}^{(k+1)}}{|w_{i-1}^{(k)}|}}{\left| r_i^{(k)} - r_{i-1}^{(k)} - |g_{i-1}| \tan\left(\frac{\theta_{i-1}}{2}\right) \frac{w_{i-1}^{(k)}}{|w_{i-1}^{(k)}|} \right|} \quad (3.126)$$

$$-t_i^1 = \frac{r_{i+1}^{(k+1)} - r_i^{(k+1)} + |g_i| \tan\left(\frac{\theta_i}{2}\right) \frac{w_i^{(k+1)}}{|w_i^{(k)}|}}{\left| r_{i+1}^{(k)} - r_i^{(k)} + |g_i| \tan\left(\frac{\theta_i}{2}\right) \frac{w_i^{(k)}}{|w_i^{(k)}|} \right|}. \quad (3.127)$$

Here, we defined the following coefficients,

$$\begin{aligned} \alpha_i &= |g_i| \tan\left(\frac{\theta_i}{2}\right) \frac{1}{|w_i^{(k)}|}, \\ \beta_i^1 &= \left| r_{i+1}^{(k)} - r_i^{(k)} - \alpha_i w_i^{(k)} \right|, \quad (3.128) \\ \beta_i^2 &= \left| r_{i+1}^{(k)} - r_i^{(k)} + \alpha_i w_i^{(k)} \right|. \end{aligned}$$

$$(1 \leq i \leq n)$$

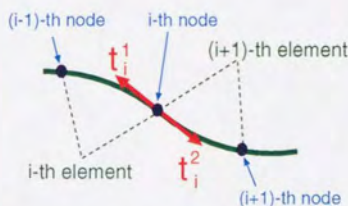


Figure 3.33: Unit vectors at the i -th node t_i^1 , t_i^2 ($2 \leq i \leq n$)

From the condition $t_i^2 = -t_i^1$ and eqs.(3.126), (3.127) and (3.128), the binding condition can be written as,

$$\beta_{i+1}^2 r_i^{(k+1)} + \alpha_i \beta_{i+1}^2 w_i^{(k+1)} - (\beta_i^1 + \beta_{i+1}^2) r_{i+1}^{(k+1)} + \alpha_{i+1} \beta_i^1 w_{i+1}^{(k+1)} + \beta_i^1 r_{i+2}^{(k+1)} = \mathbf{o}. \quad (3.129)$$

Futhermore, eq.(3.129) can be transformed as following matrix equation,

$$[M_{B,i}] \{Y_i^{(k+1)}\} = \mathbf{o}. \quad (3.130)$$

Here the matrix $[M_{B,i}]$ and $\{Y_i^{(k+1)}\}$ can be represented as

$$[M_{B,i}] = [\beta_{i+1}^2[I_3], \alpha_i \beta_{i+1}^2[I_3], -(\beta_i^2 + \beta_{i+1}^2)[I_3], \alpha_{i+1} \beta_{i+1}^2[I_3], \beta_{i+2}^2[I_3]] \quad (3.131)$$

$$\begin{aligned} \{Y_i^{(k)}\} &= \{\mathbf{r}_i^{(k)}, \mathbf{w}_i^{(k)}, \mathbf{r}_{i+1}^{(k)}, \mathbf{w}_{i+1}^{(k)}, \mathbf{r}_{i+2}^{(k)}\}^T \\ &= \{r_{i,x}^{(k)}, r_{i,y}^{(k)}, r_{i,z}^{(k)}, w_{i,x}^{(k)}, w_{i,y}^{(k)}, w_{i,z}^{(k)}, r_{i+1,x}^{(k)}, r_{i+1,y}^{(k)}, r_{i+1,z}^{(k)}, \\ &\quad w_{i+1,x}^{(k)}, w_{i+1,y}^{(k)}, w_{i+1,z}^{(k)}, r_{i+2,x}^{(k)}, r_{i+2,y}^{(k)}, r_{i+2,z}^{(k)}\}^T, \end{aligned} \quad (3.132)$$

where $[I_3]$ is the eigen matrix (3×3).

(2) Edge condition

For the edge condition of one fluxoid, it was assumed that the tangential vectors at the both nodes of the fluxoid edges, \mathbf{t}_s^1 and \mathbf{t}_{e+1}^2 , are parallel to the external magnetic flux density, B_{ex} as shown in Fig.3.34. s and e are the number of the elements of both edges of the fluxoid ($s < e$). Then the relation between \mathbf{t}_s^1 and \mathbf{t}_{e+1}^2 can be expressed as,

$$-\mathbf{t}_s^1 = \mathbf{t}_{e+1}^2 = \frac{B_{ex}}{|B_{ex}|} = \mathbf{b}_{ex} \quad (3.133)$$

where \mathbf{b}_{ex} is the normalized magnetic flux density. The tangential vectors \mathbf{t}_s^1 and \mathbf{t}_{e+1}^2 are represented as follows,

$$-\mathbf{t}_s^1 = \frac{\mathbf{r}_{s+1}^{(k+1)} - \mathbf{r}_s^{(k+1)} + |g_s| \tan\left(\frac{\theta_s}{2}\right) \frac{\mathbf{w}_s^{(k+1)}}{|\mathbf{w}_s^{(k+1)}|}}{\left| \mathbf{r}_{s+1}^{(k)} - \mathbf{r}_s^{(k)} + |g_s| \tan\left(\frac{\theta_s}{2}\right) \frac{\mathbf{w}_s^{(k)}}{|\mathbf{w}_s^{(k)}|} \right|} \quad \text{and} \quad (3.134)$$

$$\mathbf{t}_{e+1}^2 = \frac{\mathbf{r}_{e+1}^{(k+1)} - \mathbf{r}_e^{(k+1)} - |g_e| \tan\left(\frac{\theta_e}{2}\right) \frac{\mathbf{w}_e^{(k+1)}}{|\mathbf{w}_e^{(k+1)}|}}{\left| \mathbf{r}_{e+1}^{(k)} - \mathbf{r}_e^{(k)} - |g_e| \tan\left(\frac{\theta_e}{2}\right) \frac{\mathbf{w}_e^{(k)}}{|\mathbf{w}_e^{(k)}|} \right|} \quad (3.135)$$

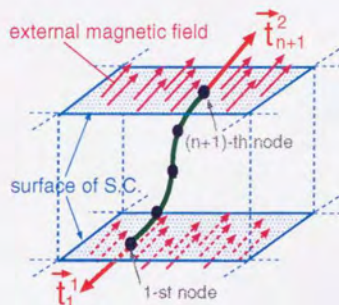


Figure 3.34: Unit vectors at the both edges of fluxoid contacting with the superconductor's surface

From eqs.(3.133), (3.134) and (3.135), the edge condition is obtained as follows,

$$-\mathbf{r}_s^{(k+1)} + \alpha_s \mathbf{w}_s^{(k+1)} + \mathbf{r}_{s+1}^{(k+1)} = \beta_s^2 \mathbf{b}_{ez} \quad (3.136)$$

$$-\mathbf{r}_e^{(k+1)} - \alpha_e \mathbf{w}_e^{(k+1)} + \mathbf{r}_{e+1}^{(k+1)} = \beta_e^1 \mathbf{b}_{ez} \quad (3.137)$$

These equations are transformed to the matrix equation,

$$[M_{E1s}] \{X_s^{(k+1)}\} = \beta_s^2 \{\mathbf{b}_{ez}\}, \quad (3.138)$$

$$[M_{E2e}] \{X_e^{(k+1)}\} = \beta_e^1 \{\mathbf{b}_{ez}\}, \quad (3.139)$$

where

$$[M_{E1s}] = [-[I_3], \alpha_s [I_3], [I_3]], \quad (3.140)$$

$$[M_{E2e}] = [-[I_3], -\alpha_e [I_3], [I_3]]. \quad (3.141)$$

Furthermore, when the surface of the superconductor is represented as $z = 0$ and $z = L_z$, the following condition can be derived concerning the two edge nodes $\mathbf{r}_s = (r_{s,x}, r_{s,y}, r_{s,z})$ and $\mathbf{r}_{e+1} = (r_{e+1,x}, r_{e+1,y}, r_{e+1,z})$,

$$r_{s,z}^{(k+1)} = 0, \quad r_{e+1,z}^{(k+1)} = L_z. \quad (3.142)$$

3.3.10 Solution of the governing equations

It is assumed that the fluxoid to be solved consists of the s -th $\sim e$ -th elements. Then from eqs.(3.75), (3.76), (3.121), (3.122), (3.130), (3.138) and (3.139), the following matrix equations can be obtained for the i -th element ($s \leq i \leq e$),

if $i = s$

$$\begin{bmatrix} [M_{C,s}], [0] \\ [M_{F,s}], [0] \\ [M_{E1,s}], [0] \end{bmatrix} \{Y_s^{(k+1)}\} = \left\{ \begin{array}{l} C_s^{ip} + C_s^{if} + C_s^M + C_s^J \\ F_s^{ip} + F_s^{if} + F_s^M + F_s^J + F_s^T + [M_{F,s}] \{X_s^{(k)}\} \\ \beta_s^2 \mathbf{b}_{ez} \end{array} \right\} = \{Z_s^{(k)}\}, \quad (3.143)$$

if $s < i < e$

$$\begin{bmatrix} [M_{C,i}], [0] \\ [M_{F,i}], [0] \\ [M_{B,i}] \end{bmatrix} \{Y_i^{(k+1)}\} = \left\{ \begin{array}{l} C_i^{ip} + C_i^{if} + C_i^M + C_i^J \\ F_i^{ip} + F_i^{if} + F_i^M + F_i^J + F_i^T + [M_{\eta,F}] \{X_i^{(k)}\} \\ \mathbf{0} \end{array} \right\} = \{Z_i^{(k)}\}, \quad (3.144)$$

if $i = e$

$$\begin{bmatrix} [M_{C,e}], [0] \\ [M_{F,e}], [0] \\ [M_{E2,e}], [0] \end{bmatrix} \{Y_e^{(k+1)}\} = \left\{ \begin{array}{l} C_e^{ip} + C_e^{if} + C_e^M + C_e^J \\ F_e^{ip} + F_e^{if} + F_e^M + F_e^J + F_e^T + [M_{\eta,F}] \{X_i^{(k)}\} \\ \beta_e^1 b_{ez} \end{array} \right\} = \{Z_e^{(k)}\}, \quad (3.145)$$

where $[0]$ is the zero matrix (3×6), and C_i^{ip} , C_i^{if} , F_i^{ip} and F_i^{if} ($s \leq i \leq e$) are represented as

$$C_i^{ip} = \sum_j C_{i,j}^p, \quad C_i^{if} = \sum_{k,k \neq i} C_{i,k}^f, \quad F_i^{ip} = \sum_j F_{i,j}^p, \quad F_i^{if} = \sum_{k,k \neq i} F_{i,k}^f. \quad (3.146)$$

The eqs.(??), (??) and (3.145) can be rewritten as

$$[M_i^a][M_i^b][M_i^c][M_i^d][M_i^e] \{Y_i^{(k+1)}\} = \{Z_i^{(k)}\}, \quad (s \leq i \leq e) \quad (3.147)$$

where $[M_i^a]$, $[M_i^b]$ and $[M_i^c]$ are (9×3) matrices.

Furthermore, the matrix equation of this fluxoid can be represented by combining eq.(??) as follows,

$$[\overline{M}] \{\overline{Y}^{(k+1)}\} = \{\overline{Z}^{(k)}\}, \quad (3.148)$$

where

$$[\overline{M}] = \begin{bmatrix} [M_s^a] & [M_s^b] & [M_s^c] & [M_s^d] & [M_s^e] & 0 & 0 & 0 \\ 0 & 0 & [M_{s+1}^a] & [M_{s+1}^b] & [M_{s+1}^c] & [M_{s+1}^d] & [M_{s+1}^e] & 0 \\ 0 & 0 & 0 & 0 & [M_{s+2}^a] & [M_{s+2}^b] & [M_{s+2}^c] & \ddots \\ & & & & \vdots & & & \\ 0 & 0 & 0 & 0 & 0 & 0 & 0 & 0 \\ 0 & 0 & 0 & 0 & 0 & 0 & 0 & 0 \\ & & 0 & 0 & 0 & 0 & 0 & 0 & 0 \\ \dots & & 0 & 0 & 0 & 0 & 0 & 0 & 0 \\ & & 0 & 0 & 0 & 0 & 0 & 0 & 0 \\ & & & & \vdots & & & & \\ \dots & [M_{e-1}^a] & [M_{e-1}^b] & [M_{e-1}^c] & [M_{e-1}^d] & [M_{e-1}^e] & 0 & 0 \\ \dots & 0 & 0 & [M_e^a] & [M_e^b] & [M_e^c] & [M_e^d] & [M_e^e] \end{bmatrix} \quad (3.149)$$

$$\{\overline{Y}^{(k+1)}\} = \begin{Bmatrix} r_s^{(k+1)} \\ w_s^{(k+1)} \\ r_{s+1}^{(k+1)} \\ \vdots \\ w_e^{(k+1)} \\ r_{e+1}^{(k+1)} \end{Bmatrix}, \quad \{\overline{Z}^{(k)}\} = \begin{Bmatrix} Z_s^{(k)} \\ Z_{s+1}^{(k)} \\ \vdots \\ Z_{e-1}^{(k)} \\ Z_e^{(k)} \end{Bmatrix}. \quad (3.150)$$

The sizes of matrices $\overline{[M]}$, $\{\overline{Y}^{(k+1)}\}$ and $\{\overline{Z}^{(k)}\}$ are

$$\begin{aligned} \overline{[M]} &: 9(e-s+1) \times (6(e-s+1)+3) \\ \{\overline{Y}^{(k+1)}\} &: (6(e-s+1)+3) \times 1 \\ \{\overline{Z}^{(k)}\} &: 9(e-s+1) \times 1 \end{aligned}$$

Furthermore, by using the boundary condition eq.(3.142), eq.(3.148) can be transformed as

$$\overline{[M]} \{\overline{Y}^{(k+1)}\} = \{\overline{Z}^{(k)}\}, \quad (3.151)$$

where the matrices $\overline{[M]}$, $\{\overline{Y}^{(k+1)}\}$ and $\{\overline{Z}^{(k)}\}$ are represented as follows,

$$\overline{[M]} = \begin{bmatrix} \overline{[M]}_{1,1} & \overline{[M]}_{1,2} & \overline{[M]}_{1,4} & \cdots & \overline{[M]}_{1,N2-2} & \overline{[M]}_{1,N2-1} \\ \overline{[M]}_{2,1} & \overline{[M]}_{2,2} & \overline{[M]}_{2,4} & \cdots & \overline{[M]}_{2,N2-2} & \overline{[M]}_{2,N2-1} \\ \vdots & & & & \vdots & \\ \overline{[M]}_{N1,1} & \overline{[M]}_{N1,2} & \overline{[M]}_{N1,4} & \cdots & \overline{[M]}_{N1,N2-2} & \overline{[M]}_{N1,N2-1} \end{bmatrix} \quad (3.152)$$

$$\{\overline{Y}^{(k+1)}\} = \{\tau_{x,s}, \tau_{y,s}, \mathbf{w}_s, \cdots, \mathbf{w}_e, \tau_{x,e+1}, \tau_{y,e+1}\}^T \quad (3.153)$$

$$\{\overline{Z}^{(k)}\} = \{\overline{Z}^{(k)}\} - 0 \begin{bmatrix} \overline{[M]}_{1,3} \\ \overline{[M]}_{2,3} \\ \vdots \\ \overline{[M]}_{N1-1,3} \\ \overline{[M]}_{N1,3} \end{bmatrix} - L_z \begin{bmatrix} \overline{[M]}_{1,N2} \\ \overline{[M]}_{2,N2} \\ \vdots \\ \overline{[M]}_{N1-1,N2} \\ \overline{[M]}_{N1,N2} \end{bmatrix} \quad (3.154)$$

where $N1 = 9(e-s+1)$ and $N2 = 6(e-s+1)+3$. Then the sizes of matrices $\overline{[M]}$, $\{\overline{Y}^{(k+1)}\}$ and $\{\overline{Z}^{(k)}\}$ are

$$\begin{aligned} \overline{[M]} &: 9(e-s+1) \times (6(e-s+1)+1) \\ \{\overline{Y}^{(k+1)}\} &: (6(e-s+1)+1) \times 1 \\ \{\overline{Z}^{(k)}\} &: 9(e-s+1) \times 1 \end{aligned}$$

The method of least squares are applied for the solution of eq.(3.151) because the number of simultaneous equations, $9(e-s+1)$ is greater than the number of unknowns, $6(e-s+1)+1$. Finally, the following matrix equation was obtained,

$$\left[\overline{[M]}^T \overline{[M]}\right] \{\overline{Y}^{(k+1)}\} = \overline{[M]}^T \{\overline{Z}^{(k)}\}. \quad (3.155)$$

Then the unknowns at the $(k+1)$ -th time steps are calculated by the following equation,

$$\{\overline{Y}^{(k+1)}\} = \left[\overline{[M]}^T \overline{[M]}\right]^{-1} \left\{ \overline{[M]}^T \{\overline{Z}^{(k)}\} \right\}. \quad (3.156)$$

Chapter 4

Prediction of critical current density of type II superconductor

4.1 2-dimensional analysis of the zero-field cooled NbTi

In this section, the behaviors of the fluxoids in NbTi superconducting film were simulated by the 2-dimensional Fluxoid Dynamics Method. In the case that the magnetic field is applied to the NbTi film after it is cooled in zero magnetic field (zero-field cooling), the fluxoids penetrate into the superconductor through its surface. When the applied magnetic field increases, the penetrating fluxoids are pushed to the inside. Then the fluxoids are affected by some kinds of forces and move in the superconductor repeating the traps and releases by the pinning center. The magnetic flux density, B , in the superconductor is determined from the distribution of the fluxoids and the shielding current density, J_s , is expressed as rotation of B . The electric field is obtained as eq.(3.66). Most of the electromagnetic quantity can be analyzed by the Fluxoid Dynamics Method.

4.1.1 Computational model near the surface of NbTi bulk

Fig.4.1 shows the computational model near of the surface of NbTi bulk. The x and z axes are coordinated to be parallel to the surface of the bulk and the y axis is coordinated to be perpendicular to the surface. The line \overline{ab} means the surface of the superconductor and $y \geq L_y$ and $y < L_y$ correspond to the air region and the superconductor region, respectively. The analytic region is the square $\square abcd$ and its size is $L_x \times L_y = 0.3\mu\text{m} \times 10.0\mu\text{m}$. the periodic boundary condition was applied to the boundary \overline{ab} and \overline{cd} , and the insulating boundary condition was applied to the boundary \overline{ad} . The green rectangles are the α -Ti pins whose size is $L_{pz} \times L_{py}$ and. The distance between each pins are d_{pz} and d_{py} . These pins are arranged parallel to the x -axis. The external magnetic field is parallel to z -axis. and the red circles correspond to the fluxoids parallel to the z -axis.

Fig.4.2 shows three sampling points of the time-variation of the magnetic flux density and the shielding current density.

Fig.4.3 is the time-variation of the applied external magnetic flux density normalized by the upper critical magnetic flux density, $\mu_0 H_{c2}$. The amplitude and frequency are 1T and 1.67×10^7 Hz, respectively.

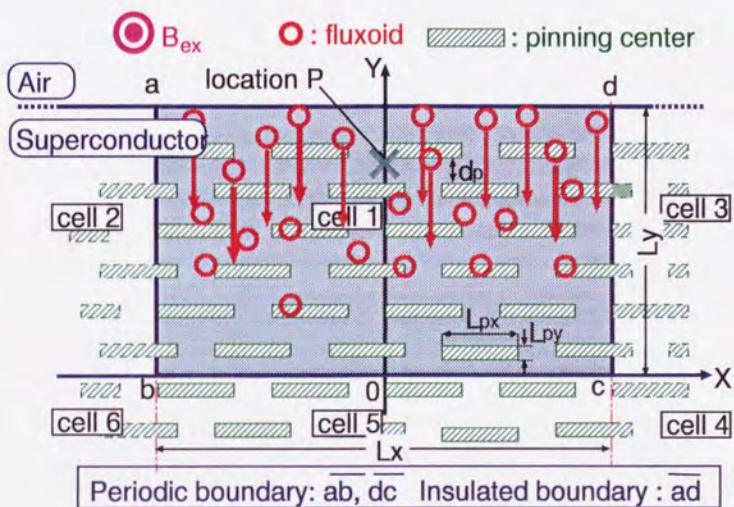


Figure 4.1: Computational model near the surface of NbTi film

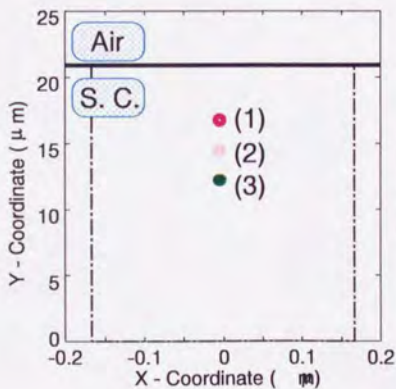


Figure 4.2: Location of the field points

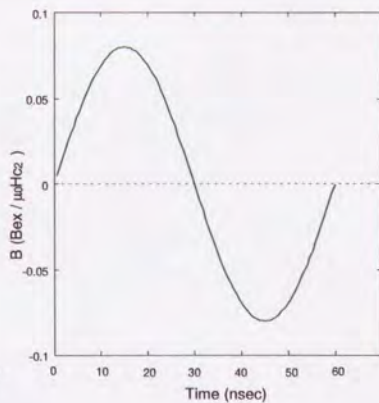


Figure 4.3: Time-variation of the applied magnetic flux density

4.1.2 Behaviors of fluxoids in NbTi bulk

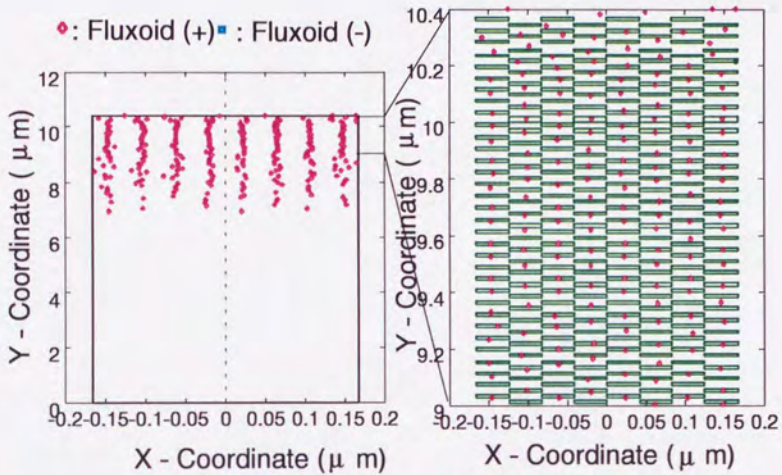
Fig.4.4 (a) shows the distribution of fluxoids at time=15 nsec. At this time the external magnetic flux density has the maximum, 1 T. The red circles correspond to the penetrating fluxoids whose direction is $(0, 0, +z)$. The fluxoids invade into the superconductor from the surface to $y \simeq 6.5 \mu\text{m}$. It can be seen that the number of the penetrating fluxoids are the most at the surface of superconductor and decreases gradually inside. The right figure in (a) shows the expanded view of the neighborhood of the surface of NbTi. The green rectangles are the α -Ti pinning centers. Most of fluxoids are trapped by the pinning centers and it can be found that the fluxoids penetrate into the superconductor repeating the trap and release by the pinning centers.

Fig.4.4 (b) and (c) show the magnetic flux density normalized by the magnetic flux density at the surface, \hat{B}_z , and the flow pattern of the shielding current density, J_s . \hat{B}_z has the maximum at the surface of the superconductor and decreases linearly with the depth from the surface. J_s is almost unique and parallel to x-axis at $y \geq 6.5 \mu\text{m}$. and zero at $y < 6.5 \mu\text{m}$.

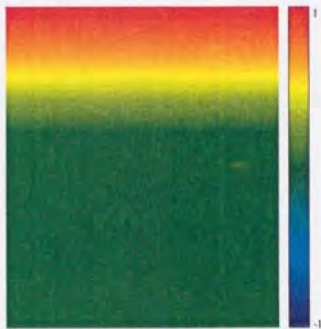
Fig.4.5 shows the distribution of fluxoids, \hat{B}_z and J_s at time = 30 nsec. The external magnetic flux density has decreased to 0 T at this time. The blue circles correspond to the reversed fluxoids whose direction is $(0, 0, -z)$. Most of the fluxoids whose direction is $(0, 0, -z)$ in the region $y \geq 8.4 \mu\text{m}$ are driven out of NbTi, and on the other hand, the fluxoids in the region $6.5 \mu\text{m} < y < 8.4 \mu\text{m}$ remain the same locations as time=15 nsec. The magnetic flux density, \hat{B}_z , has the maximum at $y \simeq 8.4 \mu\text{m}$ and the direction of shielding current density, J_s , reverses abruptly at $y \simeq 8.4 \mu\text{m}$.

In Fig.4.6 the time is 45nsec, and the external magnetic flux density has decreased to -1 T. Most of the fluxoids pointing $+z$ have been driven out of the superconductor and the reversed fluxoids penetrate to $y \simeq 7 \mu\text{m}$. The number of the reversed fluxoids has maximum at the surface of NbTi and decreases to zero linearly inside. So the \hat{B}_z is -1 T at the surface and increases to about 0 T inside. The direction of J_s is $(-1, 0, 0)$ at most part.

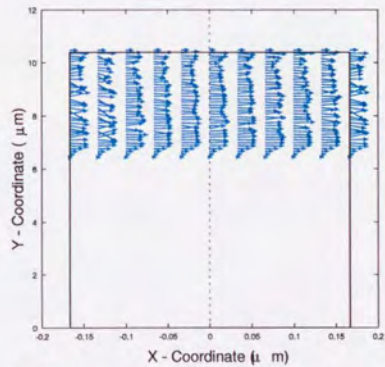
At time = 60 nsec, the external magnetic flux density increases to 0 T. It is shown in Fig.4.7 (a) that the reversed fluxoids near the surface of superconductor are driven outside but the fluxoids far from the surface are not. The magnetic flux density, \hat{B}_z , has the minimum at $y \simeq 8.4 \mu\text{m}$ and the direction of shielding current density, J_s , reverses abruptly at $y \simeq 8.4 \mu\text{m}$.



(a) Distribution of fluxoids

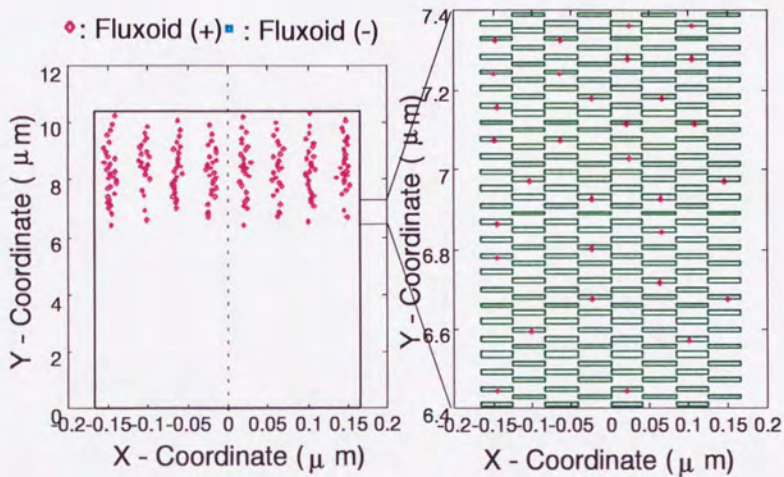


(b) Magnetic flux density ($\times B_{ez}$ (T))

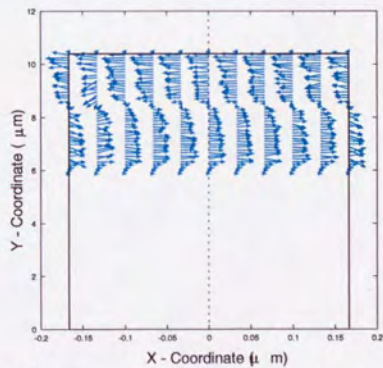
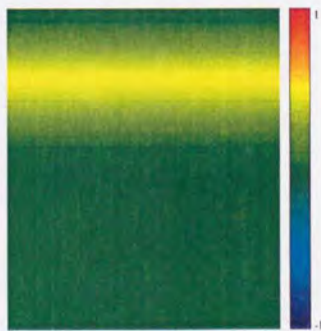


(c) Flow pattern of the shielding current

Figure 4.4: Distribution of fluxoid, magnetic flux density and shielding current (time = 15 nsec)



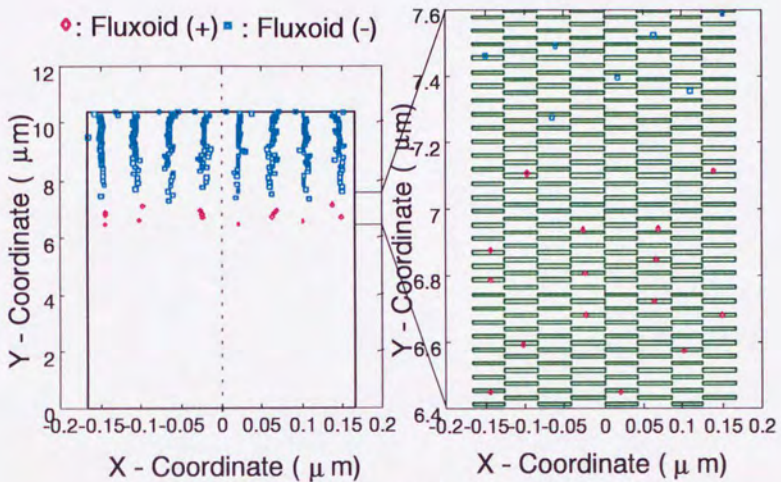
(a) Distribution of fluxoids



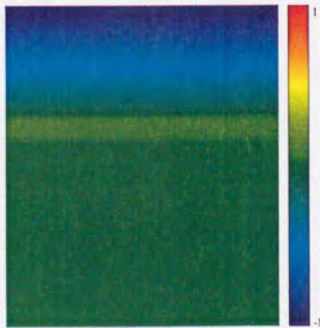
(b) Magnetic flux density ($\times B_{ez}$ (T))

(c) Flow pattern of the shielding current

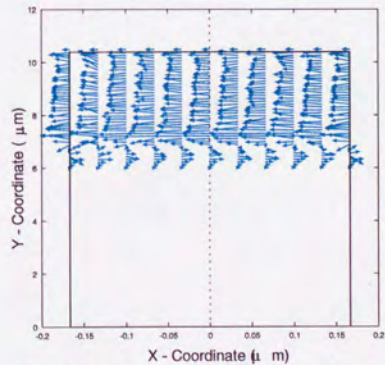
Figure 4.5: Distribution of fluxoid, magnetic flux density and shielding current (time = 30 nsec)



(a) Distribution of fluxoids

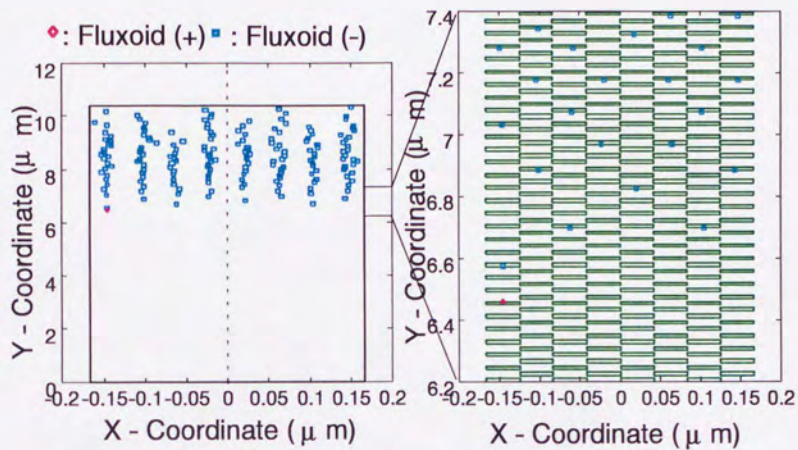


(b) Magnetic flux density ($\times B_{ex}$ (T))

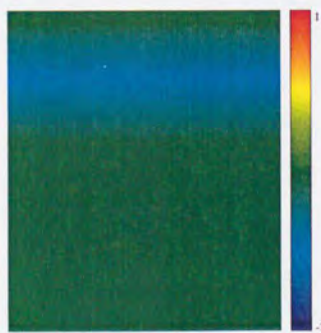


(c) Flow pattern of the shielding current

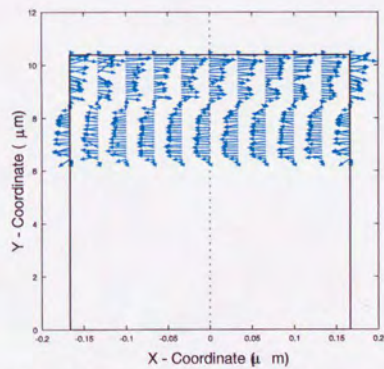
Figure 4.6: Distribution of fluxoid, magnetic flux density and shielding current (time = 45 nsec)



(a) Distribution of fluxoids



(b) Magnetic flux density ($\times B_{ex}$ (T))



(c) Flow pattern of the shielding current

Figure 4.7: Distribution of fluxoid, magnetic flux density and shielding current (time = 60 nsec)

4.1.3 Comparison with the Bean model

Fig. 4.8 (a) shows the numerical results of the time-variation of the distribution of the magnetic flux density, B , and the shielding current density, J_s , along the y -axis at the time = 15 nsec, 30 nsec, 45 nsec and 60 nsec. Fig. 4.8 (b) shows the schematic drawing of the distribution of B and J_s , obtained from the one of the well-known critical state model i.e. the Bean model. It is found that B and J_s in (a) and (b) agree well. From this agreement, the qualitative validity of this analytical method was obtained. From this agreement, furthermore, it is suggested that the critical state was satisfied at every time.

4.1.4 Relationship between J_c and B

Because the critical state is satisfied, it can be said that the shielding current density at the arbitrary location corresponds to the critical current density, J_c .

Fig. 4.9 (b) shows the relation between the applied magnetic flux density, B_s and the critical current density at location (1) in Fig. 4.2 when the external magnetic flux density B_{ez} increases linearly as shown in Fig. 4.9 (a). The red circles mean the numerical results and The green and blue dotted lines are the fitted ones for the numerical results according to the Kim model and the Yasukochi model. The yellow line is fitted one according to the original function. It can be found that the numerical results and the Kim and Yasukochi model agree very well. Fig. 4.10 and Fig. 4.11 show the numerical results of the relation between B and J_c at the location (2) and (3) in Fig. 4.2. The numerical results at locations (2) and (3) correspond to that at location (1). Then it can be found that this numerical results are not dependent on the location in the superconductor. From these result, it is concluded that this analytical method is available for the evaluation of the relationship between J_c and B of the type II superconductor.

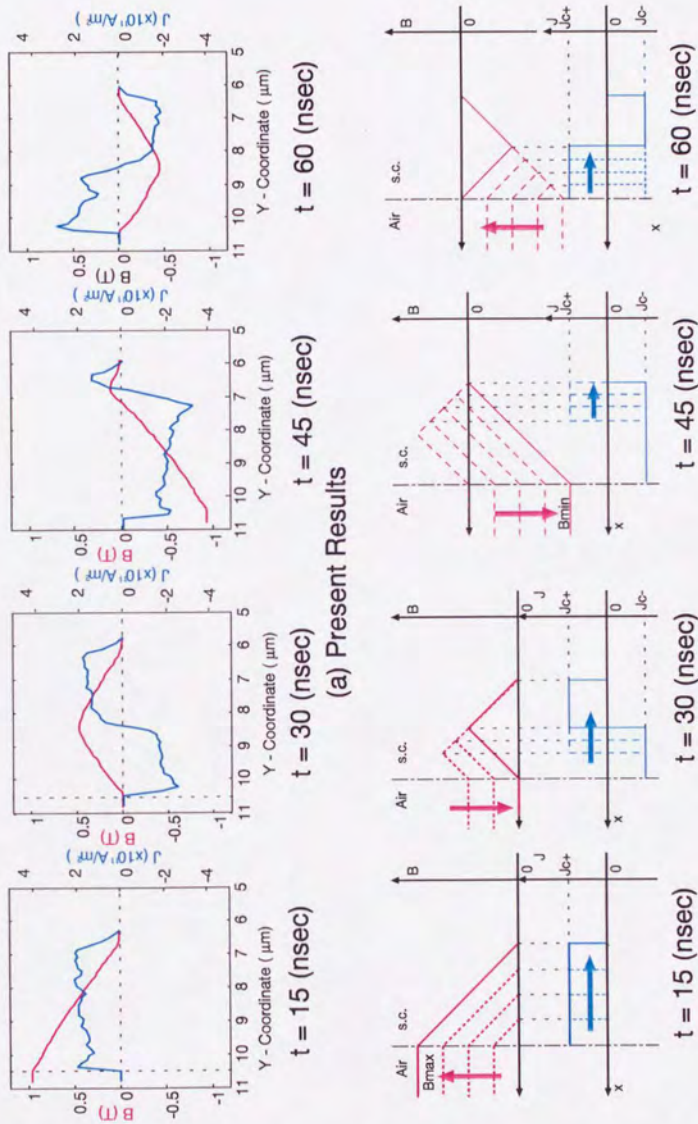
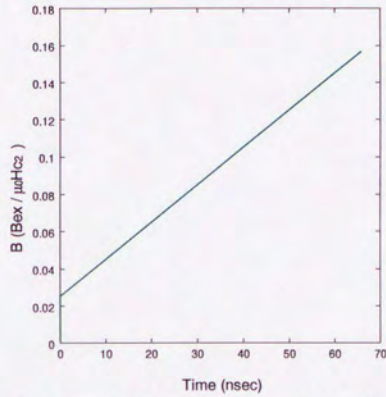
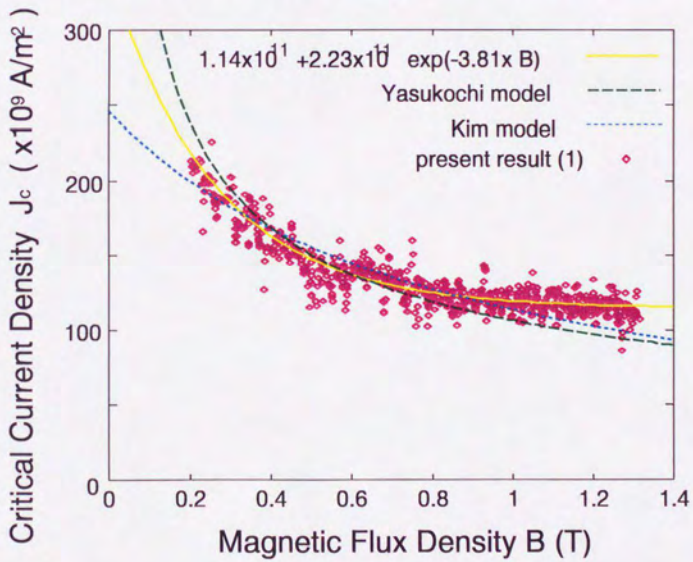


Figure 4.8: Time-variation of distribution of B , J and comparison with Bean model



(a) Time-variation of the applied magnetic flux density B_{ex}



(b) J_c - B constitutive relation

Figure 4.9: J_c - B constitutive relation & Comparison with Kim and Yasukochi models(1)

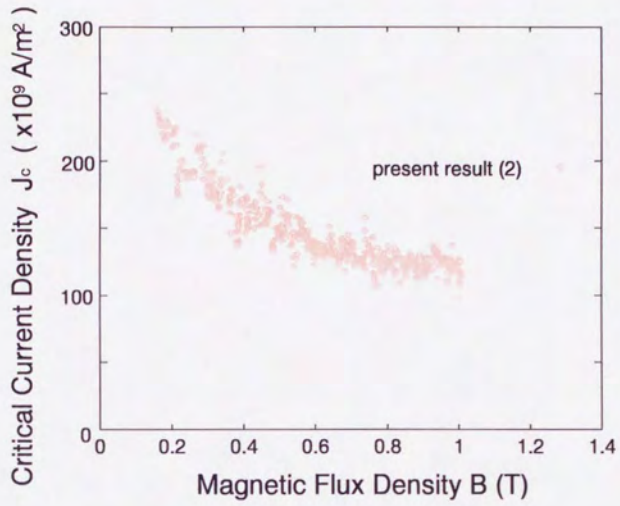


Figure 4.10: J_c - B constitutive relation at location (2)

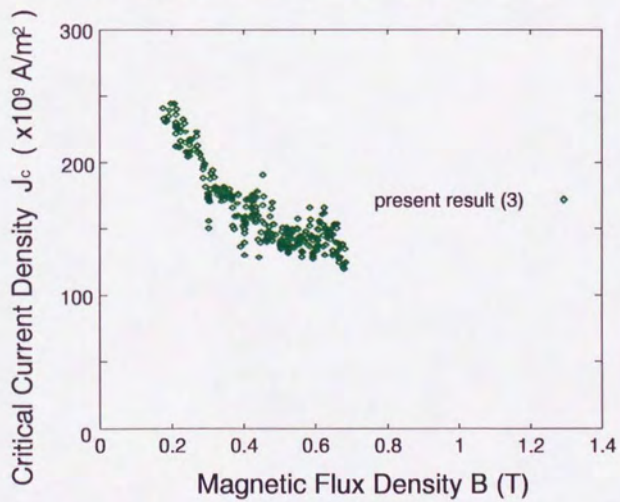


Figure 4.11: J_c - B constitutive relation at location (3)

4.2 2-dimensional analysis of the field cooled NbTi

Next, the behaviors of the fluxoids in the inner part of the field cooled NbTi was simulated in the case that the transport current was applied uniformly in x direction. Then the electrical field was calculated in some cases of the transport current density, J_{tx} , and the critical current density, J_c were evaluated. Furthermore, the constitutive relation between the applied magnetic flux density B_{ex} and J_c was obtained and compared with the existing models.

4.2.1 Computational model

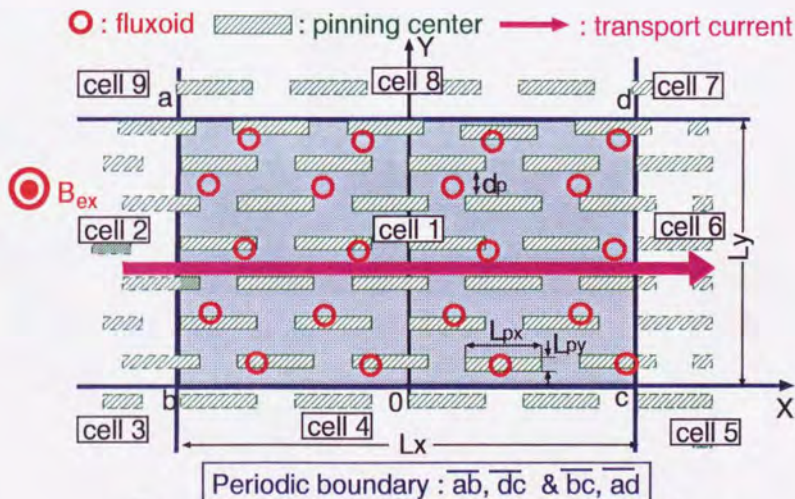


Figure 4.12: Computational model of the inner part of NbTi

Fig. 4.12 shows the schematic drawing of the 2-dimensional computational model of the inner part of NbTi used in the numerical analysis. The analyzed region is the Cell 1 ($\square abcd$) whose size is $L_x \times L_y$, and the periodic boundary condition was applied at the boundary \overline{ab} with \overline{dc} and \overline{ad} with \overline{bc} , where the fluxoids moved outside the region were

treated as ones coming inside through another boundary. Many thin α -Ti pinning centers were located parallel to the x-axis, and each pinning center's size is $L_{px} \times L_{py}$. As the repulsive force between two fluxoid, F_f , acting on the fluxoids in Cell 1, only those by the fluxoids in Cell 1 ~ 9 were taken into account. B_{ez} is the applied magnetic flux density which is parallel to z-axis and uniform in the analytical region. The transport current flows uniformly and in parallel to x-axis.

The computational parameters are shown in the following,

- Coherence length : $\xi = 5.2(nm)$
- London's penetration depth : $\lambda = 210.0(nm)$
- Ginzburg-Landau parameter : $\kappa = \lambda/\xi = 40.38$
- Size of analytical region : $L_x = L_y = 120(\xi)$
- Size of pinning centers : $L_{px} = 20(\xi), L_{py} = 6(\xi)$
- Applied magnetic flux density : $B_{ez} = 0.0956 \sim 1.0357 (T)$
- Transport current density : $J_t = 1.0 \times 10^9 \sim 10.0 \times 10^9 (A/m^2)$
- Number of pinning centers : 32

The initial distribution of fluxoids were determined according to the Abrikosov's triangular lattice and the applied magnetic field B_{ez} , and the behaviors of the each fluxoids were simulated after the transport current changing with time was induced.

4.2.2 Flows of the fluxoids

Fig. 4.13 shows the flows and the trajectories of the fluxoids in NbTi in the case that $B_{ez} = 1.3543 T$ and $J_t = 1.4 \times 10^{11} A/m^2$. The fluxoids distribute according to the Abrikosov's triangle lattice as the time $t=0$ nsec. At time $t=0.8$ nsec, most of the fluxoids are trapped by the pinning centers. And direction of the fluxoids' flow is $-y$ because the Lorentz force due to the transport current acting on the each fluxoids points in the $-y$ direction. The 5 colored lines means the trajectories of 5 fluxoids and it can be seen that the fluxoids flows in $-y$ direction with the continuous trap and release by the pinning centers.

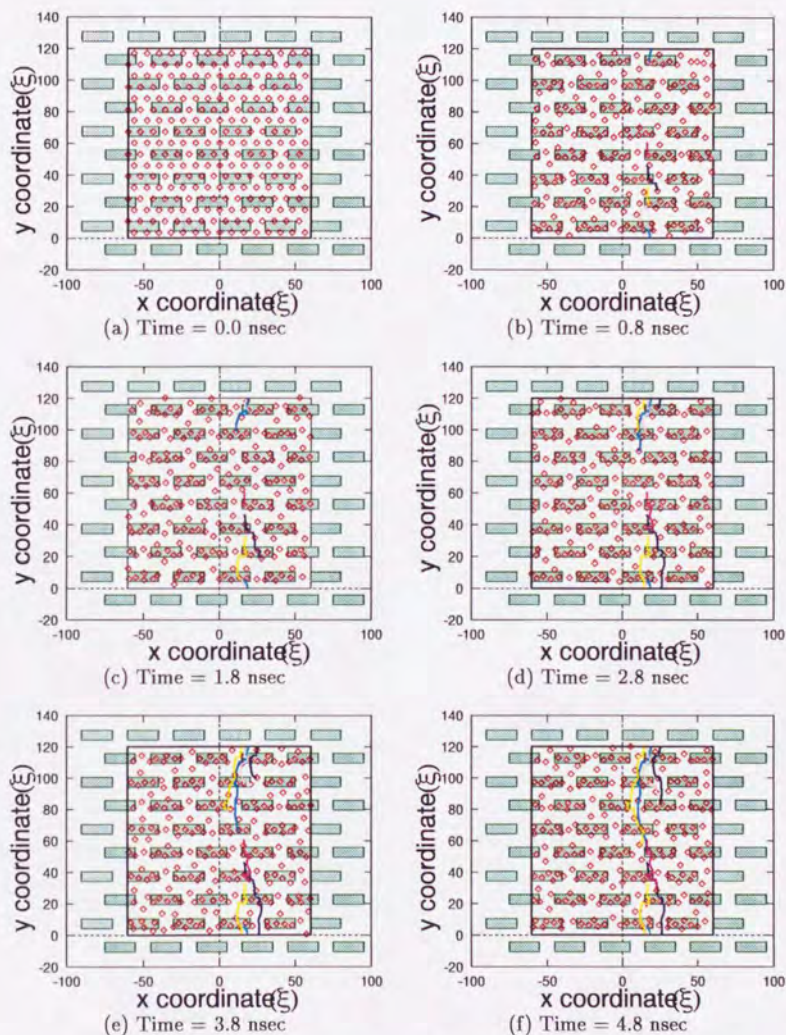


Figure 4.13: Flows of fluxoids in NbTi ($B_{ex}=1.3543T$, $J_z=1.4\times 10^{11}A/m^2$)

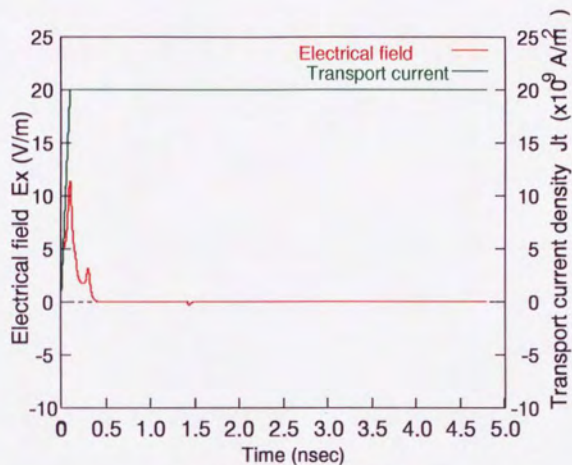
4.2.3 Time-variation of Electric field : E_x

When the fluxoids moves in the direction of $-y$ with the speed v in the magnetic flux density $B = B_{ex}e_x$, the electrical field $E \simeq E_x e_x$ is yielded due to the electromotive force in the superconductor. Fig. 4.14 shows the time-variation of the transport current density J_{tz} and the electrical field E_x . The green lines and the red ones mean J_{tz} and E_x , respectively. The applied magnetic flux density is $B_{ex} = 1.3543(\text{T})$, and the transport current density are (a) $J_t = 2.0 \times 10^{10}(\text{A}/\text{m}^2)$ and (b) $J_t = 7.5 \times 10^{10}(\text{A}/\text{m}^2)$. In case (a), the electrical field E_x converges to 0 (V/m) because the Lorentz force F_J due to J_{tz} is so small that the fluxoids are trapped by the pinning centers completely and their velocity are $v \simeq 0$. In case (b), with the larger J_{tz} , E_x converges to an equilibrium value because the Lorentz force F_J due to J_{tz} is so large enough that the fluxoids can be released from the pinning centers and the velocity are $v \neq 0$.

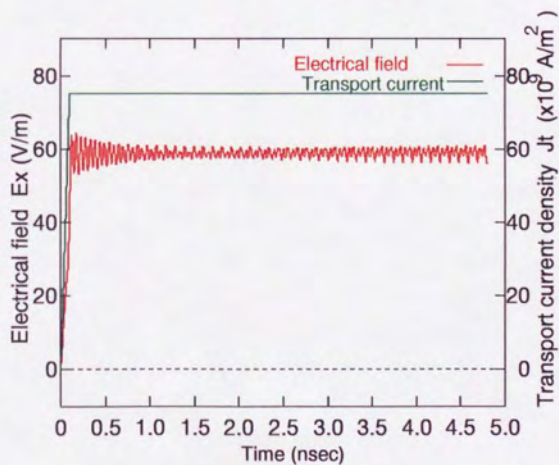
4.2.4 Relation between J_t and E_x

Fig. 4.15 shows the relation between the transport current density J_{tz} and the equilibrium value of the electrical field E_x in the case that the applied magnetic flux density is $B_{ex} = 0.4780(\text{T})$. E_x keeps 0(V/m) when $J_t < 1.5 \times 10^{10}(\text{A}/\text{m}^2)$, and rises suddenly to approach a line when $J_t > 1.5 \times 10^{10}(\text{A}/\text{m}^2)$. This phenomena corresponds to the well-known "Critical Current Model".

From this fact, it can be said that the critical current density can be predicted by using our "Fluxoid Dynamics Method". And the critical current density is determined as $J_t = 1.5 \times 10^{10}(\text{A}/\text{m}^2)$.



(a) $J_{tx} = 2.0 \times 10^{10} (\text{A/m}^2)$



(b) $J_{tx} = 7.5 \times 10^{10} (\text{A/m}^2)$

Figure 4.14: Time-variation of transport current density J_{tx} and Electrical field E_x
 $(B_{ez}=1.3543[\text{T}])$

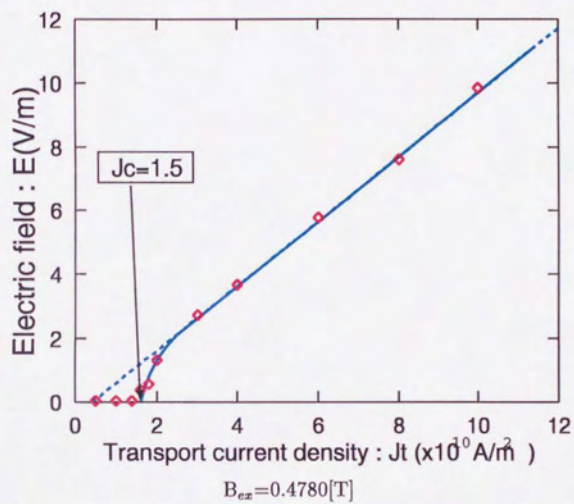


Figure 4.15: Relation between J_{tx} and E_x

4.2.5 Constitutive relation between B_{ez} and J_c

Fig. 4.16 shows the constitutive relation between the applied magnetic flux density and the transport current density J_c . When B_{ez} is large, this result corresponds to the Kim model which is the experimental approximate model,

$$J_c(B) = \frac{J_{c0}}{B + B_0} \quad (4.1)$$

where J_{c0} and B_0 are constants. When B_{ez} is small, on the other hand, J_c converges to a constant value J_c^* and J_c^* is equal to

$$J_c^* = \frac{F_p}{\Phi_0} \quad (4.2)$$

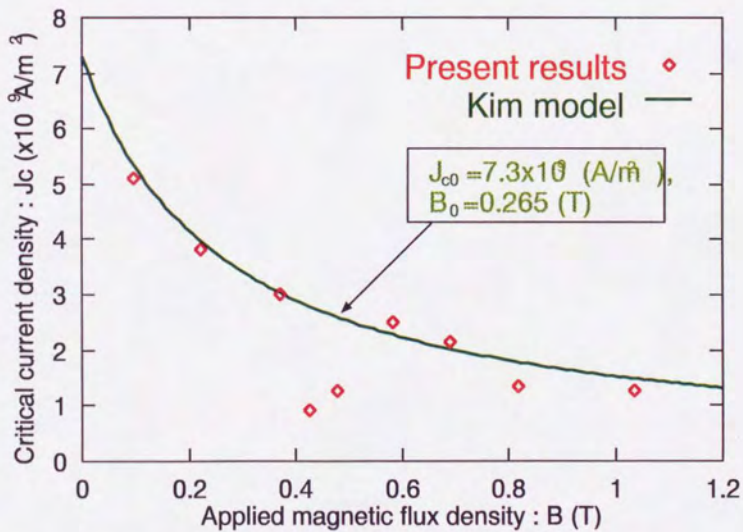


Figure 4.16: Constitutive relation between B_{ez} and J_c

Chapter 5

Numerical analysis of the anisotropy of superconductor

5.1 3D analysis of anisotropy of the shielding current in NbTi

In the simulation by the 2-dimensional Fluxoid Dynamics method the magnetic field was applied only parallel to z-axis. Usually, however, the magnetic field and the surface of the superconductor make various angles for the practical use of superconductor, and it is expected that the angle has the effect upon the relationship between the applied magnetic flux density and the critical current density. In this chapter, this effect will be evaluated by the 3-dimensional FD method for the NbTi thin film.

5.1.1 Computational model of 3-dimensional FD method

Fig. 5.1 shows the computational model of 3-dimensional Fluxoid Dynamics method.

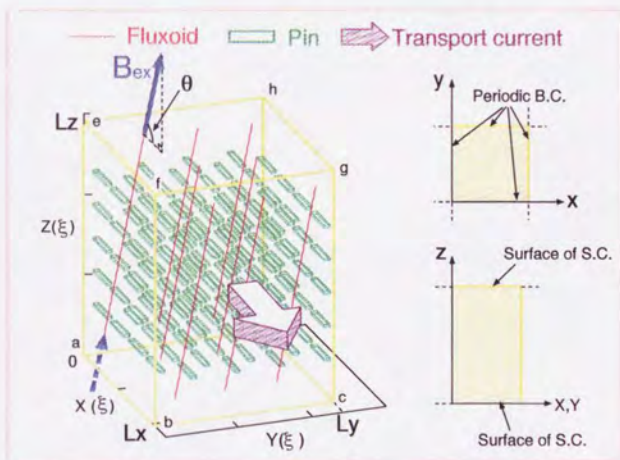


Figure 5.1: 3-dimensional computational model of NbTi thin film

The specimen is the NbTi thin film and the α -Ti impurities are adopted as the pinning centers. The analytical region is the rectangular prism $\overline{abcd-efgh}$, whose size is $L_x \times L_y \times L_z$. The boundaries $\square abcd$ and $\square efgh$ are the surfaces of the NbTi film contacting with

the air region: $z < 0$ and $z > L_z$. The periodic boundary conditions are applied for the boundaries $\square abfe$, $\square dcgh$ and $\square daeh$, $\square cbfg$. The green rectangular prisms correspond to the $n_{pz} \times n_{py} \times n_{px}$ α -Ti pins arranged parallel to the xy -plane. The size of pins are $L_{pz} \times L_{py} \times L_{px}$ and the distance between them are d_{pz} , d_{py} and d_{px} . The applied magnetic field is contained in the xz -plane and makes an angle of θ with the y -axis. The red lines correspond to the fluxoids in the superconductor, and each fluxoid consists of 20 elements. The uniform transport current is induced in the direction of $+x$.

In this study, the parameter of material were chosen as follows:

	Pin Arrange-1	Pin Arrange-2
$L_x(\xi) \times L_y(\xi) \times L_z(\xi)$	104.9 \times 121.1 \times 144.2	
$L_{pz}(\xi) \times L_{py}(\xi) \times L_{px}(\xi)$	20.0 \times 4.0 \times 1.442	20.0 \times 8.0 \times 1.442
$n_{pz} \times n_{py} \times n_{px}$	4 \times 8 \times 5	5 \times 3 \times 5

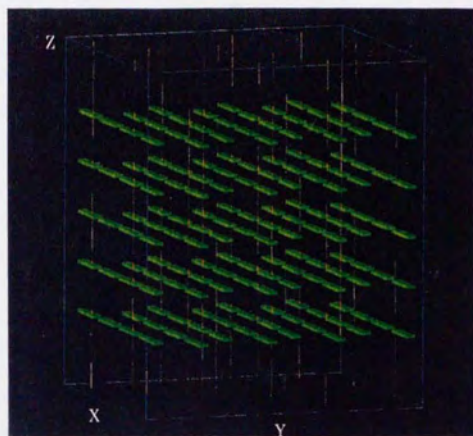
5.1.2 Initial distribution of fluxoids in equilibrium state

It is necessary to obtain the initial distribution of fluxoids in equilibrium state when no transport current is induced. It was calculated by solving the equilibrium distribution without transport current after the fluxoids were arranged according to the Abrikosov's triangle lattice at time = 0 sec in the case of Pin Arrange-1.

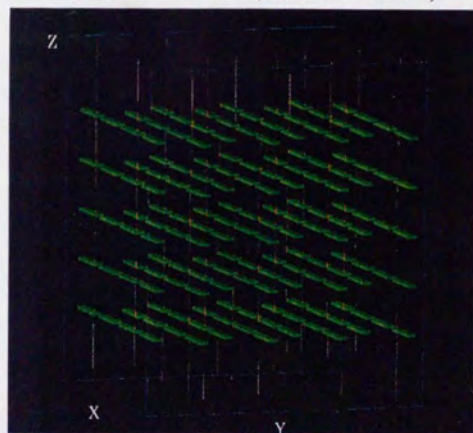
Fig.5.2 and Fig.5.3 show the time-variation of transformation of fluxoids in NbTi thin film until the equilibrium state were attained in the following cases:

	case A	case B
$\theta(deg)$	0.0	45.0
$B_{ez}(T)$	0.096280	0.136161
n_f	16	16

where B_{ez} is the applied magnetic flux density, θ is the angle of B_{ez} and n_f is the number of the fluxoids. It was observed that the fluxoids are attracted, bended and trapped by the pinning centers. When the angle θ is small, the rate of bending becomes larger and the more part of the fluxoids are trapped by the pinning centers and are kept parallel to them as shown in Fig. 5.3.

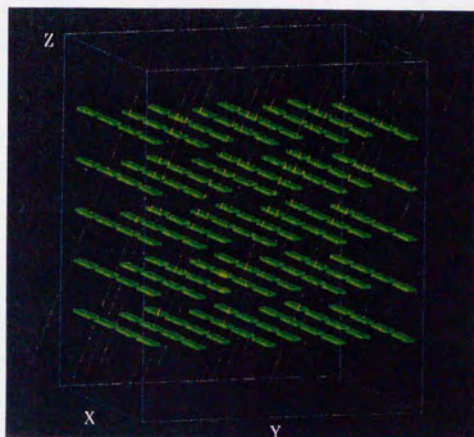


(a) time = 0.0 nsec (Abrikosov's lattice)

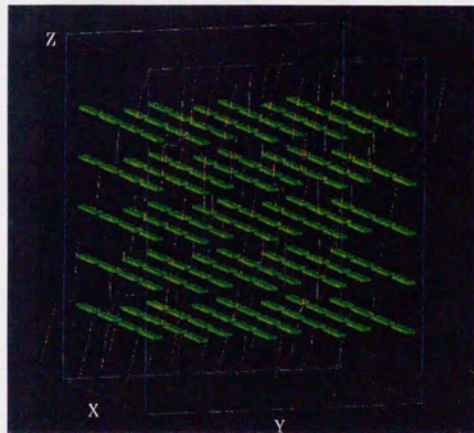


(b) time = 2.0 nsec (equilibrium distribution)

Figure 5.2: Transformation of fluxoids during the initial equilibrium simulation (case A)



(a) time = 0.0 nsec (Abrikosov's lattice)



(b) time = 2.0 nsec (equilibrium distribution)

Figure 5.3: Transformation of fluxoids during the initial equilibrium simulation (case B)

5.1.3 Flows of the fluxoids

When the uniform transport current density J_t is applied in $+x$ direction, the fluxoids flow in $-y$ direction due to the Lorentz force. Fig. 5.4 shows the time variation of the applied uniform transport current density in the case of Pin Arrange-1. The application of J_t started after the initial distribution of fluxoids in equilibrium was attained. J_t increased linearly from 0 (A/m^2) to $J_{t,max}$ (A/m^2) during 50 psec and then kept $J_t = J_{t,max}$.

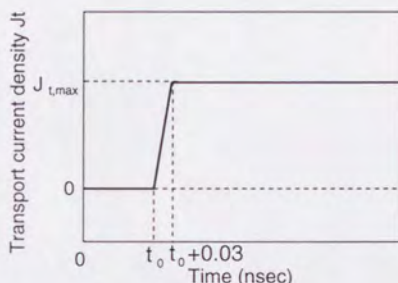
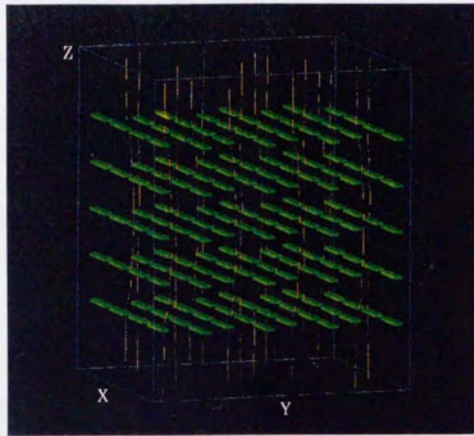


Figure 5.4: Time-variation of applied transport current density

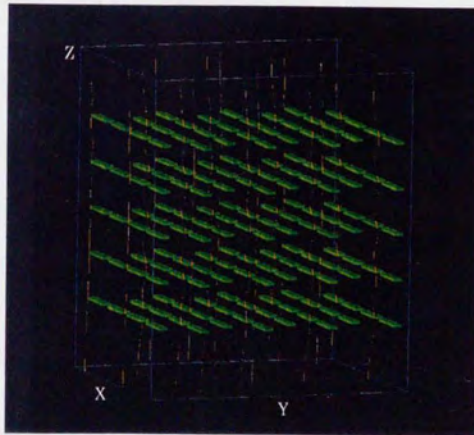
Fig.5.5 and Fig.5.6 show the flow of fluxoids in NbTi thin film in the following conditions:

	case A	case B
$\theta(deg)$	0.0	45.0
$B_{ez}(T)$	0.096280	0.136161
n_f	16	16
$J_{t,max}(A/m^2)$	10.0×10^{10}	10.0×10^{10}

It can be seen that the pinning centers capture the fluxoids and prevent the flow of fluxoids. The fluxoids are bended very much when they are released from the pinning centers. The degree of the bending is larger in case B than in case A because the more parts of fluxoids are trapped by the pinning centers. Then it can be predicted that the critical current density is higher for the smaller θ .

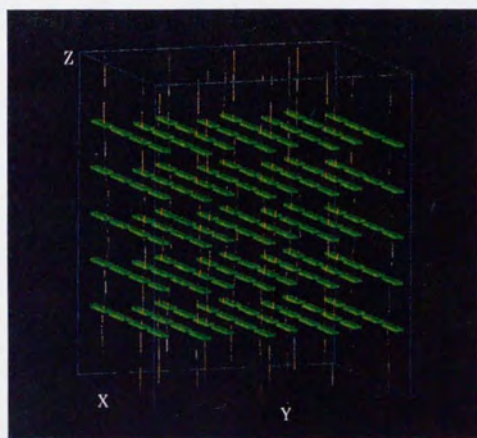


(a) time = 2.4 nsec

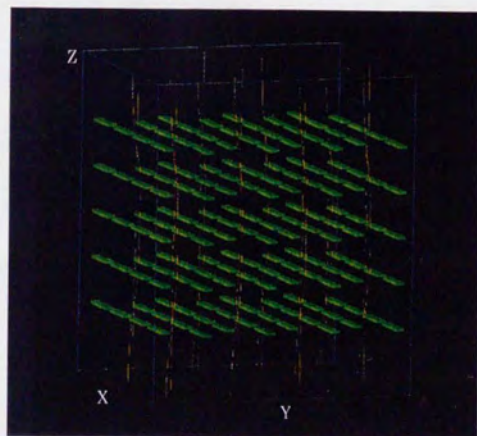


(b) time = 3.0 nsec

Figure 5.5: Flow and transformation of fluxoids (case A)

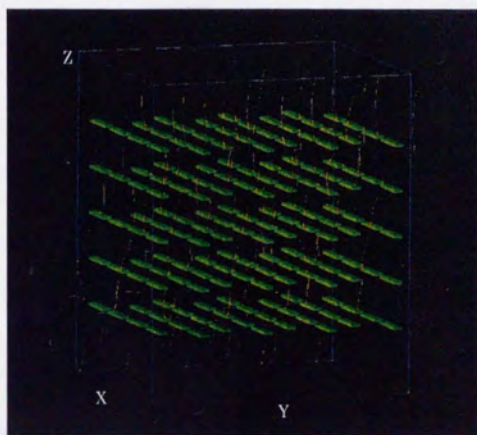


(c) time = 3.6 nsec

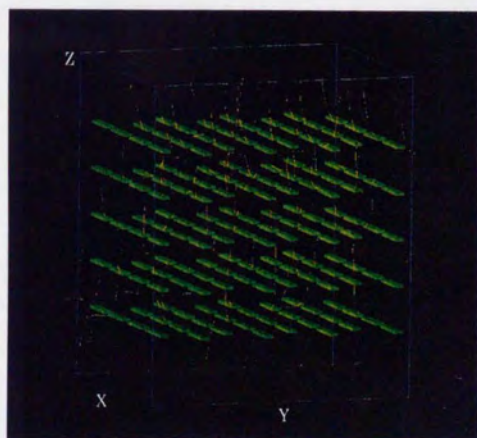


(d) time = 4.0 nsec

Figure 5.6: Flow and transformation of fluxoids (case A)

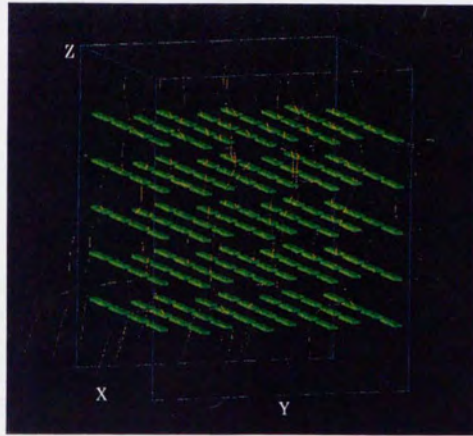


(a) time = 2.4 nsec

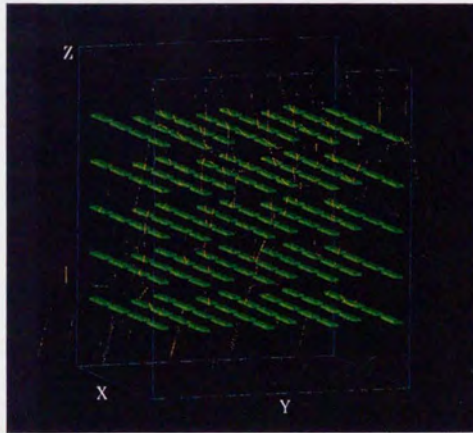


(b) time = 3.0 nsec

Figure 5.7: Flow and transformation of fluxoids (case B)



(c) time = 3.6 nsec

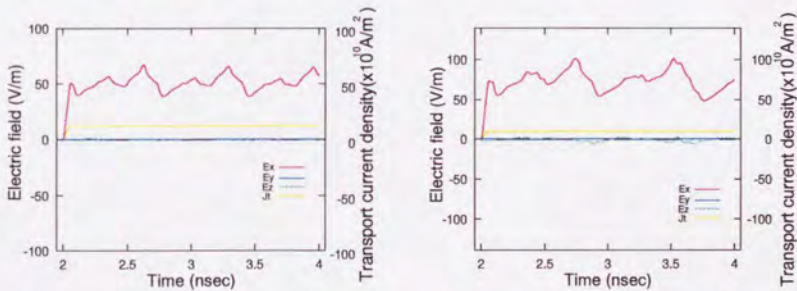


(d) time = 4.0 nsec

Figure 5.8: Flow and transformation of fluxoids (case B)

5.1.4 Time-variation of electric field

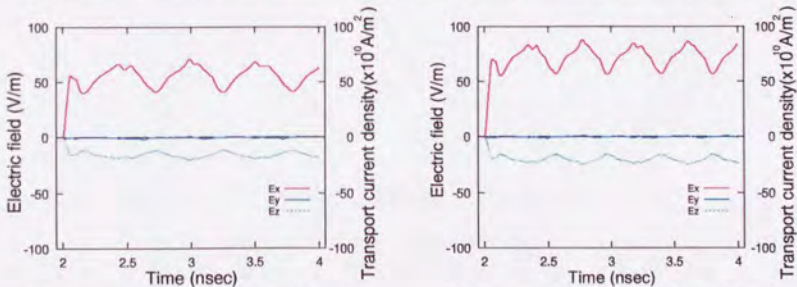
The electric field $\mathbf{E} = (E_x, E_y, E_z)$ is yielded in the superconductor when the fluxoids flow in $+y$ direction. Fig. 5.9 ~ Fig. 5.12 show the time-variation of the electric field \mathbf{E} and the transport current density J_t in the case that $\theta = 90^\circ, 75^\circ, 60^\circ$ and 45° with the Pin Arrange-1. It can be seen that E_x and E_z converges to an equilibrium value rapidly and E_y keeps 0 V/m because E_y is not yielded in this arrangement of the fluxoids and the transport current. It can be thought that the vibration of the electric field is caused by the variation of the velocity of the fluxoids while they pass through the pinning centers. The velocity of fluxoids becomes higher when they are attracted and trapped by the pinning centers and it becomes lower when they are released.



(a) $B_{ex}=0.2166\text{T}$, $J_t=12.0\times 10^{10}\text{A/m}^2$

(b) $B_{ex}=0.3851\text{T}$, $J_t=10.0\times 10^{10}\text{A/m}^2$

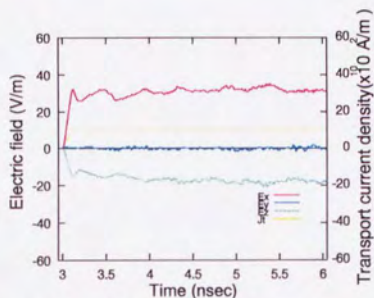
Figure 5.9: Time-variation of transport current density and electric field ($\theta = 90^\circ$)



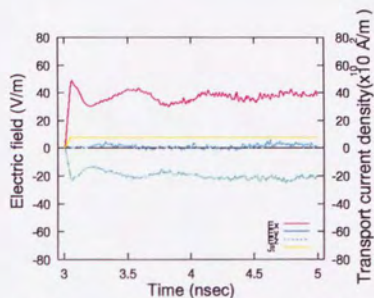
(a) $B_{ex}=0.3987\text{T}$, $J_t=8.0\times 10^{10}\text{A/m}^2$

(b) $B_{ex}=0.3987\text{T}$, $J_t=10.0\times 10^{10}\text{A/m}^2$

Figure 5.10: Time-variation of transport current density and electric field ($\theta = 75^\circ$)

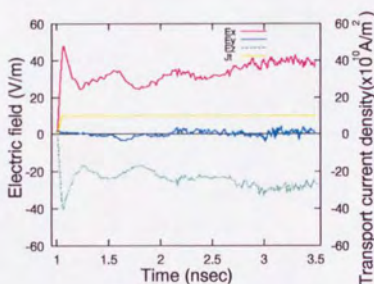


(a) $B_{ez}=0.2501\text{T}$, $J_t=10.0\times 10^{10}\text{A/m}^2$

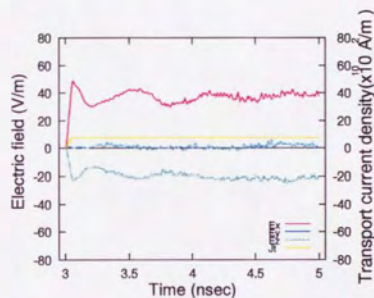


(b) $B_{ez}=0.4444\text{T}$, $J_t=8.0\times 10^{10}\text{A/m}^2$

Figure 5.11: Time-variation of transport current density and electric field ($\theta = 60^\circ$)



(a) $B_{ez}=0.3063\text{T}$, $J_t=10.0\times 10^{10}\text{A/m}^2$



(b) $B_{ez}=0.5446\text{T}$, $J_t=8.0\times 10^{10}\text{A/m}^2$

Figure 5.12: Time-variation of transport current density and electric field ($\theta = 45^\circ$)

5.1.5 Constitutive relation between J_t and E_x

Fig. 5.13 shows the numerical results of the constitutive relation between J_t and E_x for 4 cases of θ obtained from the results shown in Fig. 5.9 ~ 5.12. The dots mean the numerical results and the lines are the fitted ones. It can be found that the relations between J_t and E_x are expressed by the linear ones. Therefore, it can be thought that the intersections of these lines and the x axis correspond to the critical current density, J_c , and the inclination of these lines correspond to the flux flow resistivity, ρ . The flux flow resistivity are found to be bigger for the higher magnetic flux density for all cases of θ .

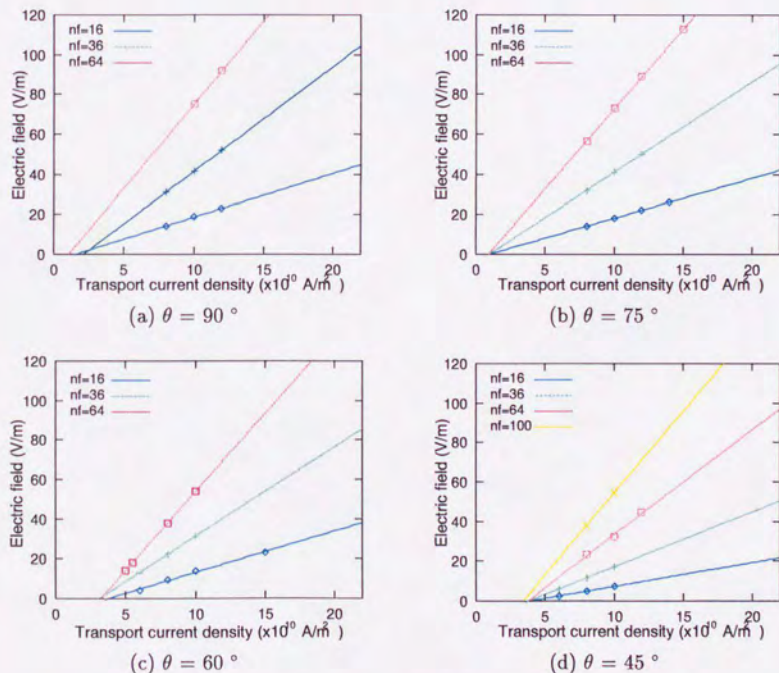


Figure 5.13: The constitutive relations between J_t and E_x

5.1.6 Relation between B_{ex} and flow resistivity

Fig. 5.14 shows the relation between the applied magnetic flux density B_{ex} and the flow resistivity ρ_f obtained from the numerical results shown in Fig. 5.13. It can be seen that ρ_f and B_{ex} are in proportion to each other. for all cases of θ . This result corresponds to the Bardeen-Stephen model[43] as expressed in eq. (2.124). Then the validity of this method was verified for the evaluation of the dependence of the flow resistivity upon the applied magnetic flux density.

By the way, the dependence of the proportional relation can be found that the proportional ratio between them is bigger for the larger θ . Fig. 5.15 shows the relation between the angle of the applied magnetic field, θ , and the incliment of the lines in Fig. 5.14, ρ_f/B_{ex} . It can be found that ρ_f/B_{ex} is proportional to the square of $\sin \theta$,

$$\rho_f/B_{ex} \propto \sin^2 \theta. \quad (5.1)$$

Then it was shown that this method is useful for the evaluation and prediction of the anisotropy of the property of the flux flow resistivity in the type II superconductor.

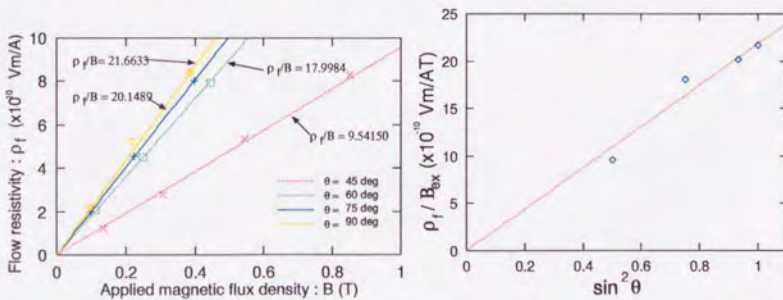
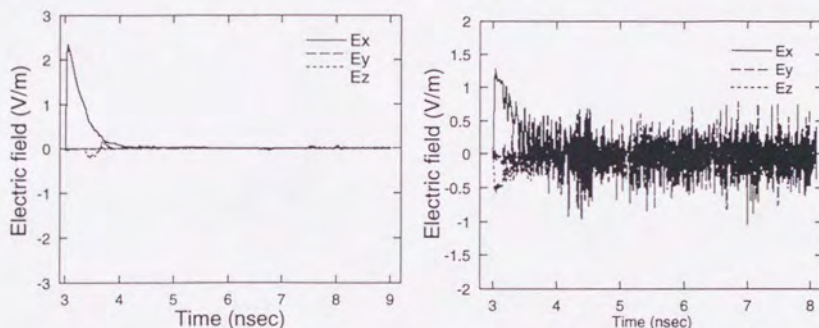


Figure 5.14: Relation between B_{ex} and ρ_f Figure 5.15: Relation between ρ_f/B_{ex} and θ

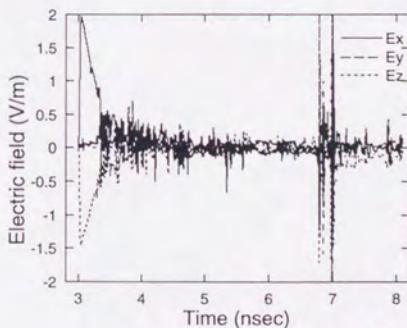
5.1.8 Time-variation of electric field-2

Fig. 5.17 shows the time-variation of the electric field E_x, E_y, E_z in the case that $\theta = 90^\circ, 60^\circ$ and 45° , the arrange of pinning centers is Pin Arrange-2 and $n_f = 4$. It can be seen that the electric field is saturated rapidly and the equilibrium value, \bar{E} are obtained. The critical current density, J_c are obtained as the transitional value of J_t giving the equilibrium of electric field which is larger than zero.



(a) $\theta=90^\circ, B_{cz}=0.024070\text{T},$
 $J_{tz} = 4.9 \times 10^{10}(\text{A/m}^2)$

(b) $\theta=60^\circ, B_{cz}=0.027794\text{T},$
 $J_{tz} = 3.0 \times 10^{10}(\text{A/m}^2)$



(c) $\theta=45^\circ, B_{cz}=0.034040\text{T},$
 $J_{tz} = 5.6 \times 10^{10}(\text{A/m}^2)$

Figure 5.17: Time-variation of electric field E_x, E_y, E_z

5.1.9 Relation between B_{ex} and J_c

Fig. 5.18 shows the numerical result of the relations between B_{ex} and J_c for 3 cases of θ . It can be found that the angle θ is smaller, the critical current density J_c becomes larger. The three lines means the fitted ones of the numerical results according to Kim model.

Table 5.1 shows the fitted constants, J_{c0} and B_0 , of Kim model in the three cases of θ . These J_{c0} and B_0 are plotted in Fig. 5.19, and it was found that J_{c0} is proportional to $1/\sin \theta$.

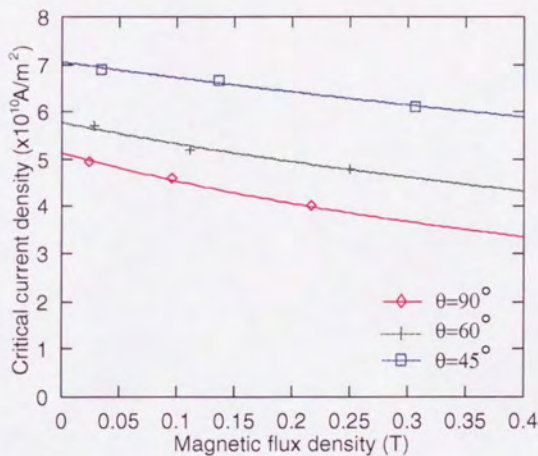


Figure 5.18: Dependence of B_{ex} - J_c relation upon θ

Table 5.1: Fitted constants J_{c0} and B_0 of Kim model

	$J_{c0}(\times 10^{10} \text{ A/m}^2)$	$B_0(\text{T})$
$\theta = 90^\circ$	5.13085	0.75528
$\theta = 60^\circ$	5.77135	1.19816
$\theta = 45^\circ$	7.05059	2.03321

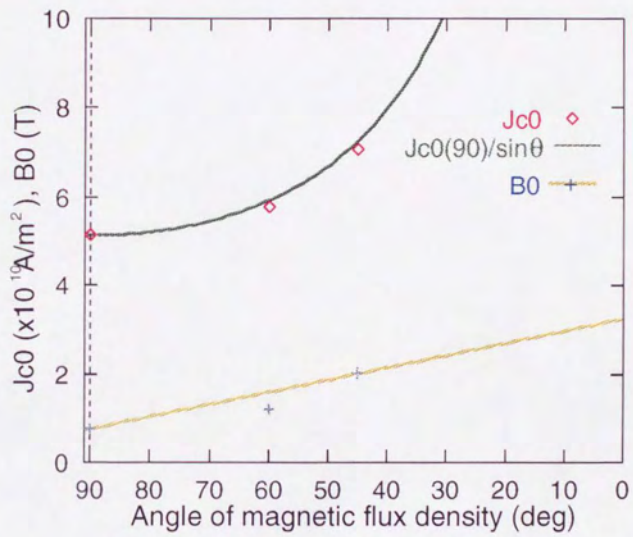


Figure 5.19: Dependence of J_{c0} and B_0 upon θ

Chapter 6

Conclusion

The new simulation method and its computational code were developed for analysis of the mesoscopic behaviors of the fluxoids in type II superconductors and the mesoscopic electromagnetic phenomena in type II superconductor was investigated through this simulation. As the conclusion of this study the following ones were obtained.

(1) The new simulation method was developed to calculate the distribution of the superconducting electrons density and the magnetic flux density in type II superconductor based on the Ginzburg-Landau theory.

- The distributions of the order parameter and the magnetic vector potential of an isolated fluxoid in NbTi were numerically calculated by this method.
- The generation of the superconducting electrons and the formation of the fluxoid lattice were simulated for the YBCO thin film.

(2) The 2-dimensional Fluxoid Dynamics method (FD-method) was proposed and developed for the new analysis method of the behaviors of fluxoids in the type-II superconductor.

- The fluxoids in the type II superconductor were assumed to be the particles of the normal conducting core surrounded by the shielding current, and their kinetic equation was defined based on the Molecular Dynamics method (MD method) considering the 5 kinds of forces affecting on the fluxoids.
- The pinning force acting on the fluxoid from the pinning centers and the viscous force due to the ohmic loss of the normal conducting core of the fluxoid was evaluated based on the Ginzburg-Landau theory for the isolated fluxoid.
- The 3 kinds of electromagnetic forces were evaluated based on the London theory and other macroscopic theories of superconductor.

(3) The 3-dimensional Fluxoid Dynamics method was also proposed and developed.

- In this method a fluxoid was discretized as the chained fluxoid arc elements and the equilibrium of forces and torques gave their movement.

- 6 kinds of forces and torques were evaluated as the integral of 2-dimensional forces along the fluxoid arc elements: the tension due to the curvature of fluxoid was added into consideration.
- (4) The mesoscopic behaviors of fluxoids and the electromagnetic phenomena in NbTi bulk were simulated by using the 2-dimensional FD method.
- The penetration of fluxoids through the surface of the NbTi bulk was simulated and their behaviors were observed when the time-variational external magnetic field was induced.
 - The numerical results agreed well with the critical state model as far to concerning the time-variation of the distribution of magnetic flux density and the shielding current density in NbTi bulk.
 - The relation between the magnetic flux density and the critical current density in the arbitrary location in NbTi was evaluated and the agreement with the Kim model and Yasukochi model was obtained.
 - The validity of this method was verified from these two agreement.
 - The behaviors of fluxoids and the electric field were simulated in the case that the transport current was induced in the NbTi bulk.
 - The flow of fluxoids were observed when the uniform transport current was induced in x-direction and the time-variation of the average electric field due to the speed electromotive force was calculated to find that the steady state is obtained very quickly : ~ 1 nsec.
 - The constitutive relation between the induced transport current density and the electric field was obtained and it was found that this method was useful to evaluate the critical current density of type II superconductor.
 - The relation between the applied magnetic flux density and the critical current density was obtained and was compared with the conventional

experimental model, Kim model. The good agreement between them gave the validity of this method.

(5) The anisotropy of critical current density was investigated by the 3-dimensional FD method.

- The difference of the trapping of fluxoids was investigated for 4 cases of the angle of the applied magnetic flux density.
- The validity of this method for the evaluation and prediction of the anisotropy of the property of the flux flow resistivity and the critical current density in the type II superconductor.

Bibliography

- [1] F. and H. London, "The electromagnetic equations of the supraconductor", *Proc. Roy. Soc. London*, Vol. A149, pp. 71-88, (1935).
- [2] V. L. Ginzburg, "Some Remarks on Phase Transitions of the Second Kind and the Microscopic theory of Ferroelectric Materials", *Soviet Phys. Solid State*, vol. 2, pp. 1824-1834, 1961.
- [3] H. Higasa, R. Takahata, H. Imaizumi and H. Miya, "Frequency response function of magnetic bearings using high temperature superconductor" (in Japanese), *Trans. IEE Japan*, Vol 115-D, No. 10, 1995.
- [4] Y. Luo, K. Miya and H. Higasa, "Geometric design of the HTSC bearing of energy storage flywheel", *Proc. ASAEM '96*, pp. 76-80, 1996.
- [5] H. Kitaguchi, H. Kumakura, K. Togano, T. Kiyoshi and K. Inoue, "Development of HTCS tapes and magnets", *Proc. 2nd Japan-Central Europe Joint Workshop*, 1996.
- [6] T. Uchimoto and K. Miya, "Design study on high Tc superconducting plasma stabilizer", *Proc. 19-th SOFT (Symp. On. Fusion Tech.)*, to be published.
- [7] C.P. Bean, "Magnetization of High-Field Superconductors", *Rev. Modern Phys.* , pp. 31-39, Jan. 1964.
- [8] Y.B. Kim, C. F. Hempstead and A. R. Strand, " Flux-Flow Resistance in Type-II Superconductors", *Phys. Rev.* , vol. 139A, pp. 1163-1172, 1965.

- [9] K. Yasuhochi, T. Ogasawara, N. Usui, "Magnetic behavior and effect of transport current on it in superconducting Nb-Zr wire", *J. Phys. Soc. Japan*, Vol. 19, No. 9, pp. 1649-1661, 1964.
- [10] P.W. Anderson, "Theory of Flux Creep in Hard Superconductors", *Phys. Rev. Lett.*, vol. 9, pp. 309-311, 1962.
- [11] K. Yamafuji and Y. Mawatari, "Electromagnetic Properties of High T_c Superconductors: Relaxation of Magnetization", *Cryogenics*, vol. 32, pp. 569-577, 1992.
- [12] T. Sugiura, H. Hashizume and K. Miya, "Numerical Electromagnetic Field Analysis of Type-II Superconductors", *Int. J. Appl. Electromagn. Mater.*, vol. 2, pp. 183-196, 1991.
- [13] H. Hashizume, T. Sugiura, K. Miya and S. Toda, "Numerical Analysis of Electromagnetic Phenomena in Superconductors", *IEEE Trans. Magn.*, vol. 28, pp. 1332-1335, 1992.
- [14] N. Takeda, M. Uesaka and K. Miya, "Influence of an applied magnetic field on shielding current paths in a high T_c superconductor", *Cryogenics*, vol. 35, pp. 893-899, 1995.
- [15] F. C. Moon, K-C. Weng and P-Z. Chang, "Dynamic magnetic forces in superconducting ceramics", *J. Appl. Phys.*, Vol. 66, No. 11, pp. 5643-5645, 1989.
- [16] F. C. Moon, "Magnetic forces in high- T_c superconducting bearings", *Appl. Electromag. Mater.*, Vol. 1, pp. 29-35, 1990.
- [17] M. Uesaka, Y. Yoshida, N. Takeda and K. Miya, "Experimental and numerical analysis of three-dimensional high- T_c superconducting levitation systems", *Int. J. Appl. Electromag. Mater.*, vol. 4, pp. 13-25, 1993.

- [18] Y. Yoshida, M. Uesaka and K. Miya, "Magnetic Field and Force Analysis of High T_c Superconductor with Flux Flow and Creep", *IEEE Trans. Magn.*, vol. 30, pp. 3503-3506, 1994.
- [19] K. Watanabe, A. Awaji, N. Kobayashi, H. Yamane, T. Hirai and Y. Muto, "Angular dependence of the upper critical field and the critical current density for $Y_1Ba_2Cu_3O_{7-\delta}$ films", *J. Appl. Phys.* Vol. 69, No. 3, pp. 1543-1545, 1991.
- [20] N. Nakamura, G. D. Gu and N. Koshizuka, "Self-field effect on critical current density in single-crystal $Bi_2Sr_2CaCu_2O_x$ ", *Physica C*, Vol. 225, pp. 65-70, 1994.
- [21] R. H. Koch, V. Foglietti, W. J. Gallagher, G. Koren, A. Gupta and M. P. A. Fisher, "Experimental evidence for vortex-glass superconductivity in Y-Ba-Cu-O",
- [22] D. R. Nelson and H. S. Seung, "Theory of melted flux liquids", *Phys. Rev.*, Vol. B39, No. 13, pp. 9153-9174, 1989. *Phys. Rev. Lett.*, Vol. 63, No. 14, pp. 1511-1514, 1989.
- [23] D. R. Nelson and V. M. Vinokur, "Boson localization and pinning by correlated disorder in high-temperature superconductors", *Phys. Rev. Lett.*, Vol. 68, No. 15, pp. 2398-2401, 1992.
- [24] H. Q. Ding, N. Karasawa, W. A. Goddard III, "Atomic level simulation on a million particles: The cell multipole method for Coulomb and London nonbond interactions", *J. Chem. Phys.*, vol. 97, No. 15, pp. 4309-4315, 1992.
- [25] H. Hsieh and R. S. Averback, "Molecular-dynamics simulations of collisions between energetic clusters of atoms and metal substrates", *Phys. Rev.*, vol. B45, No. 8, pp. 4417-4431, 1992.
- [26] A. Brass and H. J. Jensen, "Algorithm for computer simulations of flux-lattice melting in type-II superconductors", *Phys. Rev.*, Vol. B39, No. 13, pp. 9587-9590, 1989.

- [27] W. H. Kleiner, L. M. Roth and S. H. Autler, "Bulk solution of Ginzburg-Landau equations for type II superconductors: upper critical field region", *Phys. Rev.*, Vol. 133, No. 5A, pp. 1226-1227, 1964.
- [28] A. A. Abrikosov, "On the magnetic properties of superconductors of the second group", *Soviet Phys. JFTP*, Vol. 5, No. 6, pp. 1174-1182, 1957.
- [29] D. Saint-James and P. G. de Gennes, *Phys. Lett.*, Vol. 7 p. 306, 1963.
- [30] F. Caroli and K. Maki, "Motion of the vortex structure in type-II superconductors in high magnetic field", *Phys. Rev.*, Vol 164, No. 2, pp. 591-607, 1967.
- [31] L. P. Gorkov and G. M. Eliashberg, "Generalization of the Ginzburg-Landau equations for non-stationary problems in the case of alloys with paramagnetic impurities", *Soviet Phys. - JFTP*, Vol. 27, No.2, pp. 328-334, 1968.
- [32] L. P. Gorkov "Microscopic derivation of the Ginzburg-Landau equations in the theory of superconductivity", *Soviet Phys. - JFTP*, Vol. 36, No.9 pp. 1364-13667, 1968.
- [33] C. R. Hu and R. S. Thompson, "Dynamic structure of vortices in superconductors $\Pi H < H_{c2}$ ", *Phys. Rev.* Vol. B6, pp. 110-120, 1972.
- [34] C. J. Carpenter, "Comparison of Alternative Formulations of 3-Dimensional Magnetic-field and Eddy-current Problems at Power Frequencies", *Proc. IEE*, Vol. 124, pp. 1026-1034, 1979.
- [35] W. D. Gropp, H. G. Kaper, G. K. Leaf, D. M. Levine, M. Palumbo and V. M. Vinokur, "Numerical simulation of vortex dynamics in type II superconductors", *J. Comp. Phys.*, Vol. 123, pp. 254-266, 1996.
- [36] K. J. M. Moriarty, E. Myers and C. Rebbi, "A vector code for the numerical simulation of cosmic strings and flux vortices in superconductors on the ETA-10", *Comp. Phys. Commun.*, vol. 54, pp.273-294, 1989.

- [37] F. Liu, M. Mondello and N. Goldenfeld, "Kinetics of the superconducting transition", *Phys. Rev. Lett.*, vol. 66, No. 23, pp. 3071-3074, 1991.
- [38] H. Frahm, S. Ullah and A. T. Dorsey, "Flux dynamics and the growth of the superconducting phase", *Phys. Rev. Lett.*, vol. 66, No. 23, pp. 3067-3070, 1991.
- [39] R. Kato, Y. Enomoto and S. Maekawa, "Computer simulations of dynamics of flux lines in type-II superconductors", *Phys. Rev.*, vol. B44, No. 13, pp. 6916-6920, 1991.
- [40] R. Kato, Y. Enomoto and S. Maekawa, "Effects of the surface boundary on the magnetization process in type-II superconductors", *Phys. Rev.*, vol. B47, No. 13, pp. 8016-8024, 1993.
- [41] M. Machida and H. Kaburaki, "Direct simulation of the time-dependent Ginzburg-Landau equation for type-II superconducting thin film: vortex dynamics and V-I characteristics", *Phys. Rev. Lett.*, vol. 71, No. 19, pp. 3206-3209, 1993.
- [42] M. Machida and H. Kaburaki, "Numerical simulation of flux-pinning dynamics for a defect in a type-II superconductor", *Phys. Rev.*, vol. B50, No. 2, pp. 1286-1289, 1994.
- [43] J. Bardeen and M. J. Stephen, *Phys. Rev.* Vol. A140, p. 1197, 1965.
- [44] K. Demachi, Y. Yoshida, H. Asakura and K. Miya, "Numerical analysis of magnetization processes in type II superconductors based on Ginzburg-Landau theory", *IEEE Trans. Magn.*, Vol. 32, No. 3, pp. 1156-1159, 1996.
- [45] K. Demachi, H. Asakura, Y. Yoshida, K. Miya, "Numerical analysis of type II superconductor based on Ginzburg-Landau theory", *Proc. 3rd Japanese-Czech-Slovak Joint Semin. Appl. Electromagn.*, pp. 77-82, 1995.
- [46] H. Hashizume, S. Toda, T. Kurusu and K. Maeda, "Numerical Simulation of Fluxoid Dynamics by MD Method", *Proc. 4-th Japanese-Polish Joint. Semin.*, pp. 176-179, 1995.

- [47] K. Demachi, H. Tsumori and K. Miya, "Numerical analysis of the behaviors of fluxoids in type-II superconductor based on the molecular dynamics method combined with the Ginzburg-Landau theory", *Proc. 8-th Int. Work. Crit. Curr. Supercon.*, pp. 263-270, 1996.

Appendix

The change of the energy by its infinitesimal variation δE can be written as

$$\begin{aligned}
 E + \delta E &= \int_v \left[f_n + \alpha(\psi + \delta\psi)(\psi^* + \delta\psi^*) + \frac{\beta}{2}(\psi + \delta\psi)^2(\psi^* + \delta\psi^*)^2 \right. \\
 &+ \frac{1}{2m^*} \left\{ \left(\frac{\hbar}{i} \nabla - e^* \mathbf{A} + \delta \mathbf{A} \right) (\psi + \delta\psi) \right\} \left\{ \left(-\frac{\hbar}{i} \nabla + e^* \mathbf{A} + \delta \mathbf{A} \right) (\psi^* + \delta\psi^*) \right\} \\
 &+ \left. \frac{(\nabla \times (\mathbf{A} + \delta \mathbf{A}))^2}{2\mu_0} \right] dV. \tag{A.1}
 \end{aligned}$$

By neglecting the higher order terms, δE is represented as follows;

$$\begin{aligned}
 \delta E &= \int_v \left[\alpha(\psi \delta\psi^* + \psi^* \delta\psi) + \beta|\psi|^2(\psi \delta\psi^* + \psi^* \delta\psi) \right. \\
 &+ \frac{1}{2m^*} \left\{ \left(\frac{\hbar}{i} \nabla \psi + e^* \mathbf{A} \psi \right) \cdot \left(-\frac{\hbar}{i} \nabla \delta\psi^* + e^* \mathbf{A} \delta\psi^* \right) \right. \\
 &+ \left. \left(-\frac{\hbar}{i} \nabla \psi^* + e^* \mathbf{A} \psi^* \right) \cdot \left(\frac{\hbar}{i} \nabla \delta\psi + e^* \mathbf{A} \delta\psi \right) \right. \\
 &+ \left. \left(\frac{\hbar}{i} (\nabla \psi) e^* \psi^* + e^{*2} \mathbf{A} |\psi|^2 - \frac{\hbar}{i} (\nabla \psi^*) e^* \psi + e^{*2} \mathbf{A} |\psi|^2 \right) \cdot \delta \mathbf{A} \right\} \\
 &+ \left. \frac{1}{\mu_0} (\nabla \times \delta \mathbf{A}) \cdot (\nabla \times \mathbf{A}) \right] dV, \tag{A.2}
 \end{aligned}$$

where

$$\alpha(\psi \delta\psi^* + \psi^* \delta\psi) + \beta|\psi|^2(\psi \delta\psi^* + \psi^* \delta\psi) = (\alpha + \beta|\psi|^2)\psi \delta\psi^* + (\alpha + \beta|\psi|^2)\psi^* \delta\psi, \tag{A.3}$$

$$\begin{aligned}
 \left(\frac{\hbar}{i} \nabla \psi + e^* \mathbf{A} \psi \right) \cdot \left(-\frac{\hbar}{i} \nabla \delta\psi^* + e^* \mathbf{A} \delta\psi^* \right) &= \mathbf{u} \cdot \left(-\frac{\hbar}{i} \nabla \varphi + e^* \mathbf{A} \varphi \right) \\
 &= -\frac{\hbar}{i} \mathbf{u} \cdot (\nabla \varphi) + \mathbf{u} \cdot (e^* \mathbf{A} \varphi), \tag{A.4}
 \end{aligned}$$

$$\left(\frac{\hbar}{i} \nabla \psi + e^* \mathbf{A} \psi \right) \equiv \mathbf{u}, \tag{A.5}$$

$$\delta\psi^* \equiv \varphi. \tag{A.6}$$

By using the following formula of vector identity,

$$\nabla \cdot (\varphi \mathbf{u}) = (\nabla \varphi) \cdot \mathbf{u} + \varphi \nabla \cdot \mathbf{u}, \tag{A.7}$$

the first term of the right hand side of eq. (A.4) is transformed as

$$\mathbf{u} \cdot (\nabla \varphi) = \nabla \cdot (\varphi \mathbf{u}) - \varphi \nabla \cdot \mathbf{u}. \tag{A.8}$$

By substituting eq. (A.8), eq. (A.4) is transformed as

$$\begin{aligned} -\frac{\hbar}{i}\mathbf{u}\cdot(\nabla\varphi)+\mathbf{u}\cdot(e^*\mathbf{A}\varphi) &= -\frac{\hbar}{i}[\nabla\cdot(\varphi\mathbf{u})-\varphi\nabla\cdot\mathbf{u}]+\mathbf{u}\cdot(e^*\mathbf{A}\varphi) \\ &= -\frac{\hbar}{i}\nabla\cdot(\varphi\mathbf{u})+\left\{\frac{\hbar}{i}\nabla\cdot\mathbf{u}+\mathbf{u}\cdot(e^*\mathbf{A})\right\}\varphi. \end{aligned} \quad (\text{A.9})$$

The second term of the right hand side of eq. (A.9) is transformed by substituting eq. (A.5) as follows,

$$\begin{aligned} \frac{\hbar}{i}\nabla\cdot\mathbf{u}+\mathbf{u}\cdot(e^*\mathbf{A}) &= \frac{\hbar}{i}\nabla\cdot\left(\frac{\hbar}{i}\nabla\psi+e^*\mathbf{A}\psi\right)+\left(\frac{\hbar}{i}\nabla\psi+e^*\mathbf{A}\psi\right)\cdot(e^*\mathbf{A}) \\ &= \left(\frac{\hbar}{i}\right)^2\nabla^2\psi+2\frac{\hbar}{i}e^*\mathbf{A}\cdot\nabla\psi+(e^*\mathbf{A})^2\psi \quad (\text{A.10}) \\ &= \left(\frac{\hbar}{i}\nabla+e^*\mathbf{A}\right)^2\psi. \quad (\because\nabla\cdot\mathbf{A}=0) \quad (\text{A.11}) \end{aligned}$$

Then eq. (A.4) is represented as

$$(A.4) = -\frac{\hbar}{i}\nabla\cdot\left\{\delta\psi^*\left(\frac{\hbar}{i}\nabla\psi+e^*\mathbf{A}\psi\right)\right\}+\left\{\left(\frac{\hbar}{i}\nabla+e^*\mathbf{A}\right)^2\psi\right\}\delta\psi^* \quad (\text{A.12})$$

The following term in eq. (A.4) corresponds to the complex pair of eq. (A.12),

$$\left(-\frac{\hbar}{i}\nabla\psi^*+e^*\mathbf{A}\psi^*\right)\cdot\left(\frac{\hbar}{i}\nabla\delta\psi+e^*\mathbf{A}\delta\psi\right). \quad (\text{A.13})$$

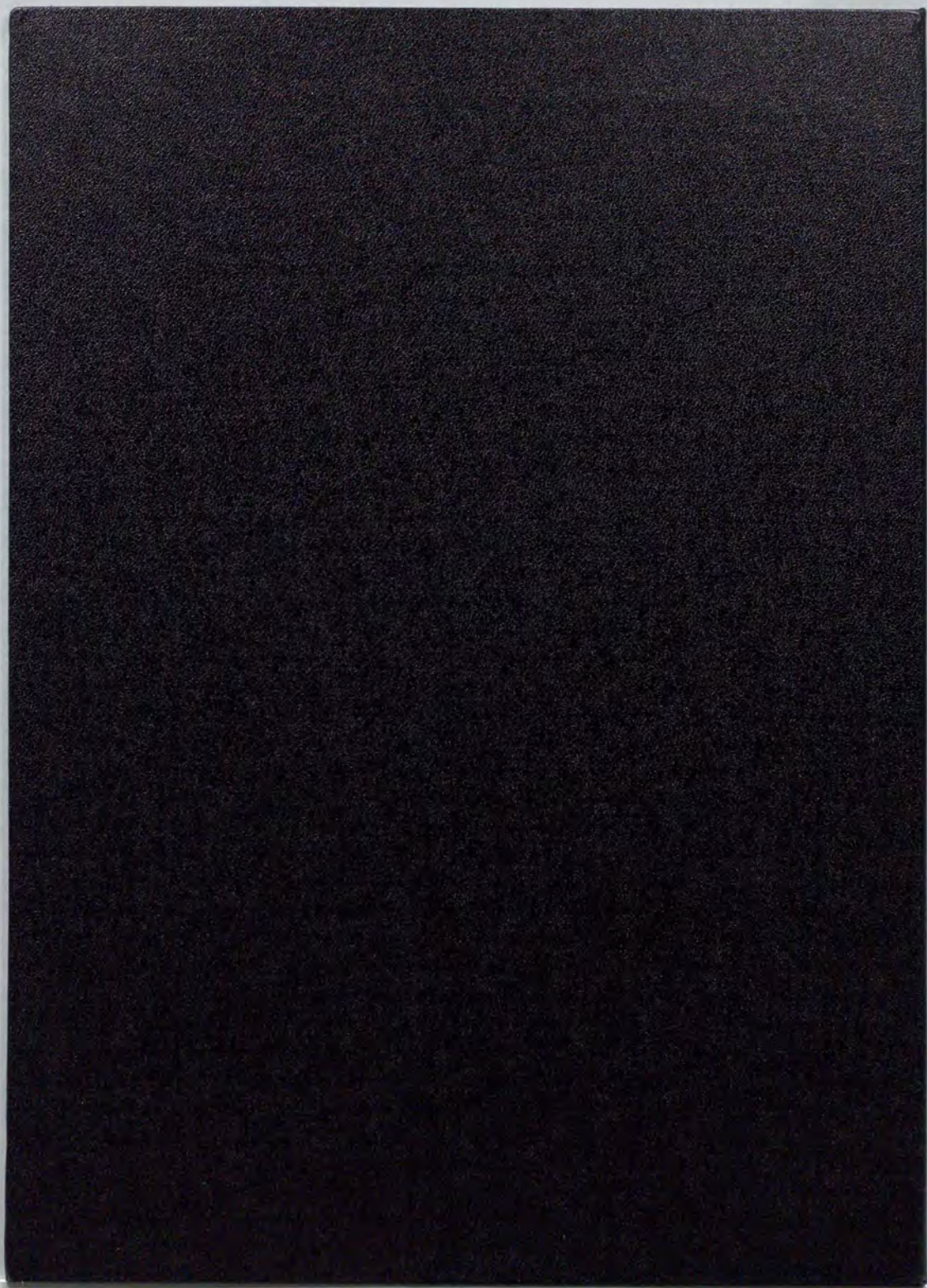
Furthermore the terms in eq. (A.2) are represented as follows

$$\begin{aligned} &\left(\frac{\hbar}{i}(\nabla\psi)e^*\psi^*+e^*{}^2\mathbf{A}|\psi|^2-\frac{\hbar}{i}(\nabla\psi^*)e^*\psi+e^*{}^2\mathbf{A}|\psi|^2\right)\delta\mathbf{A} \\ &= \left\{\frac{\hbar e^*}{i}(\psi^*\nabla\psi-\psi\nabla\psi^*)+2e^*{}^2\mathbf{A}|\psi|^2\right\}\delta\mathbf{A}, \end{aligned} \quad (\text{A.14})$$

$$\begin{aligned} (\nabla\times\delta\mathbf{A})\cdot(\nabla\times\mathbf{A}) &= (\nabla\times\mathbf{u})\cdot\mathbf{v} \quad (\because\delta\mathbf{A}=\mathbf{u},\nabla\times\mathbf{A}=\mathbf{v}) \\ &= \mathbf{u}\cdot(\nabla\times\mathbf{v})+\nabla\cdot(\mathbf{u}\times\mathbf{v}) \\ &= \delta\mathbf{A}\cdot(\nabla\times\nabla\times\mathbf{A})+\nabla\cdot\{\delta\mathbf{A}\times(\nabla\times\mathbf{A})\}, \end{aligned} \quad (\text{A.15})$$

By substituting eqs. (A.13), (A.14) and (A.15) into eq. (A.2) and by applying the Gauss theorem, δE is represented as follows

$$\begin{aligned}
\delta E &= \int_v \left[\left\{ \alpha\psi + \beta|\psi|^2\psi + \frac{1}{2m^*} \left(\frac{\hbar}{i} \nabla + e^* \mathbf{A} \right)^2 \psi \right\} \delta\psi^* + \{C.C.\} \delta\psi \right. \\
&+ \left. \left\{ -\frac{1}{2m^*} \left(\frac{\hbar e^*}{i} (\psi^* \nabla \psi - \psi \nabla \psi^*) + 2e^{*2} \mathbf{A} |\psi|^2 \right) + \frac{1}{\mu_0} (\nabla \times \nabla \times \mathbf{A}) \right\} \delta \mathbf{A} \right] dv \\
&+ \int_S \left[\frac{1}{2m^*} \left\{ -\frac{\hbar}{i} \delta\psi^* \left(\frac{\hbar}{i} \nabla \psi + e^* \mathbf{A} \psi \right) + (C.C.) \right\} + \frac{1}{\mu_0} \delta \mathbf{A} \times (\nabla \times \mathbf{A}) \right] dS. \quad (A.16)
\end{aligned}$$



inches
1 2 3 4 5 6 7 8
cm
1 2 3 4 5 6 7 8 9 10 11 12 13 14 15 16 17 18 19 20

Kodak Color Control Patches

© Kodak, 2007 TM Kodak



Kodak Gray Scale



© Kodak, 2007 TM Kodak

A 1 2 3 4 5 6 **M** 8 9 10 11 12 13 14 15 **B** 17 18 19

